Università degli Studi di Catania
Dottorato di Ricerca in Fisica – XXIII ciclo

RIZZO CARMELO

Symmetry Energy Effects in Low Energy Heavy Ion Collisions with Exotic Beams

PHD Thesis

Tutors:
Prof. M. Di Toro
Dott. M. Colonna
Prof. V. Baran

PHD Coordinator:
Prof. F. Riggi

Anno Accademico 2010 – 2011

Alla donna che mi ha reso felice, Beatrice.

Contents

Introduction

Heavy ion collisions provide a unique tool to explore the nuclear matter phase diagram and Equation of State (EoS). In the case of Asymmetric Nuclear Matter, that is a mixture of neutrons and protons with different concentrations, it becomes possible to investigate the density dependence of the symmetry energy, a quantity that is known, from the Bethe-Weiszäcker mass formula, only around normal conditions.

The knowledge of the EoS of asymmetric matter at low density is very important for the study of structure properties of neutron-rich and exotic systems, such as neutron skins and properties of nuclei at the drip lines, as well as in the astrophysical context, for all phenomena where low-density clustering is concerned, like in the crust of neutron stars. On the other hand, the high density behavior of the symmetry energy affects the neutron star mass/radius and cooling, the formation of black holes, as well as the possible formation of hybrid structures, with a transition to the deconfined phase in the inner core.

The symmetry term gets a kinetic contribution directly from basic Pauli correlations and a potential part from the highly controversial isospin dependence of the effective interactions. Both at sub-saturation and supra-saturation densities, different many-body

techniques lead to different predictions, especially in the high density regime. Hence, it is appealing to try to get information on the density behavior of the symmetry energy from the study of reaction mechanisms involving asymmetric systems.

Dissipative heavy ion collisions offer a unique opportunity to study phenomena occurring in nuclear matter under extreme conditions with respect to shape, intrinsic excitation energy, spin, N/Z ratio (isospin), together with the possibility to control these conditions by choosing appropriate entrance and exit channels. It is possible to probe the mechanisms of nuclear excitation, how intrinsic degrees of freedom are converted into collective modes, how these modes decay and how relaxation processes occur within a small quantal system that is initially far from equilibrium. The velocity and the angular distribution of the reaction products furnish natural clocks from which it is possible to determine the equilibration times of the various degrees of freedom (e.g. N/Z ratio, mass, excitation energy) and discuss whether non-equilibrium features in light particle and fragment emissions are present. Hence it becomes possible to investigate the details of the nuclear interaction away from normal density.

For dissipative collisions at low energy, interaction times are quite long and therefore a large coupling among various mean-field modes is expected. In some cases, due to a combined Coulomb and angular momentum (deformation) effect, some instabilities can show up, like in fission decays. These processes, in heavy-ion reactions with exotic systems, can provide a new access to the dynamics of nuclear scission, allowing to probe the role of the isovector part of the nuclear

interaction. One can investigate whether the development of surface (neck-like) instabilities is sensitive to the structure of the symmetry term. In particular one can study the competition between reaction mechanisms: in mid-peripheral collisions a large variety of phenomena is observed, ranging from incomplete fusion to highly dissipative binary evens up to neck break-up and non-statistical light fragment emission. The interplay between different mechanisms takes place in transition regions where dynamical "bifurcations" will appear. We can expect a large influence of dynamical fluctuations coupled to a larger role of usually small contributions of the in-medium effective nuclear interaction, like the symmetry terms. This is the main idea behind the present thesis project, to exploit a new transport approach to the reaction dynamics, the Stochastic Mean Field (SMF) theory, where fluctuations are consistently treated and the isovector part of the nuclear EoS is microscopically tested in the used effective forces.

We see also effects of the different interaction times on the charge equilibration mechanism, probed starting from entrance channels with large N/Z asymmetries, that is directly driven by the strength of the symmetry term, just below normal density. In fact, the density is expected to be below saturation in the portion of the di-nuclear system along the way toward fusion and it is just in this phase that the proton-neutron fluxes occur leading the system to charge equilibration.

For more central collisions this has been studied also experimentally via the direct measurement of the prompt Dynamical Dipole Resonance (DDR), a nucleus-nucleus collective

bremsstrahlung radiation emitted during the time of charge equilibration. In fact, for charge asymmetric entrance channels, one expects pre-equilibrium photon emission from the dipole oscillation in the fast isospin transfer dynamics observed in fusion and deep-inelastic reactions, in addition to the photons originating from the Giant Dipole Resonance (GDR) thermally excited in the final hot compound nucleus or fragments.

The isospin effects on the observables discussed before, competition between dissipative reaction mechanisms and prompt dipole emissions, will be more clearly measured using the new available exotic beams, neutron or proton rich. We can have larger isospin contents in the composite systems as well as larger N/Z asymmetries in the entrance channels. We note that the energy range of the radioactive beams presently planned in the new European facilities, Spiral2 at Ganil, SPES at Legnaro and HIE-Isolde at Cern, seems to be well suited for the measurements proposed in this thesis project. In fact some of the results presented here have already been included in some Letter Of Intent (LOI) for such new facilities.

In particular we think that some of the SPES heavy n-rich beams will be very well suited to this kind of investigation. In fact we note that the beam energies, corresponding to the ALPI reacceleration, nicely cover the range of the predicted maximum in DDR strength (8-12MeV/A).

In this work we investigate isospin effects in reactions induced by ^{132}Sn (SPIRAL2, SPES) and also by other SPES ion beams (n-rich ^{142}Cs and ^{90}Kr).

As we will discuss in the following, this study reveals new interesting features, opening the possibility to access independent information on the symmetry energy.

The reaction theory developed at the LNS, based on a Stochastic Mean Field Transport Approach, is particularly suitable for these studies. The mean field dynamics, essential at these low energies, is very accurately treated but fluctuations are also consistently accounted for, in order to reproduce the stochastic effects of dynamical instabilities. The simulations are performed with two choices of the isovector part of the nuclear interaction in the medium, "Asystiff", corresponding to a potential part of symmetry energy with a positive slope around saturation, and "Asysoft", for the case of a flat behaviour and eventually a decrease above saturation.

The thesis is organized as it follows:

In Chapter 1 the semi-classical approximation of the many-body problem is presented, leading to the BNV transport equation for the one-body distribution function and the its resolutions by the test particles approach.

In Chapter 2 is devoted to the description of the effective interactions used in the transport code, focusing on the symmetry energy.

In Chapter 3 we report the properties of the prompt dipole radiation, produced via a collective "bremsstrahlung" mechanism, in fusion reactions with exotic beams. We will show the gamma yield and we will find that the angular distribution of the emitted photons from such collective dipole mode.

In Chapter 4 we will focus on the interplay between reaction mechanisms, fusion vs. break-up, that in exotic systems is expected to be influenced by the symmetry energy term at densities around the normal value. The method described, based on the event by event evolution of phase space Quadrupole collective modes will nicely allow to extract the fusion probability at relatively early times. Fusion probabilities for reactions induced by ^{132}Sn on ^{64,58}Ni targets at 10MeV/A are evaluated. Finally a collective charge equilibration mechanism is revealed in both fusion and break-up events. Finally we investigate the effect of the mass asymmetry in the entrance channel for systems with the same overall isospin content and similar initial charge asymmetry.

Chapter 1 : MANY-BODY PROBLEM

There are various models that describe the dynamics in heavy ion collisions, the one used in this thesis is the BNV (Boltzmann Nordheim, Vlasov): it is based on the description of the nuclear dynamics as a many-body system via the equations of transport Landau-Vlasov, these semi-classical equations provide an approximation of the many-body problem. The evolution of the system in the ion collisions is determined by a competition between mean field and two-body correlations.

The nuclear interactions between nucleons are independent of their charge, we know that this property of nuclear forces acting between two nucleons is a consequence of their composite nature (i.e. they are composed of three quarks which have mass much smaller than the mass of a nucleon). This leads us to believe that the "nucleon" is characterized by a freedom degree called "isotopic spin", which distinguishes between two different states: proton and neutron. The mean field must take into account this freedom degree as well as the various properties of the nuclear matter when you depart from the symmetry between protons and neutrons.

1.1 The Hierarchy of equations BBGG in N-body theory.

The nucleus is described by a many-body systems interacting via Coulomb and nuclear interaction, and because the actions of its constituent particles are comparable with the value of Planck's constant, it is a quantum system. The N-body Schroedinger equation is difficult to solve because the potential of the system is the sum of two or more interaction terms.

$$H = \sum_{i=1}^{N} \hat{T}_i + \sum_{i<j=1}^{N} \hat{U}_{ij}$$

equ. 1.1

The Hamiltonian of the system is the sum of kinetic energy operators of all individual particles and the operators describing the interaction between two bodies of the system. From the N-body wave function ϕ, solution of the Schroedinger equation, we can obtain the N-body density operator in the coordinate space:

$$\rho_N = \rho_N\left(\vec{r}_1,\ldots,\vec{r}_N,\vec{r}'_1,\ldots,\vec{r}'_N\right) = \phi\left(\vec{r}_1,\ldots,\vec{r}_N\right)\phi^*\left(\vec{r}'_1,\ldots,\vec{r}'_N\right)$$

equ. 1.2

The density matrix is itself the solution of equation Von Neumann:

$$i\hbar\frac{\partial\rho_N}{\partial t} = \left[H,\rho_N\right]$$

equ. 1.3

Von Neumann's equation corresponds to that of Schroedinger in the formalism of the density operator. It can not be solved exactly but it

represents the starting point for further approximations. Introducing the Liouville operators and replacing them in the equation of Von Neumann, we get:

$$\hat{L}_i \equiv \left[\hat{T}_i, \rho_N\right] \qquad\qquad \hat{M}_{ij} \equiv \left[\hat{U}_{ij}, \rho_N\right]$$

equ. 1.4

$$i\hbar \frac{\partial \rho_N}{\partial t} = \left(\sum_{i=1}^{N} \hat{L}_i + \sum_{i<j=1}^{N} \hat{M}_{ij} \right) \rho_N$$

equ. 1.5

With suitable approximations, one can go from a discussion of many bodies, of which you can not solve the problem analytically, to a reduced two-body which can be solved. For this purpose we consider the density matrix of order K:

$$\rho_K = \rho_K\left(\vec{r}_1,...,\vec{r}_K,\vec{r}_1^{'},...,\vec{r}_K^{'}\right) = \frac{N!}{(N-K)!}\int d\vec{r}_{K+1}...d\vec{r}_N...d\vec{r}_{K+1}^{'}...d\vec{r}_N^{'}\rho_N\left(\vec{r}_1,...,\vec{r}_N,\vec{r}_1^{'},...,\vec{r}_N^{'}\right)$$

equ. 1.6

The effect of integration is to reduce the number of variables on which it depends, taking them from *N* to *K*, while the factorial term *N!/(N-K)!*, consider the integration over the remaining *(N-K)* variables. Substituting the density of order *K* in the equation of Von Neumann, we get:

$$i\hbar \frac{\partial \rho_K}{\partial t} = \frac{N!}{(N-K)!} Tr_{(K+1,...,N)}\left(\sum_{i=1}^{K} \hat{L}_i + \sum_{i<j=1}^{K} \hat{M}_{ij} + (N-K)\sum_{i=1}^{K} \hat{M}_{i,K+1} \right) \rho_N$$

equ. 1.7

where the trace indicates the integration. Extracting the integral index *K+1*, we obtain:

$$i\hbar\frac{\partial\rho_K}{\partial t}=\left(\sum_{i=1}^{K}\hat{L}_i+\sum_{i<j=1}^{K}\hat{M}_{ij}\right)\rho_N+Tr_{(K+1)}\left(\sum_{i=1}^{K}\hat{M}_{i,K+1}\right)\rho_{K+1}$$

equ. 1.8

In the last term appears in the density operator (*K+1)*-body that enters in the correlation of order *K+1* in the density operator *K*-body. So starting from the problem many-body you can go down to lower order of density through these equations related to each other and called "**BBGG Hierarchy"** [BON94], by Bogoliubov, Born, Green and Gurov. This is a problem, because, if you want to know the density of one-body we should also know that of two, and so on the other hand this is a nice approximation scheme, if you have some knowledge of higher order terms, as we will see in the following.

1.2 The time dependent Hartree-Fock equation.

Introducing the hierarchy BBGG, the very first step is to consider only the first equation for k=1, so we can exploit the temporal evolution of the one-body density:

$$i\hbar\frac{\partial}{\partial t}\rho_1\left(\vec{r}_1,\vec{r}_1^{'},t\right)=\hat{L}_1\rho_1\left(\vec{r}_1,\vec{r}_1^{'},t\right)+Tr_{(2)}\hat{M}_{12}\rho_2\left(\vec{r}_1,\vec{r}_1^{'},\vec{r}_2,\vec{r}_2^{'},t\right)$$

equ. 1.9

In order to obtain a resolution of this equation, we introduce the Hartree-Fock approximation (TDHF), which expresses the two-body density operator through a anti-symmetric product of one-body densities. Such two-body density do not show effects of interaction correlations between the nucleons, the only correlation being the anti-symmetry of the total N-body wave function. We note that it is the term, typically quantum, of exchange that makes anti-symmetric the two-body density operator with respect to the exchange, $\vec{r}_1^{'}\leftrightarrow\vec{r}_2^{'}$:

$$\rho_2^{(TDHF)}\left(\vec{r}_1,\vec{r}_1^{'},\vec{r}_2,\vec{r}_2^{'},t\right)=\rho_1\left(\vec{r}_1,\vec{r}_1^{'},t\right)\rho_1\left(\vec{r}_2,\vec{r}_2^{'},t\right)-\rho_1\left(\vec{r}_1,\vec{r}_2^{'},t\right)\rho_1\left(\vec{r}_2,\vec{r}_1^{'},t\right)$$

equ. 1.10

In this case we can describe the many-body Hamiltonian as a sum of independent single-particle Hamiltonians, each of which with a potential term which does not depend on the relative coordinates between two particles; in so doing, the motion of each particle of the system is governed by the presence of a mean field self-consistently produced by the interaction with the other particles. Using the TDHF we can write the trace of the temporal evolution of the one-body density as:

$$Tr_{(2)}\hat{M}_{12}\rho_2^{(TDHF)}=Tr_{(2)}\left[\hat{V}_{12},\rho_2^{(TDHF)}\right]=\left[\hat{U}_{direct}\ \left(\rho_1\right)+\hat{U}_{exchange}\left(\rho_1\right),\rho_1\right]=\left[Tr_{(1)}\left(\hat{V}\rho_1\right),\rho_1\right]$$

equ. 1.11

where $\hat{V}$ is the interaction operator anti symmetrized. Through these results we obtain the time-dependent Hartree-Fock equation:

$$i\hbar \frac{\partial}{\partial t} \rho_1(t) = \left[\hat{T} + Tr_{(1)}\left(\hat{V}\rho_1\right), \rho_1 \right]$$

equ. 1.12

where $\hat{T} + Tr_1(\hat{V}\rho_1)$ is the Hamiltonian of the Hartree-Fock self-consistent, where there is a mean field. We have reduced the problem from a quantum N-body to a one-body problem. This approximation reproduces the dynamics only if the nuclear mean field effects are dominant [BER88] over the residual interactions between nucleons [RIN80]. When the Fermi spheres of the two nuclei overlap, the direct two-body interactions are inhibited and the phase space is called Pauli-blocked. So the TDHF equation, although affected by strong approximations, can describe very well some nuclear properties in an energy range of about 10MEV per nucleon. It can also describe rather well some collective properties of nuclei as well as single particle proprieties, like energy levels. The equation retains the expectation value of some operators, a necessary condition for an equation that does not lose physical meaning: the number of particles is conserved, as well as the total energy, the total momentum and angular momentum of the system; it is also preserved the anti symmetry of the total wave function. This equation is not a good description of the dynamics at medium-high energies, because now it is fundamental to consider the effect of explicit two-body collision terms, not present in TDHF. It is also important to note that it does not give information about quantum probability but only the time evolution average values of one-body operators.

1.3 Wigner transform and distribution.

A equivalent formulation can be derived from definition of phase space like a 6-N dimensional space generated by the canonical coordinates of the particles. One point of this space represents one state of the system. Gibbs introduced the statistical ensemble: once a macroscopic state is fixed, there is an entire ensemble of microscopic states of system corresponding to it. The system may be described by the phase space distribution function $f_N=f_N(s_1,\ldots,s_N,t)$ which represents the probability to find a given ensemble. The time evolution of f_N is fixed by the Liouville Theorem: since the total number of microscopic systems in an ensemble is conserved. So the density of states in a given phase space point is constant in time or in other words the distribution function is a constant of motion, which amounts to saying that the system behaves like an incompressible fluid in phase space [HUA63]. This statement can be expressed in formulas as follows:

$$\frac{\partial f_N}{\partial t} = \{H, f_N\}$$

equ. 1.13

It represents, when { } is a Poisson bracket, formally the semi classical limit of the Von Neumann equation, if we replace the Poisson brackets with the commutators. We can express this equation in terms of phase space coordinates of the particles as:

$$\frac{\partial f_N}{\partial t} + \sum_{i=1}^{N} \left[\frac{\partial f_N}{\partial \mathbf{r}_i} \dot{\mathbf{r}}_i + \frac{\partial f_N}{\partial \mathbf{p}_i} \dot{\mathbf{p}}_i \right] = 0$$

$$\dot{\mathbf{r}}_i = \frac{\partial H}{\partial \mathbf{p}_i}, \quad \dot{\mathbf{p}}_i = -\frac{\partial H}{\partial \mathbf{r}_i}$$

equ. 1.14

Starting from this equation, one can consider the reduced distribution function of order *K*, in the same way as shown in the previous paragraph, from which we derive a classical statistical hierarchy, called "BBGKY Hierarchy", by Born, Bogoliubov, Green, Kirkwood and Yvon. As the quantum BBGG Hierarchy, these equations are exact, since no approximations have been made up.

The connection between the classical and quantum hierarchies is given by the Wigner transform [WIG32]: it is the Fourier transform of the density matrix in coordinate space with respect to a combination of the canonical variables.

$$f_N\left(\vec{r}_1,...,\vec{r}_N,\vec{p}_1,...,\vec{p}_N,t\right) = \frac{1}{\left(2\pi\hbar\right)^3}\int d^3\vec{s}_1..d^3\vec{s}_N \prod_{i=1}^{N} e^{-i\frac{\vec{p}_i\cdot\vec{s}_i}{\hbar}} \rho_N\left(\vec{r}_1+\frac{\vec{s}_1}{2},...,\vec{r}_N+\frac{\vec{s}_N}{2},\vec{r}_1-\frac{\vec{s}_1}{2},...,\vec{r}_N-\frac{\vec{s}_N}{2},t\right)$$

equ. 1.15

where $\vec{s}$ is the vector which has components for the relative coordinates of two particles and $\vec{r}$ is the vector which has components for the coordinates of the center of mass of two particles.

From its definition and the Von Neumann equation a different hierarchy was derived. Although the Wigner transform formally resembles the classical distribution function f_N, the variables on which it depends are not canonical conjugate. In fact there are conceptual

differences between a classical distribution function and the Wigner transform defined above: firstly, the variables are not phase space conjugate coordinates, but those that resulting from a Fourier transform. Moreover, the classical N-body distribution function is defined always positive, while the quantum f_N does not have a defined sign, we can only say that this is a real function because the density matrix is Hermitian [DIT84]. But we can demonstrate by making an expression in power of $\hbar$ that in classical limit $\hbar \to 0$ these variables indeed reduce to classical canonical variables. In fact the condition $\hbar \to 0$ is not appropriate. In general all the semi-classical results described here are derived from the assumption that f_N does not change quickly with position and momentum. The Wigner function in the classical limit is positive and can be associated with a probability.

1.4 The Vlasov equation.

Consider the TDHF equation in which appears the density operator to one-body, ρ_1, and f is the Wigner transform of this operator: applying the Wigner transform to both sides of the TDHF equation for $\hbar \to 0$ and introducing the Hamiltonian of the Hartree-Fock self-consistent:

$$f\left(\vec{r},\vec{p},t\right)=\frac{1}{\left(2\pi\hbar\right)^3}\int d^3\vec{s}\,e^{-i\frac{\vec{p}\cdot\vec{s}}{\hbar}}\rho_1\left(\vec{r}+\frac{\vec{s}}{2},\vec{r}-\frac{\vec{s}}{2},t\right)$$

equ. 1.16

$$H^{HF} = \frac{\hat{\vec{P}}^2}{2m} + \hat{W}(f)$$

equ. 1.17

where $\hat{W}(f)$ is the Wigner transform of the self-consistent one-body potential (mean field). We obtain an equation formally identical to the *equ.1.12*, called the Vlasov equation [VLA45] from which you can obtain the time evolution of *f*.

$$\frac{\partial}{\partial t} f(\vec{r}, \vec{p}, t) = \left\{ H^{HF}(f), f \right\}$$

equ. 1.18

The knowledge of the Wigner transform of the one-body density *f* is very important because it has properties that are identical to those of the classical one-body distribution function in phase space, even if from the conceptual point of view it is the same thing. Although this equation is semi classical, can well describe the evolution quantum systems at low energies, i.e. those conditions in which collisions are Pauli-blocked. In this case the Pauli exclusion principle dominates (this is expressed through anti-symmetrization in the two body density operator of Hartree-Fock approximation), in other words, the system evolves so as not to violate it at every instant of time, since Liouville's theorem is valid.

1.5 The collision integral.

The direct two-body interactions play an important role in medium-high energies, where the nucleon-nucleon collisions are not prohibited by the Pauli-blocking. By varying the energy we then have different reaction mechanisms: a low-energy one-body dynamics prevail, with mean-field effects, whereas at higher energies effects of NN-collisions will not be negligible and must put in place new mechanisms, due to two or many-body contributions. The Vlasov equation neglects correlations in the second order up, but this approximation is not valid increasing energy, because we cannot neglect the direct nucleon-nucleon collisions as mentioned above. So in a semi-classical context we can introduce a collision term in the Vlasov equation that allows systems to deal with intermediate energies, where there is strong competition between the dynamics of the field and that due to nucleon-nucleon collisions. This term is the so-called two-body collision integral, introduced by Boltzmann to describe kinetically a gas, and is a function of the distribution function. The Vlasov equation associated with the collision term does not guarantee the incompressibility of phase space, with respect to the Liouville theorem and the Pauli-blocking, because the direct collisions are changing the momentum of particles and the occupation in phase space. Consequently, the second member of *equ.1.18* should be different from zero, because local density in phase space will not be constant.

Now consider a system of two point particles colliding in a point of the ordinary space and that the impact changes only their momenta, in

the phase space one can calculate the number of particles emerging from an infinitesimal volume $d^3\vec{p}d^3\vec{r}$, by the integral:

$$\frac{d\vec{p}d\vec{r}}{\hbar^3}\int\frac{d^3p_1d^3r_1}{\hbar^3}\frac{d^3p'd^3r'}{\hbar^3}\frac{d^3p_1'd^3r_1'}{\hbar^3}\omega\left(\vec{p}\vec{p}_1\rightarrow\vec{p}'\vec{p}_1'\right)ff_1\delta\left(\vec{r}'-\vec{r}_1'\right)\delta\left(\vec{r}'-\vec{r}_1\right)\delta\left(\vec{r}_1'-\vec{r}_1\right)$$

equ. 1.19

where ω is the transition probability for nucleon-nucleon collisions, and where the remaining terms in the integral represent the occupation of the states, where appear the Dirac delta δ (point system) and classical distributions, *f*. We can replace the classic distributions ff_1 in the integral, with $ff_1(1-f')(1-f'_1)$, i.e. multiplying the initial distribution by a term which denies the possibility that the final states are occupied by other particles, so the collision is inhibited if the probability distribution of possible final state is close to one, this simulation of the Pauli-blocking was introduced by Nordheim. So the collision integral is the difference between the term of the outgoing flow of probability, and the term entry:

$$I_{coll}\left(f\right)=\int d^3\vec{p}_1d^3\vec{p}'d^3\vec{p}_1'\omega\left(\vec{p}\vec{p}_1\rightarrow\vec{p}'\vec{p}_1'\right)\left[f'f_1'\left(1-f\right)\left(1-f_1\right)-ff_1\left(1-f'\right)\left(1-f_1'\right)\right]$$

equ. 1.20

Finally, putting this integral in the Vlasov equation, we obtain the Landau-Vlasov equation, also called the Boltzmann-Nordheim-Vlasov (BNV):

$$\frac{\partial}{\partial t}f\left(\vec{r},\vec{p},t\right)-\left\{H\left(f\right),f\right\}=I_{coll}\left(f\right)$$

equ. 1.21

where *H(f)* is the effective Hamiltonian containing the mean field potential. So the variation in distribution over the time is given by a kinetic term, a term self-consistent mean field and one of collision. Since the distribution function concerns not only the first term but also others, and especially the mean field and the integral of collisions in a non-linear way, this equation is difficult to integrate analytically; we solve the equation using numerical methods such as the "test particles". In particular, if we advance the hypothesis that the potential is local and not dependent on momentum, it has been widely used to describe reactions with dynamic mean field and with collision dynamics.

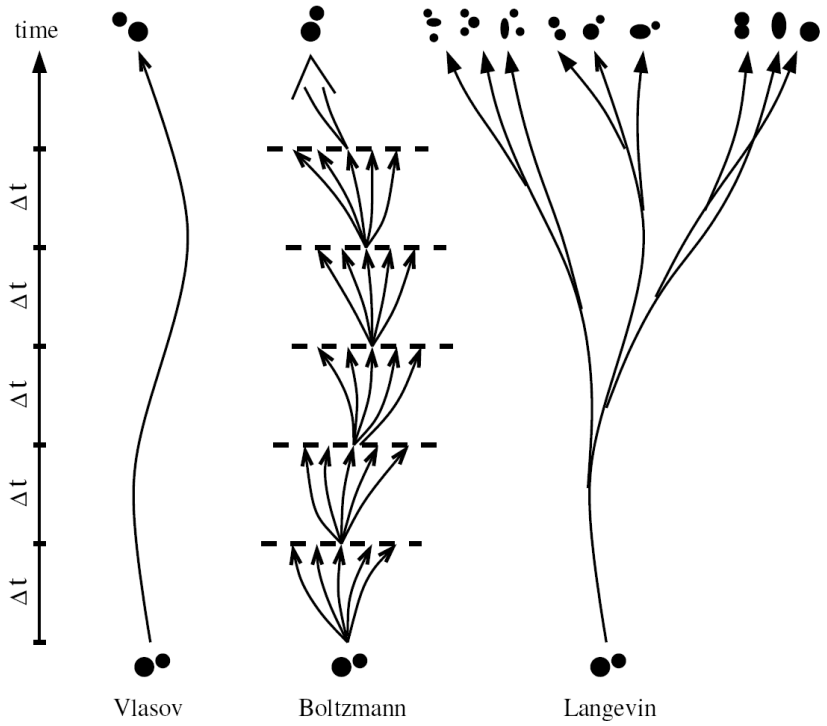

Fig. 1

This equation is purely deterministic because the treatment BNV keeps the average effect of this term, and therefore produces a unique

trajectory in phase space, which is different from the pure Vlasov approach. Fluctuations only arise from numerical noise. The time evolution of the trajectory in phase space for different approaches is described in Fig.1.

The Vlasov equation drives the system along a single dynamic path, when the Boltzmann collision integral included various possible outcomes of collisions are on average at every step, and the system ends in a single final configuration, different from only Vlasov. The approach discussed in this section allows the system to follow different paths, leading to a continuous path branching, and end up with a whole ensemble of different configurations. The validity of mean field treatment is therefore limited to phenomena that show a small degree of fluctuation. In fact, the BNF-based models are more suitable to study the temporal evolution of one-body observables, but are not sufficient to describe the processes characterized by bifurcations, where a small fluctuation of the spatial density can be amplified, thereby producing a divergence of irreversible possible outcomes, in addition, the correlations in the emission of light particles and the fluctuations of one-body observables can not be correctly reproduced. In such cases, the average trajectory is no longer a physical information and treatment is needed along with a stochastic methods. The treatment of nuclear Boltzmann-Langevin includes a stochastic part of the collision term. This leads to a splitting of the dynamics trajectories, as all possible results of the remaining collisions are allowed to develop independently, each with its own self-consistent field. In this way we get a whole different set of dynamical paths, although starting from a single initial state identified by the phase

space density of one-body. The Stochasticity is introduced by the addition of a fluctuating collision term into the linearized Boltzmann formula. The resulting equation is not analytically derived from the BBGKY hierarchy, but is based on physical hypotheses.

1.6 Derivation of the Boltzmann-Langevin fluctuating collision integral.

The proposed method considers the first two developments of the equations of the BBGG hierarchy as a starting point for dealing with fluctuations [AYI88]. We rewrite them in a compact form, using Liouville operators:

$$\mathcal{L}_0\rho_1 = \mathcal{L}_1\rho_1 + \sum_2 M_{12}\rho_2$$
$$\mathcal{L}_0\rho_2 = (\mathcal{L}_1 + \mathcal{L}_2 + M_{12})\rho_2 + \sum_3 (M_{13} + M_{23})\rho_3$$

equ. 1.22

We recall that the two-body density contains the effects of all order correlations and fluctuations; it can be decomposed into an average uncorrelated part σ_o and a term containing the fluctuations and the correlations $\delta\sigma$:

$$\rho_2(1\ 2, 1'\ 2', t) = \sigma_0(1\ 2, 1'\ 2', t) + \delta\sigma(1\ 2, 1'\ 2', t)$$

equ. 1.23

The interaction term ($L_1+L_2+M_{12}$), can be divided in a mean field part and in a term including the residual interaction: ($L_1+L_2+M_{12}$)=$L_{MF}+L_v$. The introduction of this term and of the two-body density in the second *equ.1.22*, and by taking the weak coupling approximation, which allows us to neglect the term of the second order in $L_v\delta\sigma$, we can write down the expression for the time evolution of the fluctuation term $\delta\sigma$:

$$\mathcal{L}_0\delta\sigma = \mathcal{L}_{MF}\delta\sigma + L_v\sigma_0$$

equ. 1.24

By the development of this operator we explicitly yields the evolution of the two-body distribution function:

$$\rho_2(t) = \sigma_0(t) - \frac{i}{\hbar}\int_{t_0}^{t} dt' G(t-t')\mathcal{L}_v\sigma_0(t) + G(t-t_0)\delta\sigma(t_0)$$

equ. 1.25

where $G(t) = e^{\frac{iL_{MF}t}{\hbar}}$ is the mean field propagator. We recognize three components, the first component is not correlated, which evolves according to the L_{MF} mean field potential in the absence of fluctuations, the second describes the average variation of ρ_2 due to two-body collisions and gives rise to collision term of the equation transport, the last term propagates the initial correlations and gives the fluctuating collision term we are looking for. The replacement of the expression in *equ.1.25* into the first equation of the BBGKY hierarchy with k=1, leads to the following equation for the one-body density:

$$\frac{\partial}{\partial t}\rho_1(t) + \frac{i}{\hbar}[h, \rho_1] = I(\rho_1) + \delta I(\rho_1)$$

equ. 1.26

It is similar to the semi-classical BNV equation, *equ.1.21*, for distribution function with an important difference given by the term *δI*. In this last expression shows *h(ρ)* representing the mean field Hamiltonian, $I(\rho_1)$, which is the term of a collision and finally appears $\delta I(\rho_1)$ which describes the fluctuations of the collision term:

$$I(\rho_1) = -\frac{1}{\hbar^2}\sum_2 \int_{t_0}^{t} dt' \langle 12|\mathcal{L}_v G(t-t')\mathcal{L}_v \sigma_0|1'2\rangle$$

equ. 1.27

$$\delta I(\rho_1) = -\frac{i}{\hbar}\sum_2 \langle 12|\mathcal{L}_v G(t-t_0)\delta\sigma(t_0)|1'2\rangle$$

equ. 1.28

This semi-classical equation is the so-called Boltzmann-Langevin, BLE, equation:

$$\frac{\partial f}{\partial t} - \{h(f), f\} = I_{coll}(f) + \delta I(\mathbf{r}, \mathbf{p}, t)$$

equ. 1.29

where I_{coll} is the collision integral given by *equ.1.20*. If the two-body distribution function is not initially related, from *equ.1.29* back to the BNV equation. The BLE carries extensive information about dissipation and fluctuation, but is not useful without further approximations, since there is no way to assess the fluctuation term *δI*. The simplest approximation that can be done is to assume that the fluctuating density evolves in a stochastic way, as is the case for the

Brownian motion of a pollen grain hit by water molecules. In this case the fluctuating variable is not the position of the grain, but the same density, which receives random kicks from the force δI.

Exact solutions of the Boltzmann-Langevin equation can be difficult to obtain, because the fluctuating collision term can be approximated by a fluctuating Brownian force, with a null average value, as done in Stochastic Mean Field simulations, SMF. More quantal approaches make use of Gaussian wave packets to represent the A particles.

Concerning the ingredients of code of simulation, the isoscalar term of the nuclear interaction, following the results of the last two decades, is chosen soft, with an incompressibility parameter $K=200\text{-}230\ MeV$. This value is compatible with the measurements of the energy of the isoscalar monopole resonance in nuclei. The collision term depends on a collision rate containing a differential nucleon-nucleon cross section. Note that, although the nucleon-nucleon interaction is splitted between mean field and residual interaction, it is a single interaction. This means that the cross section in the collision term should not be chosen independently of the mean field but evaluated from imaginary part the Brückner G-matrix, the real part of which being the mean field. Practically however both terms are not consistently calculated, and the residual interaction is implemented either with the free $\sigma_{NN}(E,I,\theta)$ or with some recipe for in-medium correction.

The comparisons between experimental data and models presented in the next sections were made in such a way that the properties of

symmetric matter and the residual interaction were fixed, whereas the form of E_{sym} was varied.

1.7 The test particles.

The BNV model is more comprehensive than cascade-type models [BER84], because the nucleons are propagating with the correct self-consistent mean field. In the initialization procedure, assigning the momentum of nucleon according to the Fermi distribution and mass-formula binding energies, we can prepare nuclei that evolve during the collision. This thesis has made use of a simulation program that solves the equation of Landau-Vlasov, BNV model [CHO93, BAR96, BAR05], through the test particle method [WON82] which discretize the distribution function introducing in place of each nucleon, a series of N_{test} pseudo-particles called, precisely, "test particles" that simulate simultaneous N_{test} runs. In this context each event is not clearly identifiable because a mixing between events is introduced unless fluctuating terms are explicitly included (see next sections), so nucleons lose their identity. On the other hand, this procedure is used to ensure some continuity in the distribution of nucleons in nuclear volume, necessary to perform properly the mean field dynamics in the computer simulation. This method introduces a mapping of phase space the more accurate the larger the number of test particles per

nucleon which should theoretically be infinite, even if the computation time grows very quickly with it.

The one-body distribution function in this context takes the form:

$$f\left(\vec{r},\vec{p},t\right)=\sum_{i=1}^{N}\omega_i S\left(\vec{r}-\vec{r}_i\right)S\left(\vec{p}-\vec{p}_i\right)$$

equ. 1.30

where *S* is the test particle form factor depending on the coordinates in the phase space of the ith test particle, where ω_i are the statistic weights and where *N* is the total number of test particles given by $N=N_{test}\cdot A_{tot}$, N_{test} represents the number of test particles per nucleon and A_{tot} is the total number of mass of the two nuclei involved in the reaction. However, replacing the Dirac delta functions (as in the BUU simulations) in the above expression we do not get a continuous distribution function, necessary to derive the Vlasov equation from Liouville's theorem. We can then use a form factor to solve the problem. One other function certainly more continuous than the Dirac delta, is the Gaussian functions that give rise to the BNV approach used in this thesis. The use of this form implies some benefits especially from its smoothness: we can treat the correlations between particles and describe more accurately the effects of surface. In fact a Gaussian form factor has approximately the shape of a surface term analogous to the Skyrme one [CHA97]. So we consider a Gaussian form factor for test particles as:

$$S(\mathbf{r},\mathbf{r}')=e^{-(\mathbf{r}'-\mathbf{r})^2/2\sigma^2}$$

equ. 1.31

and we build an effective density, then taking the Fourier transform we can expand the effective density in plane wave:

$$\varrho_{eff}(\mathbf{r}) \sim \int d^3\mathbf{r}' S(\mathbf{r},\mathbf{r}')\varrho(\mathbf{r}') \sim \sum_{\mathbf{k}} \varrho_{eff}^{\mathbf{k}}\, e^{i\mathbf{k}\cdot\mathbf{r}}$$

equ. 1.32

the coefficient corresponding to wave number k results from the convolution of the form factor and the density:

$$\varrho_{eff}^{\mathbf{k}} = \int d^3\mathbf{r} e^{-i\mathbf{k}\cdot\mathbf{r}} \varrho_{eff}(\mathbf{r}) \sim \varrho_k e^{-k^2\sigma^2/2} \approx \varrho_k \left(1 - \frac{\sigma^2 k^2}{2}\right)$$

equ. 1.33

Consider two nuclei in a closed box of *40fm* from the side, this means that are significant only particles that are less than *20fm* from the center of the box. The idea is to discretize the phase space, the box, into cells of unit volume (*1fm*^{3}), so all physical quantities are identified by their average value in each cell, we also assume that all particles in each of them feel the same nuclear mean field and Coulomb field. Define the pseudo particles with the Gaussian form factor we follow their evolution, which is described by classical equations of motion. At each time step we calculate the evolution which determine the density of the system. We can show that the Vlasov equation is satisfied if the test point particles of the system evolve in time as if each were to follow the classical equations of Hamilton [BER88]:

$$\dot{\vec{p}}_i = -\frac{\partial H}{\partial \vec{r}_i} = -\vec{\nabla}_{\vec{r}}^{(i)} U\left(\vec{r}_i, \vec{p}_i\right) \qquad \dot{\vec{r}}_i = \frac{\partial H}{\partial \vec{p}_i} = \frac{\vec{p}_i}{m} + \vec{\nabla}_{\vec{p}}^{(i)} U\left(\vec{r}_i, \vec{p}_i\right)$$

equ. 1.34

Can not consider the time a continuous variable, the equations are developed in series at intervals of width Δt, truncated to first order:

$$\vec{p}_i\left(t+\Delta t\right)=\vec{p}_i\left(t\right)-\vec{\nabla}_{\vec{r}}^{(i)}U\left(\vec{r}_i\left(t+\frac{\Delta t}{2}\right),\vec{p}_i\left(t\right)\right)\Delta t$$

$$\vec{r}\left(t+\frac{\Delta t}{2}\right)=\vec{r}\left(t-\frac{\Delta t}{2}\right)+\frac{\vec{p}_i\left(t\right)}{m}\Delta t+\vec{\nabla}_{\vec{p}}^{(i)}U\left(\vec{r}_i\left(t-\frac{\Delta t}{2}\right),\vec{p}_i\left(t\right)\right)\Delta t$$

equ. 1.35

which represents a linearization of the equations of Hamilton. From these we calculate the potential, which is used again to determine the next evolution of test particles.

The division into cells, however, breaks the homogeneity of space, so do not verify the Galilean invariance for translations: the generator of translations, the momentum, is not preserved and therefore and therefore the distribution function is chosen to minimize this problem and return the total number of nucleons. The function *S* is not located on a single cell but extends over $(2n)^3$ cells. Consequently, if a single test particle change the density in his cell, change it in other nearby cells. In general, the calculations made on the lattice, as mentioned above involve a discretization of the space show that the incidence of this will be smaller if the function *S* has a smooth trend as in the case of the Gaussian. The minimum number of test particles per nucleon used in the code is *100*: for smaller values fluctuations are not negligible, while for higher values the calculation time becomes too large. This could be a problem especially because we need many events to get a good statistics. However, for studying heavy ion collisions at low energies where the effects of mean field are much

stronger we are forced to use a large number of test particles at the expense of computation time.

1.8 The collision integral in simulation code.

Let's see how we can introduce the nucleon-nucleon collisions given by equ.1.20 in the simulation [BON89]. It is based on the concept of mean free path λ is related to the nucleon-nucleon cross section by the relation $\lambda=(\sigma_{NN}\rho)^{-1}$.

We use a parallel ensemble procedure: the same algorithm is applied to N_{test} sets of A particles. For each particle i_1 in a given set, the collision partner i_2 is chosen as the nearest particle in coordinate space within a distance *d=2fm*. Then the relative velocity v_{12}, density $\rho(r)$ and cross section σ_{NN} are evaluated, in order by the λ will also give the characteristic time between two successive collisions suffered by a particle which moves with velocity v_{12}, $t_{coll}=\lambda/v_{12}$. A minimum value for t_{coll} can be estimated at normal density and for σ_{NN} =40mb is about *3fm/c*; it is a reasonable value for the time step between two calls of the routine that is set in the simulation code to Δt=1fm/c. In elementary scattering theory the probability of a collision between two bodies during a time Δt is:

$$P_{coll} = 1 - e^{-\Delta t / t_{coll}} \sim \frac{\Delta t}{t_{coll}} \quad \text{for} \quad \Delta t << t_{coll}$$

equ. 1.36

As for the cross section in the literature are different parameterizations. The more comprehensive approach is that of Li and Machleidt deriving from the Bonn potential for an expression of the elastic cross section which depends on the density and the energy of the colliding particles. The different parameterizations of the Bonn potential agree well with experimental data on nucleon-nucleon scattering. From the Dirac-Brueckner theory, Li and Machleidt got the trend in the nuclear middle of σ_{nn}, which is decreasing at increasing densities. In the collision integral I_{coll}, an in-medium depending nucleon-nucleon cross section, via the local density, is employed in the simulation code [LI94]:

$$\sigma_{NN} = \sigma_{NN}^{free}(1 + \alpha \frac{\rho}{\rho_0})$$

equ. 1.37

where α=-0,2. The energy dependence of σ_{NN}^{free} is given in Fig.2. The cross section is set equal to zero for nucleon-nucleon collisions below 50MeV of relative energy. In this way we avoid spurious effects, that may dominate in a low energy range when the calculation time becomes too large. In spite of that, for low energy collisions, the simulations cannot be trusted on the time scale of a compound nucleus formation, mainly for the increasing numerical noise.

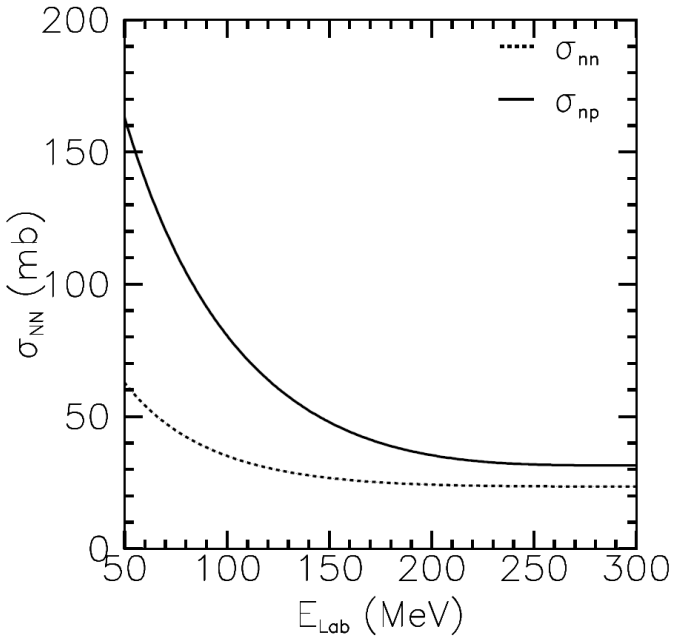

Fig. 2 Cross section of nucleon-nucleon to ρ = 0 as a function of energy of the colliding particles. The dotted line refers to pp or nn collisions, while the solid line refers to np collisions.

It should be emphasized that the cross section between test particles is smaller by a N_{test} factor, compared to nucleon-nucleon. This will also reduce the stochastic effect on the reaction dynamics, due to the random nature of two-body collisions. In code, the probability is compared with a random number, between 1 and 0, and if this number is smaller than in *equ.1.36*, P_{coll}, the collision may take place on condition that the final state is Pauli blocked. Moreover, the true mean free path is larger than what we calculated, because of Pauli blocking. In this sense, it must be simply regarded as a factor used to evaluate numerically the number of collisions in a definite time step, whose rate is given by *equ.1.20*. Apart from the Pauli blocking the other factors f and f_1 are automatically taken into account by choosing at random the partners of collision. We will show that the choice of the nearest

partner is in fact only useful in order to preserve as much as possible the locality of the collision but this prescription does not affect the collision rate. The Pauli blocking factors for the final states are evaluated after a Montecarlo choice of the final momenta, by means of Gaussian distribution in momentum space around p', p_1' built using particles within spheres of radius σ_r and centre around the positions r', r_1'. The parallel ensemble choice should lead to a mean field accurate because the phase space should be filled completely, although we cannot use a infinite number of test particles. Also, in order to reduce the number of spurious collisions, our control on the Pauli blocking is done taking into account all the particles of the system.

1.9 The fluctuations.

In fact the use of test particles in solving the BNV equation introduces fluctuations numeric type: the space discretization involves a fluctuation in the distribution function of its trajectory around a mean value, generating the final situation different. One other cause that creates differences of the final state is the collision integral: it introduces a certain ambiguity in determining the asymptotic trajectories of test particles. The effects of the collision integral becomes unimportant when considering short time paths and a large number of test particles per nucleon, because in this case there is a

strong mediation that hides the dubious collisions, favoring the most likely trajectory average. However if you do not consider the collision integral, then the Vlasov equation is completely deterministic set the initial conditions, because the evolution of the distribution function is uniquely determined by the mean field. The effect of collisions is to expand the package of *f* around the mean value.

A purely physical factor, which causes fluctuations of the final state, comes from the presence of correlations two or more bodies. The equation we are trying to solve numerically does not take into account these correlations, being derived from the TDHF equation, which is a truncation of the hierarchy BBGG in the level of operators to one-body.

In general, we can introduce these correlation effects in the distribution function so that it can be written as: $f = \bar{f} + \delta f$,where $\bar{f}$ indicates the trajectory average (on statistic ensemble) and the δf term includes all correlation effects. These fluctuations have been introduced into the transport equation of Boltzmann-Langevin [RIZ08]. Since it introduces the concept of variance σ_f^2 [RAN90,COL98], which is a measure of the fluctuations of the distribution function in a fixed location and at a fixed time: $\sigma_f^2(\vec{r},\vec{p},t) = \{f_n^2\} - \bar{f}^2$, where f_n indicates the distribution function that describes the n system of the ensemble, the {} is the average of the elements ensemble, and $\bar{f}$ is the average of f_n. It can be shown that its value at the statistical balance is:

$$\sigma_0^2(\vec{r},\vec{p},t_{eq}) = f_0(\vec{r},\vec{p},t_{eq})(1-f_0(\vec{r},\vec{p},t_{eq}))$$

equ. 1.38

and also that his time evolution is of the same form, assuming a local thermal equilibrium. In this way we can locally approximate the variance with its statistical value. Introduce fluctuations in the phase space of interaction, there considerable computational time: our program then uses a projection of the *equ.1.38* only in the coordinate space:

$$\sigma_p^2(\vec{r},t) = \frac{4}{V}\int d^3\vec{p}\,/\,h^3\sigma_f^2(\vec{r},\vec{p},t)$$

equ. 1.39

thus introducing the density fluctuations. The σ_ρ is calculated assuming that you have in each cell the thermal equilibrium, so that we can consider the nucleus as a Fermi gas in equilibrium, and write the function f of the statistic Fermi-Dirac:

$$f(\vec{r},\vec{p},t) = (1+e^{\frac{E(\vec{p})-\mu(\vec{r},t)}{T(\vec{r},t)}})^{-1}$$

equ. 1.40

with $E(\vec{p}) = \frac{p^2}{2m}$, μ and T are respectively the chemical potential and the local temperature. By the development of Sommerfield around $E=\mu$, for small values of T/E_F results a more explicit expression for the variance:

$$\sigma_p = \frac{T}{\frac{2}{3}\frac{E_F}{\rho}V}\left[1-\frac{\pi^2}{12}\left(\frac{T}{E_F}\right)^2+\ldots\right]$$

equ. 1.41

At this point, considering an i^{th} cell with its density, the simulation assigns a new value of density in the range $\rho\pm\delta\rho$ with $\delta\rho$ chosen according to a Gaussian distribution of the type $\exp-(\delta\rho/\sigma_\rho)^2/2$. Are then recalculated the energy and the impulses of the test particles, which are distributed according to the *equ.1.39* with the chemical potential and temperature, they also recalculated. is important to note that the definition of variance given in this context is only local: in a more complete treatment should also cover the variance in momentum space and you should add the correlation (covariance) between the different cells of the phase space .

CHAPTER 2 : THE EOS OF ASYMMETRIC NUCLEAR MATTER.

To describe a macroscopic system we can find equations an express the observable as a function of others. The famous example of such equations, so-called Equation of State, is the law which connects pressure, volume and temperature of an ideal gas at equilibrium: $PV=nRT$. In recent years, including the nuclear interactions we are searching for a equation of state can describe variables such as pressure, density and temperature for the nuclear matter. There is no precise analytical form describing the strong interaction between the nucleons, so the nuclear equation of state are based on semi-empirical potential, seeking to reproduce the characteristics of nuclear matter.

As the forces between molecules are attractive for long-range repulsive range and smaller, the nuclear forces also have this important feature, so we can treat the nuclei in a way a little more classic defining a liquid phase, corresponding to nuclei composed of bound nucleons and a gaseous phase, associated to a state in which the nucleons are free. Of particular interest appear the corresponding conditions of density and isospin asymmetry, as well as interesting is the behavior of nuclear matter in intermediate states between the liquid and gaseous phase, i.e. in a situation where we say that classically there is a phase transition.

2.1 The nuclear matter Equation of State.

As is already done for the water, in nuclear matter we can construct an Equation Of State, EOS, that allows the study of liquid-vapor phase transitions observed at low densities and beam energies of the order of tens of MeV. In principle, the equation of state is derived from a fundamental nucleon-nucleon interaction model. The approach starts from an effective potential felt by all the nucleons of the system dependent on a set of parameters that are set to reproduce the characteristics of nuclear matter around saturation (equilibrium at zero temperature). At low energy we prefer a description of mean field because the direct correlations between nucleons are strongly blocked by the Pauli principle. We describe in this work the main properties of nuclear matter that can be obtained from the equation of state.

The energy density, $\varepsilon = \int_0^{\rho} H(\rho')dp'$, where H is the Hamiltonian of the system, is obtained from the state of emptiness, adding a nucleon at a time until it reaches the density ρ, which corresponds to a system of *A* particles occupying a volume V, it is related to the energy per nucleon by the expression $\varepsilon = \frac{E}{A}\rho$.

Since the functional is identified with the EOS has the dimension of energy per nucleon as a function of density, we can write:

$$\frac{E}{A} = \frac{E}{A}(\rho)$$

equ. 2.1

Similar to the definition of pressure for a classical thermodynamic system, the state can be characterized by the pressure of nuclear matter, given by the change of energy with volume:

$$P(V,T) = \rho^2 \left(\frac{\partial}{\partial \rho} \frac{E}{A}(\rho) \right)_{T=\text{cost}}$$

equ. 2.2

We can relate the pressure at the saturation density by the equilibrium condition:

$$\left. \frac{\partial}{\partial \rho} \frac{E}{A}(\rho) \right|_{\rho=\rho_0} = 0$$

equ. 2.3

Introducing the compression module, which expresses the pressure response to a change of density, we can derive the constant compressibility:

$$\chi = -\frac{1}{V}\frac{\partial V}{\partial P} = \frac{1}{\rho}\left(\frac{\partial}{\partial \rho} P(\rho) \right)^{-1}$$

$$K = \frac{9}{\rho\chi} = 18\frac{P}{\rho} + 9\rho^2 \frac{\partial^2}{\partial \rho^2}\frac{E}{A}(\rho)$$

equ. 2.4

This formula, given the density around saturation where the pressure is zero, expresses the curvature of the equation of state of nuclear matter that is the ability to respond to the efforts of the pressure.

2.2 The Local mean field.

A method for obtaining information on the equation of state is using phenomenological mean field models. The self consistent local mean field we used is that given by the standard Skyrme parameters [BER88]:

$$U(\rho) = A\left(\frac{\rho}{\rho_0}\right) + B\left(\frac{\rho}{\rho_0}\right)^{\sigma}$$

equ. 2.5

The first term (attractive) is responsible for the forces that tend to keep the compact nucleus, while the second (repulsive) to avoid the collapse when the density increases. The constant σ is greater than one to prevent the collapse of the nucleus. The parameterization of A, B and σ is chosen by three conditions: that the density of the minimum energy per nucleon is equal to that of saturation, which in this minimum energy is equal to the binding energy of the nucleus and that the equation of state gives the effective nuclear compressibility.

The Fig.2.1 shows the trends of two potential obtained with the following parameterizations:

SOFT: A = -358,1MeV; B = 304,8MeV; σ = 7/6.

STIFF: A = -123,6MeV; B = 70,4MeV; σ = 2.

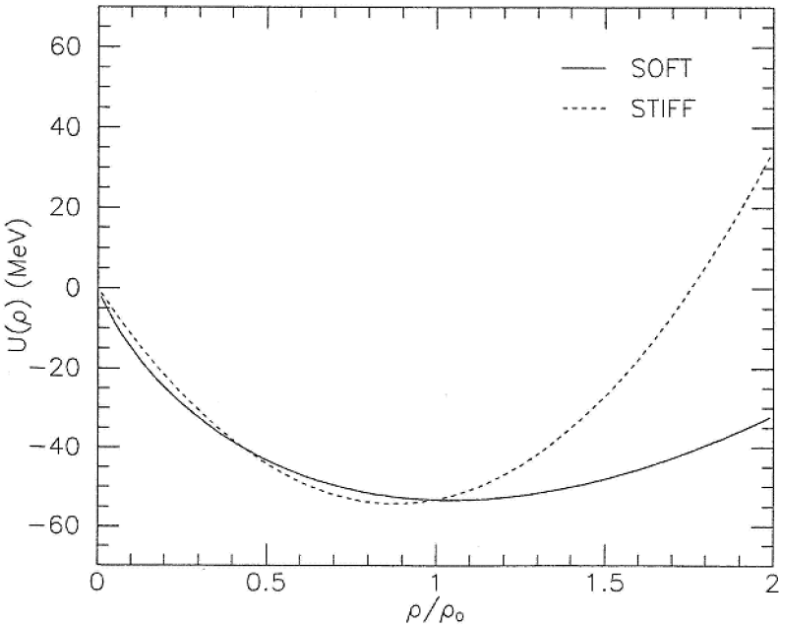

Fig. 2.1 Mean field as a function of local density. The solid line corresponds to the Soft EOS, while the dashed line Stiff EOS.

The parameterizations of the mean field as those just described give a constant value of compressibility of 200MeV and 377MeV respectively for Soft and Stiff EOS.

2.3 The EOS of asymmetric nuclear matter.

Since the 70's the construction of Heavy ion accelerators increasing power has allowed a deeper experimental research, resulting in a theoretical effort to understand the basic mechanisms of the nuclear interaction. It is seen that the equation of state depends on

the symmetry term [TSA89], when we treat the asymmetric nuclear matter far from normal conditions. To a good approximation, at zero temperature, the EOS of asymmetric nuclear matter reads:

$$\frac{E}{A}(\rho, I) = \frac{E}{A}(\rho, 0) + \frac{E_{sym}}{A}(\rho) I^2$$

equ. 2.6

the general expression takes into account the parabolic dependence on the parameter of asymmetry *I*. The first term is the isoscalar term, invariant under proton and neutron exchange, while the second (isovector) one gives the correction brought by neutron-proton asymmetry. For I=1 this terms gives the equation of state of neutron matter. Note that because I is, for most nuclei, smaller than *0.3*, the isovector term is much smaller than the symmetric part, which implies that isospin effects should be rather small and all the more difficult to evidence. The availability of Exotic Isotopes Beams will, in the future, allow to vary I on a larger range. This equation derived on an empirical basis can be viewed as a series expansion in powers of the energy per nucleon of I^2, truncated at lowest order. Small deviations from the parabolic trajectory calculations were found in the Dirac-Brueckener only at high density [BOM91], attributed to many-body correlations that are certainly negligible at energies presented in this thesis. The symmetry energy per nucleon can be defined as the difference between the energies for pure neutron matter ($I=1$) and matter perfectly symmetrical ($I=0$):

$$\frac{E_{sym}}{A}(\rho)=\frac{1}{2}\frac{\partial^2}{\partial I^2}\frac{E}{A}(\rho,I)\Big|_{I=0}$$

equ. 2.7

In symmetric nuclei neutrons and protons occupy the same energy level of the Fermi gas, the increase of the asymmetry change the occupation of the shell. The term of symmetry has a kinetic contribution directly due to the different degree of occupation of phase space for protons and neutrons and a potential contribution due to the properties of the isovector part of the nuclear effective interactions in the middle:

$$\frac{E_{sym}}{A}(\rho)=\frac{E_{sym}^{KIN}}{A}(\rho)+\frac{E_{sym}^{POT}}{A}(\rho)=\frac{\varepsilon_F(\rho)}{3}+\frac{C}{2}F(u)$$

equ. 2.8

where ε_F is the energy corresponding to the Fermi momentum calculated at the density ρ. Evaluated the kinetic part, the discourse is reduced to the function *F(u)* of the reduced density $u\equiv\rho/\rho_o$. If the density coincides with the saturation we obtain *F(1)=1* and *C* is the order of 32MeV to have the a_4 term of the formula of the Bethe-Weizsacker mass. The potential contribution of the symmetry term versus the nuclear density is still unknown, our current knowledge is substantially reduced to the coefficient a_4, i.e. around saturation we do not know the isospin dependence of nuclear effective interactions in-medium and the existing many-body techniques are showing the difficulty of the problem. Essentially all the effective interactions are adjusted to reproduce the a_4 term but take a contrasting behavior above and below the saturation density. Microscopic approaches

based on realistic nucleon-nucleon interaction, Brueckner type or variational or on effective field theories, show a rich variety of predictions. In this work we will refer to equation of state (EOS) "*Asy-stiff*", if we consider a potential contribution of the term of symmetry that grows linearly with nuclear density and with a constant coefficient, C=32MeV, and "*Asy-soft*" EOS, $C(\rho)/\rho_0 = 482 - 1638\rho$, where the symmetry term shows an increase at low density, a saturation and possibly a decline around ρ_0=0.16fm^{-3}. Also we consider the different trend "*Asy-(super)stiff*" EOS, $C(\rho)/\rho_0 = \frac{32}{\rho_0}\frac{2\rho}{\rho+\rho_0}$, which increases in a parabolic way around the normal density, [COL98+, BAR02].

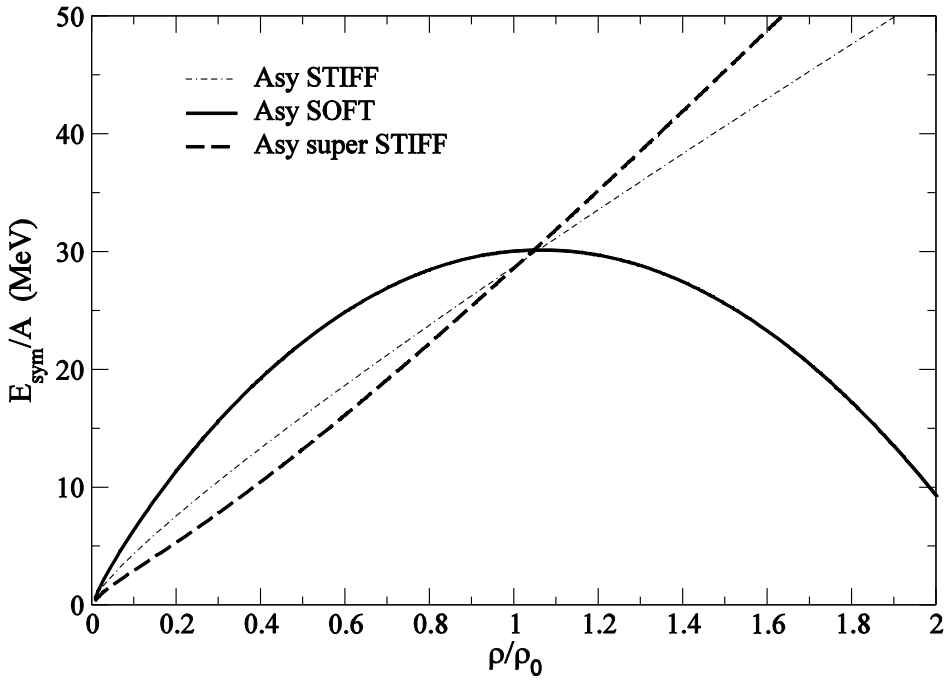

Fig. 2.2 Density dependence of the symmetry energy for the two parameterizations. Solid line: Asysoft. Dashed line: Asystiff. Point and dashed line: super Asystiff.

The asymmetry is clearly related to the properties of a single particle; the dependence on the density of the mean fields of neutrons and protons for various parameterizations is shown in Fig.2.3, for a system with N=1.5 Z:

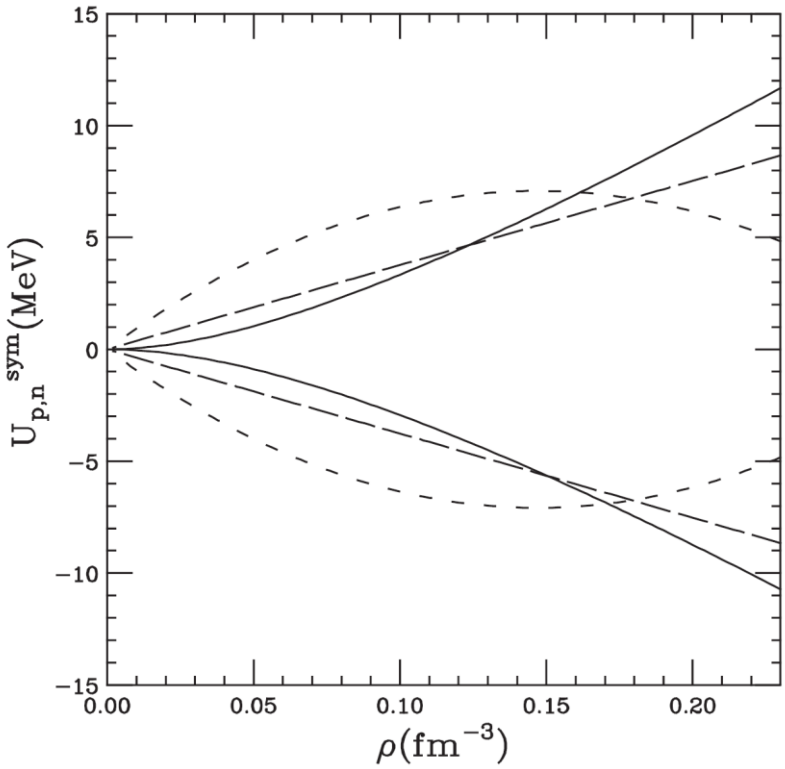

Fig. 2.3 Symmetry contribution to the mean field for I = 0.2 (average asymmetry of 124Sn), negative for the protons and positive for the neutrons. Dotted line with short lines: asy-soft (Skyrme type), long dash: asy-stiff (such as Brueckner), solid line: super asy-stiff (such as RMF).

The mean field is built from Skyrme forces:

$$U_{n,p} = A\frac{\rho}{\rho_0} + B(\frac{\rho}{\rho_0})^{\alpha+1} + C(\rho)\frac{\rho_n - \rho_p}{\rho_0}\tau_q + \\ + \frac{1}{2}\frac{\partial C}{\partial \rho}\frac{(\rho_n - \rho_p)^2}{\rho_0}$$

equ. 2.9

where $q=n$, p and $\tau_n=+1$, $\tau_p=-1$. The coefficients A, B and the exponent α, characterizing the isoscalar part of the mean-field, are fixed in simulation code requiring that the saturation properties of symmetric nuclear matter ($\rho_0=0.145 fm^{-3}$, E/A=−16MeV), with a compressibility modulus around 200MeV, are reproduced. In regions outside the normal density, the field seen by the neutrons and protons in the three cases is quite different, these trends affect the characteristics of nuclear matter at equilibrium. The symmetry potential is repulsive (U>0) for neutrons. At sub-saturation densities it is more repulsive in the asy-soft case, whereas above normal density the repulsive character increases with the asy-stiffness. Conversely the symmetry potential is attractive for protons, which means that it acts in opposition with the Coulomb potential. So Significant consequences of these effects are predicted on a wide spectrum of observables, including isospin content of the particle emission, the equilibration charge, the collective flows, the charge distribution and other. We stress that these trend strongly affect the dynamic in reactions induced on neutron-rich nuclei beam. Observable effects can be found yet at densities non much different than the saturation value, provided the system lies for a sufficient time at density slightly higher or slightly lower than the normal one. The stiffness of the symmetry energy has important consequences at low density on the neutron skin structure, for example, while the knowledge in high density regions is important for the neutron star properties.

Consider the series expansion of the symmetry energy arrested to the second order around the normal density in terms of the curvature parameter K_{sym} and of the slope L:

$$\frac{E_{sym}}{A}(\rho) \equiv a_4 + \frac{L}{3}\left(\frac{\rho-\rho_o}{\rho_o}\right) + \frac{K_{sym}}{18}\left(\frac{\rho-\rho_o}{\rho_o}\right)^2$$

equ. 2.10

$$K_{sym} \equiv 9\rho_o^2\left(\frac{d^2}{d\rho^2}\frac{E_{sym}}{A}(\rho)\right)_{\rho=\rho_o}$$

$$L \equiv 3\rho_o\left(\frac{d}{d\rho}\frac{E_{sym}}{A}(\rho)\right)_{\rho=\rho_o} = 3\frac{P_{sym}}{\rho_o}$$

equ. 2.11

where L define the "asy-stiffness" of the EOS around normal density. The symmetry pressure

$$P_{sym} = \rho^2\left(\frac{d}{d\rho}\frac{E_{sym}}{A}(\rho)\right)_{\rho=\rho_o}$$

equ. 2.12

adding to nuclear pressure in normal condition, move the density from the equilibrium value ρ_0. The shift in density can be calculated by a series expansion around ρ_0:

$$\Delta\rho(I) = -9\rho_0^2\left(\frac{1}{K}\right)_{I=0}\frac{d}{d\rho}\frac{E_{sym}}{A}(\rho)\Big|_{\rho=\rho_0}\cdot I^2$$

equ. 2.13

This value is always negative, as the first derivative of the energy is always positive.

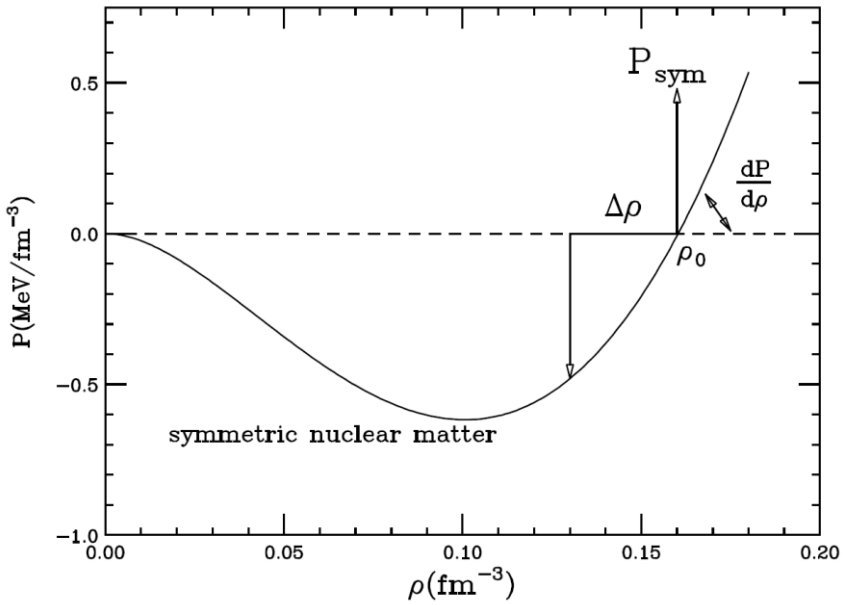

Fig. 2.4 Geometric representation of the density variation inside the asymmetric matter.

Similarly, the compressibility of nuclear matter is modified by the asymmetry. The shift of the constant of compressibility at equilibrium is negative because it depends on the slope and curvature of the E_{sym}/A around the value ρ_0:

$$\Delta K(I) = 9\rho_0 \left(\rho_0 \frac{d^2}{d\rho^2} - 2\frac{d}{d\rho} \right) \frac{E_{sym}}{A}(\rho) \Bigg|_{\rho=\rho_0} \cdot I^2 = \left(K_{sym} - 6L \right) \cdot I^2$$

equ. 2.14

Knowing the trend of the equation of state is of fundamental importance in this context, because the various behaviors of the potential part of the symmetry energy as a function of density around the saturation affect L and K_{sym}:

$$L = \frac{2}{3}\varepsilon_F + \frac{3}{2} C \frac{d}{du} F(u) \Big|_{u=1} \qquad K_{sym} = -\frac{2}{3}\varepsilon_F + \frac{9}{2} C \frac{d^2}{du^2} F(u) \Big|_{u=1}$$

equ. 2.15

Chapter 3: PHENOMENOLOGY OF THE CHARGE EQUILIBRIUM.

Through a semi classical approach, we can estimate the non-statistical dipole radiation of a heavy-ion collisions in the period preceding the charge equilibrium of the nuclear matter. The origin of this dynamic radiation is related to the asymmetry in charge in the entrance channel, i.e. when the *N/Z* ratios of the two colliding nuclei is different. We will see that could generate a collective dynamical mode in the dipole degree of freedom finally leading to charge equilibration.

The dynamics of dissipative heavy-ion reactions is described by a approach based on the *Stochastic extension of microscopic transport equation BNV*, where the mean field and two-body collisions are treated in a self consistent way and where we have used the effective Skyrme interactions corresponding to a Soft EoS in symmetric matter, in agreement with the data of the isoscalar monopole giant resonances. The numerical accuracy of the code has been tested extensively at low energies, just above the threshold of fusion [BAR96, BAR01, CAB98]. The physical observables depend strongly on the reaction mechanism corresponding to the various input parameters (incident energy of the projectile, the angular momentum, charge and total mass of the nuclei) [LEF76].

In this chapter we will analyze the dynamics of charge equilibration in dissipative reactions between ions with different N/Z ratios in the entrance channel (N neutrons number and Z protons number), illustrating the sensitivity of the pre equilibrium dipole emission to the isovector part of the nuclear interaction. We also discuss the peculiar features of this radiation, such as the angular anisotropy that is related to the lifetime of the dipole oscillation.

Although the low density behavior of symmetry energy has been certainly investigated in the Fermi energy regime, through the definition of suitable observables (imbalance ratio, N/Z of pre equilibrium emission, isoscaling, …), a completely independent new information can be obtained from the study of collective oscillations in fusion reactions just above the Coulomb barrier (～10MeV/A).

3.1 The charge equilibration in fusion reactions with the charge asymmetry in the input channel.

For a fusion reaction there are three main stages [BAR00]: during the approach phase, the two nuclei exceed the Coulomb barrier and begin to feel the nuclear attraction, see a first damping of the available kinetic energy although the two partners still keep intact their individual properties. In this phase the region of overlap between the two nuclei, so-called the neck, does not have a significant size to allow a significant exchange of nucleons.

In the second phase it follows a period corresponding to a di-nuclear configuration in which the two nuclei form a typical molecular state. In this phase generates a growing role of other degrees of freedom within the system because the energy of relative motion is replaced by that of collective and thermal motions. The enlargement of the neck creates a communication door between the two nuclei, through which we see a significant shift of mass and energy. So the two nuclei lose their identity and the system acquires the structure of the composite system, with a common mean field. Finally during the third stage, a thermal equilibrated compound nucleus is formed, followed by a statistical particle-radiation emission.

To understand the mechanism of the charge equilibration, we study the effect of isospin asymmetry in the input channel. We consider a collision of fusion between two systems that show a large difference in the ratio N on Z at energies above the Coulomb barrier,

in the energy order of tens of MeV. In the approaching phase we observe a polarization of protons that move away from the center of mass of the system due to Coulomb repulsion.

The exchange of nucleons between the two colliding nuclei will start in the di-nuclear phase, here we observe a fast mechanism of equilibration of the charge that tends to diminish the ratio *N/Z* towards an equilibrium value of the compound nucleus. In this phase, the centers of mass of protons and neutrons do not coincide, contrary to what happens in the fusion of nuclei with the same *N/Z*.

This exchange of charge can be dominated by a stochastic sequence of individual migrations of nucleons or a collective motion of protons and neutrons of iso vectorial character. The second mechanism is predominant in reactions between intermediate mass and heavy ions [BAR01]. Good observable of collective motion are the dipole moment in coordinate space, D(t), and his conjugate in momentum space, DK(t):

$$D(t)=\frac{NZ}{A}\left(X_p(t)-X_n(t)\right) \qquad DK(t)=\frac{A}{2NZ}\left(P_p(t)-P_n(t)\right)$$

$$X_n(t)=\sum_{i=1}^{N}\frac{x_i^n}{n_i^n}(t) \qquad X_p(t)=\sum_{i=1}^{Z}\frac{x_i^p}{n_i^p}(t)$$

$$P_n(t)=\sum_{i=1}^{N}p_i^n(t) \qquad P_p(t)=\sum_{i=1}^{Z}p_i^p(t)$$

Equ.3. 1

where X_n and X_p are respectively the coordinates of the center of mass (c.o.m.) of neutrons (N) and protons (Z) along the dynamics of fusion, i.e. along the symmetry axis of the system, while P_n and P_p are the momentum of neutrons and protons c.o.m.. The two dipole

moments, as operators, are significant because the quantum commutator calculated along the symmetry axis is exactly $i\hbar$:

$$\left[D, DK\right] = \frac{NZ}{A}\frac{A}{2NZ}\left(\frac{\sum_{i=1}^{Z}\left[x_i^p, p_i^p\right]}{Z} + \frac{\sum_{i=1}^{N}\left[x_i^n, p_i^n\right]}{N}\right) =$$

$$= \frac{1}{2}\left(\frac{Zi\hbar}{Z} + \frac{Ni\hbar}{N}\right) = i\hbar$$

Equ.3. 2

The time evolution of the dipole in the space of coordinates and momenta, performs damped harmonic oscillations. This makes us to understand that the charge equilibration is not through a slow and gradual rapprochement between the centers of mass of protons and neutrons, but by making coherent oscillation around the center of mass of the system. The damping will be caused by the neutron-proton collisions that reduce the relative particle flow and by the emission of fast nucleons, mainly neutrons, which tends to reduce the charge asymmetry. This process takes place on short time scales, before the full equilibration time corresponding to the formation of a compound nucleus (C.N.). The C.N. can decay in a statistical way emitting also dipolar photons, the Giant Dipole Resonance (GDR). For this reason we call the dipole radiation emitted in the initial phase of the charge equilibration, the Dynamical Dipole Resonance (DDR).

The origin time of the dipole oscillation coincides with the start of di-nuclear phase. i.e. after a short delay with respect to the contact configuration (t=0) between projectile and target, when the dipole has just the “ geometrical” value:

$$D(t=0)=\frac{NZ}{A}\left(X_p(t=0)-X_n(t=0)\right)=$$
$$=\frac{r_0\left(A_{pr}^{1/3}+A_{tar}^{1/3}\right)}{A}Z_{pr}Z_{tar}\left|\left(\frac{N_{tar}}{Z_{tar}}\right)-\left(\frac{N_{pr}}{Z_{pr}}\right)\right|$$

Equ.3. 3

The delay between the start of the dipole oscillation and the contact time is due to the formation time of a di-nuclear mean field regulating collective oscillation. During this time the spread of non-collective nucleon tends to reduce the initial geometric dipole D(t=0). This effect will be governed by the dynamics of fusion (incident energy and mass asymmetry).

The effect of the symmetry energy is maximum in the initial di-nuclear phase of the reaction, when the overlap region becomes large enough. We see something like an extended spring on the isovector degree of freedom, with the symmetry energy acting like a restoring force. The value of the dipole moment at this time step does not coincide with that the one associated with the contact configuration, because the creation of a di-nuclear mean field takes time. An easy way to tell when the collective dipole oscillation begins, is to follow the correlation between the dipoles in the space of coordinates and of momentum. The trend of the correlation between D(t) and DK(t) depends on the reaction dynamics: in fact, when the neck becomes large enough and when the non-collective exchange of mass between the two configurations ends, it assumes a shape of a "spiral" (out of phase damped oscillation): it triggers the collective dynamics of the charge equilibration in a fast way [BAR01]. This behavior is due to the forces of attraction resulting from the symmetry term of the di-

nuclear mean field which smoothly tends to minimize the charge asymmetry of the system.

When the spiral goes to the center, the dipole mechanism for the charge equilibration stops. The excited residual will still emit dipolar radiation, but this will be statistical, similar to that of the Giant Dipole Resonance (GDR) in nuclei. The main differences between the two radiation are: the dynamic dipole has a clear anisotropy due to the privileged axis of oscillation, rotating on the reaction plan, and the oscillation frequency is at lower values, because the system is very deformed, with a large elongation around the oscillation axis.

The prompt dipole radiation also represents a nice cooling mechanism on the fusion path. It could be a way to pass from a warm to a cold fusion in the synthesis of heavy elements with a noticeable increase of the survival probability [BON04]:

$$\frac{P_{surv,dipole}}{P_{surv}} = \frac{P_\gamma P_{surv}(E^* - E_\gamma)}{P_{surv}(E^*)} + (1 - P_\gamma) > 1, \frac{P_{surv}(E^* - E_\gamma)}{P_{surv}(E^*)} > 1$$

Equ.3. 4

3.2 The Dipole resonances.

The Giant Dipole Resonance (GDR) are statistical collective excitations of iso-vector type of nuclear matter at equilibrium, i.e. out phase oscillations between protons and neutrons. To observe these resonances, we may radiate a mass with a beam of photons, the nuclei in the ground state absorb photons that have a resonance frequency close to that, obtaining the cross section of photo-absorption. These

resonances exist for all nuclei in the periodic table, because they are distinctive collective responses of nuclear matter with properties that do not depend strongly on the nature of nucleus on which they are located. The photo absorption cross section can be represented by a Lorentzian curve peak on the resonance frequency. The parameters of the Lorentzian, centroid and width of resonance, don't change much with the mass number A: the resonance energy varies from 13 to 24 MeV and the width varies from 4 to 8 MeV [SNO86]. To reproduce the experimental data, the phenomenological model of Myers [MYE77] requires that the resonance energy depends on nuclear mass given by the linear combination of $A^{-1/3}$ (Steinwedel-Jensen volume modes) and $A^{-1/6}$ (Goldhaber-Teller surface modes). At the beginning it was thought that the giant resonances were excitations of the ground state of the nucleus, now with the accelerators for heavy ions we can study these resonances in systems excited or "hot" [SNO86, GAA92]. In 1955, Brink showed that the GDR, as excitation of nuclear matter, could be built on any energy state and the energy of the GDR will not much depend on the structure of the energetic state on which it is built. Experimentally the bombardment of light nuclei with protons, generated γ emissions that left nuclei to the excited states, the energy of these photons was the same as that obtained by the emissions of GDR γ at the ground state.

Following this discovery, the γ emission was studied through the use of compound nuclei excited to prove conclusively the validity of the Brink hypothesis. So the radiation GDR, built on the ground state and on excited states, is established on a system where all the freedom degrees are in statistical equilibrium.

However, during the di-nuclear phase of a heavy ions reaction, we can have an issue like GDR γ far from equilibrium conditions. We can estimate a period of oscillation of $2\pi\hbar/E_{GDR} \approx 80$ - 100fm/c and a lifetime of $\hbar/\Gamma_{GDR} \approx 50$fm/c. The diffusion width is the main contribution to total width Γ_{GDR}, and 50fm/c corresponds to the time needed to build the GDR collective mode on a compound nucleus. These times are relatively short and this makes the GDR an ideal probe to study nuclear systems in extreme conditions.

Moreover we have seen that the charge asymmetry in the input channel generates a mechanism of isospin equilibration in the early stages of the reaction that leads to dipolar oscillations of collective nature at high frequency. The equilibrium charge prevails in time range of 200-300fm/c. So in charge asymmetric entrance channel, we expect a extra contribution of photons, so-called of pre-equilibrium, which is in addition to the photons spectrum in the GDR region in statistical equilibrium. The idea is to form a composite di-nuclear system with non charge equilibration and then leads to an extra dipole emission of non statistical origin.

We can apply an bremsstrahlung approach to estimate the contribution of pre equilibrium photons, and specifically to determine the probability of γ emission from a moving charged system [BAR01]:

$$\frac{dP}{dE_\gamma} = \frac{2e^2}{3\pi\hbar c^3 E_\gamma} \mid D''(\omega) \mid^2$$

Equ.3. 5

where $E=\hbar\omega$ is the photon energy and $D''(\omega)$ is the Fourier transform of the dipole acceleration: $D''(\omega) = \int_{t_0}^{t_{max}} D''(t)e^{i\omega t}dt$. For each event t_0 represents the onset-time of the collective dipole response and t_{max} the "damping time". i.e. the time step corresponding to an almost flat D(t) behaviour.

In this work, we discuss isospin effects in dissipative collisions at low energies, between 6 and 16 MeV/A, where unstable ion beams with large asymmetry will be soon available. In this energy range, for dissipative reactions between nuclei with different N/Z ratios, the charge equilibration process in the entrance channel has a collective character resembling a large amplitude Giant Dipole Resonance. The gamma yield resulting from the decay of such pre-equilibrium isovector mode can encode information about the early stage of the reaction [CHO93, BAR96, SIM07, BAR00, BAR01]. This collective response is appearing in the lower density intermediate neck region, while the system is still in a highly deformed di-nuclear configuration. It is therefore of interest to look at the influence of density dependence of symmetry energy below saturation upon the excitation and dynamics of the prompt dipole mode. The corresponding emission rates can be evaluated, through a "bremsstrahlung" mechanism, in a consistent transport approach to the reaction dynamics, which can account for the whole contribution along the dissipative non equilibrium path, in fusion or deep-inelastic processes.

3.3 Dynamical dipole mode in fusion reactions of ^{132}Ce with exotic nuclear beams at 6-16 MeV/A energy range: beam energy dependence and anisotropy.

The experimental prompt γ-ray emission was investigated in the 6-16 MeV/A energy region by means of the ^{36,40}Ar+^{96,92}Zr fusion reactions leading to a compound nucleus in the vicinity of ^{132}Ce. The case at 16AMev has been recently studied at LNS in a Medea exp. where it has been possible to measure even the anisotropy of this prompt dipole radiation. The aim of this experiment was to investigate the prompt γ radiation, emitted in the decay of the dynamical dipole mode and to map its beam energy dependence [MAR08].

The reactions populate, through entrance channels having different charge asymmetries, a compound nucleus in the region of Ce under the same conditions of excitation energy and spin. By studying the γ ray spectra of the initial charge symmetric reaction ^{40}Ar + ^{92}Zr, the statistical giant dipole resonance (GDR) parameters and angular distribution are extracted, and a comparison of the γ -ray emission of the two reactions revealed a extra yield in the GDR energy region for the more initial charge asymmetric system.

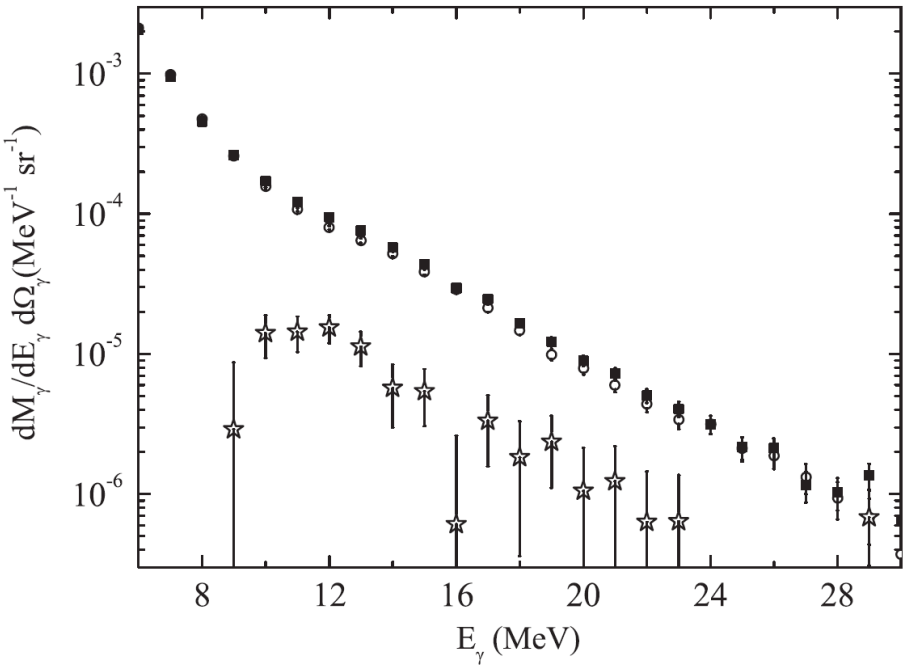

Fig.3. 1 90◦ bremsstrahlung-subtracted γ -ray spectra in coincidence with the fusionlike residues for the ^{40}Ar + ^{92}Zr (open circles) and for the ^{36}Ar + ^{96}Zr (solid squares) reaction. The stars represent the difference between the two spectra.

In Fig.3.1 the γ spectra of the two reactions obtained at $\theta_{lab} = 90◦$ resulting after the subtraction of the *np* bremsstrahlung component are presented. The γ ray multiplicity related with the charge asymmetric reaction is clearly larger than that of the charge symmetric one. This excess cannot be ascribed to differences in the statistical GDR in the compound nucleus formed in the two reactions, being identical all the reaction parameters, except for the entrance channel charge asymmetry. Therefore, it is related to entrance channel charge asymmetry effects and it is attributed to the dynamical dipole mode present at the beginning of the di-nuclear system formation.

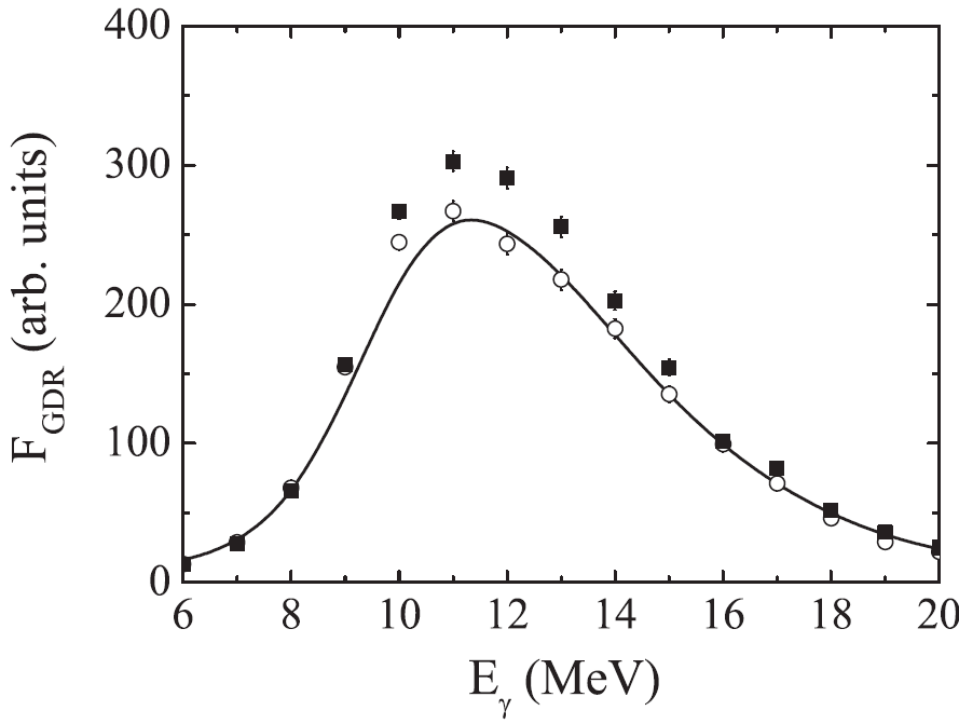

Fig.3. 2 90◦ bremsstrahlung-subtracted γ -ray spectra of the $^{40}Ar + ^{92}Zr$ (open circles) reaction and the $^{36}Ar + ^{96}Zr$ (solid squares) reaction. The solid line represents the theoretical spectrum calculated with the code CASCADE for the charge symmetric reaction $^{40}Ar + ^{92}Zr$.

To better evidence details in the GDR energy region, the data (solid squares and open circles of Fig.3.2) is linearized, dividing it by a theoretical spectrum [MAR08]. The latter was obtained by using the CASCADE code but with a constant dipole strength function instead of a Lorentzian one and folded by the response function of the experimental apparatus. The resulting linearized data is shown in Fig.3.2. By integrating over energy these data, from 8 to 21 MeV, a 12% increase of the γ ray intensity is found in the charge asymmetric system.

Reaction	E_{lab} (A MeV)	E^* (MeV)	$D(t=0)$ (fm)	Δ	Increase (%)	E_{dd} (MeV)	Γ_{dd} (MeV)
$^{32}S + ^{100}Mo$	6.125	117	18.2	0.19	1.6 ± 2.0		
$^{36}S + ^{96}Mo$	5.95	117	1.7	0.16			
$^{32}S + ^{100}Mo$	9.3	174	18.2	0.19	25 ± 2	11.4 ± 0.3	3.0 ± 0.5
$^{36}S + ^{96}Mo$	8.9	174	1.7	0.16			
$^{36}Ar + ^{96}Zr$	16	285 ± 9	20.6	0.16	12 ± 2	12.2 ± 0.6	3.7 ± 1.4
$^{40}Ar + ^{92}Zr$	15.1	284 ± 9	4.0	0.14			

Tab. I Reaction pair, incident energy, compound nucleus excitation energy, initial dipole moment $D(t = 0)$, initial mass asymmetry Δ=(Rt-Rp)/(Rt+Rp) where Rt and Rp are the target and projectile radius, percent increase of the intensity in the 90◦ linearized γ ray spectra for the charge asymmetric system and centroid energy E_{dd} and width Γ_{dd} of the dynamical dipole mode obtained by the Lorentzian fit of the data.

In the Tab.I we report the present status of the Dynamical Dipole data, obtained from fusion reactions. We note the dependence of the extra strength on the interplay between initial dipole moment, the beam energy and initial mass asymmetry: this clearly indicates the relevance of the fusion dynamics. From Tab. I, where the percent increase of the 90◦ linearized spectra for the studied three beam energies is shown, we can see that the prompt dipole radiation intensity presents a maximum at 9 MeV/A decreasing toward lower and higher energies. Although diminished with respect to its value at 9 MeV/A, it is still observed at nuclear excitation energies as high as ~280 MeV, excluding a fast increase of the dynamical dipole mode damping width with excitation energy. In fact the dynamical dipole mode is a pre-equilibrium collective oscillation present before the thermalization of the mechanical energy. The damping is related to fast processes, the pre-equilibrium nucleon emissions (mostly neutrons, that are reducing the charge asymmetry), and (*p*,*n*) direct collisions that will damp the isovector oscillation. From calculations we expect that both mechanisms are smoothly increasing in the

present range of beam energies. We analyze the pre-equilibrium component observed at two beam energies at 9 and 16 MeV/A, to deduce the characteristics of the dynamical dipole mode and their evolution with beam energy.

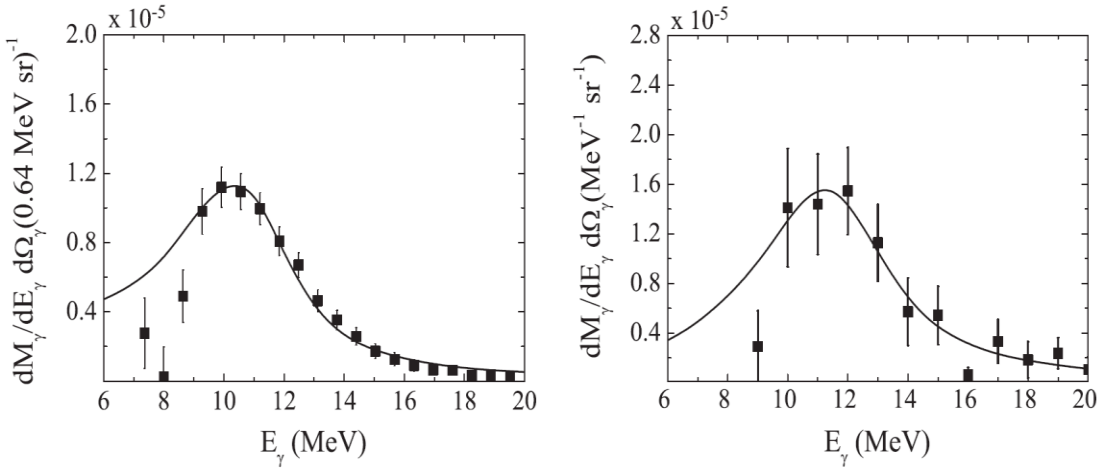

Fig.3. 3 90◦ difference spectra of the ^{32,36}S + ^{100,96}Mo reactions at 9 MeV/nucleon (left-hand side) and of the ^{36,40}Ar + ^{96,92}Zr reactions at 16 MeV/nucleon (right-hand side).

In Fig.3.3 we report the difference spectra obtained for the ^{32,36}S + ^{100,96}Mo reactions at 9 MeV/A (left side) and for the ^{36,40}Ar + ^{96,92}Zr reactions at 16 MeV/A (right side). The centroid energy E_{dd} and the width Γ_{dd} of the dynamical dipole mode were extracted fitting the observed γ ray excess with a Lorentzian curve folded by the corresponding experimental apparatus response function (solid lines in the figure). The values obtained are reported in Tab. I.

It is worth noting that for both beam energies, $E_{dd}\sim$12MeV was found to be lower than the centroid energy of the compound GDR (E_{GDR}=14 MeV), implying a deformation of the composite system at the moment of the prompt dipole radiation. In fact from a simple

geometrical di-nuclear model we would expect a centroid around ~10 MeV. The fact that it was found to be somewhat larger than predicted is consistent with the expectation that some density overlap already exists at the start-up of the dipole oscillation [BAR00]. We notice that centroid energy and width remain constant within errors by increasing the beam energy.

In our simulations the dynamical dipole yield for the more charge symmetric reactions, ^{40}Ar(N/Z=1.22) + ^{92}Zr(N/Z=1.3) and ^{36}S(N/Z=1.25) + ^{96}Mo(N/Z=1.28), was found to be negligible [PIE09]. Therefore, the calculations presented in the following refer to the dynamical dipole yield related to the more charge asymmetric partner of each system, namely ^{36}Ar(N/Z=1) + ^{96}Zr(N/Z=1.4) and ^{32}S(N/Z=1) + ^{100}Mo(N/Z=1.38). In the transport equation a test particle approach with Gaussian phase space wave packets is considered. In the simulation 200 test particles has been employed and we have considered 20 events for each initial reaction set.

In Fig.3.4 we present the total prompt dipole radiation yields evaluated for the ^{36}Ar + ^{96}Zr and ^{32}S + ^{100}Mo reactions, together with the available data (points in the figure) obtained by integrating the γ ray excess over energy and over solid angle and by taking into account the corresponding experimental setup efficiency. In the integration of the data over solid angle an $a_2 = -1$ anisotropy coefficient for the dynamical dipole yield was considered. There are different sets of calculations. In figure we show theoretical calculations obtained with cross sections with an overall reduction, $(1-\alpha\rho/\rho_0)$ with α=0.2, corresponding to a constant nuclear density,

ρ=0.14fm^{-3}, that is slightly lower than the saturation value ρ=0.16fm^{-3} for infinite nuclear matter (upper curves). In the same panel we show the results obtained using free *nn* cross sections (lower curves). In the collision integral an in-medium N-N cross section going to zero for nucleon-nucleon collision below 50MeV of relative energy, is considered. This is to eliminate spurious NN collisions, that should be Pauli blocked at these low energies.

Reduced *nn* cross sections are leading to larger dipole radiation rates because we have a less fast nucleon emission, in particular for neutrons that decrease the dipole strength, and we have a reduced attenuation of the dipole *pn* oscillation due to a smaller number of *pn* direct collisions. In Fig.3.4 we display the calculations done with in-medium reduced *nn* cross sections corresponding to nuclear densities that change "locally" during the reaction dynamics at each time step of the collisional procedure. In Fig.3.4 we can see that the theoretical results for the reactions ^{32}S + ^{100}Mo and ^{36}Ar + ^{96}Zr are rather close, independent of the used *nn* cross section. By the bremsstrahlung formula, the total direct photon emission probability is systematically higher for the ^{36}Ar + ^{96}Zr reaction. However, differences are small, within 20%, and the direct comparison at different beam energies made in the present work is fully justified.

The experimental results for 6 and 16 MeV/A are in good agreement with the theoretical ones if we use free *nn* cross sections but also if we use a "local" nuclear density and in-medium reduced *nn* cross sections. The experimental result obtained at 9 MeV/A can be better reproduced by using reduced *nn* cross sections corresponding at constant nuclear density ρ=0.14fm^{-3}. In fact the calculation with

“local nuclear density” modified cross sections gives a multiplicity approximately 40% lower than the experimental value at 9 MeV/A. In any case the data show a maximum at 9 MeV/A while the calculations have a smoother behaviour with energy. Further investigation, from both a theoretical and an experimental point of view, around the maximum value of the dynamical dipole yield could give a more detailed mapping of its dependence on incident energy. At higher beam energies the prompt dipole mode is expected to be over damped because of a larger number of *np* collisions and fast neutron emissions. This point must be investigated in more details. The experimental excitation function of the dipole mode, as a function of energy, depends on the reaction mechanism that we are observing.

The experimental selection is based only on fusion-evaporation events while the theoretical curves refer also to the more peripheral fusion-fission and dissipative break-up events, where the DDR strength is smaller. Therefore a theory selection on fusion-evaporation events, possible via a coupling to sequential evaporation code which will give the C.N. fission probability, would also increase the γ-multiplicity per event to compare with the fusion-evaporation data.

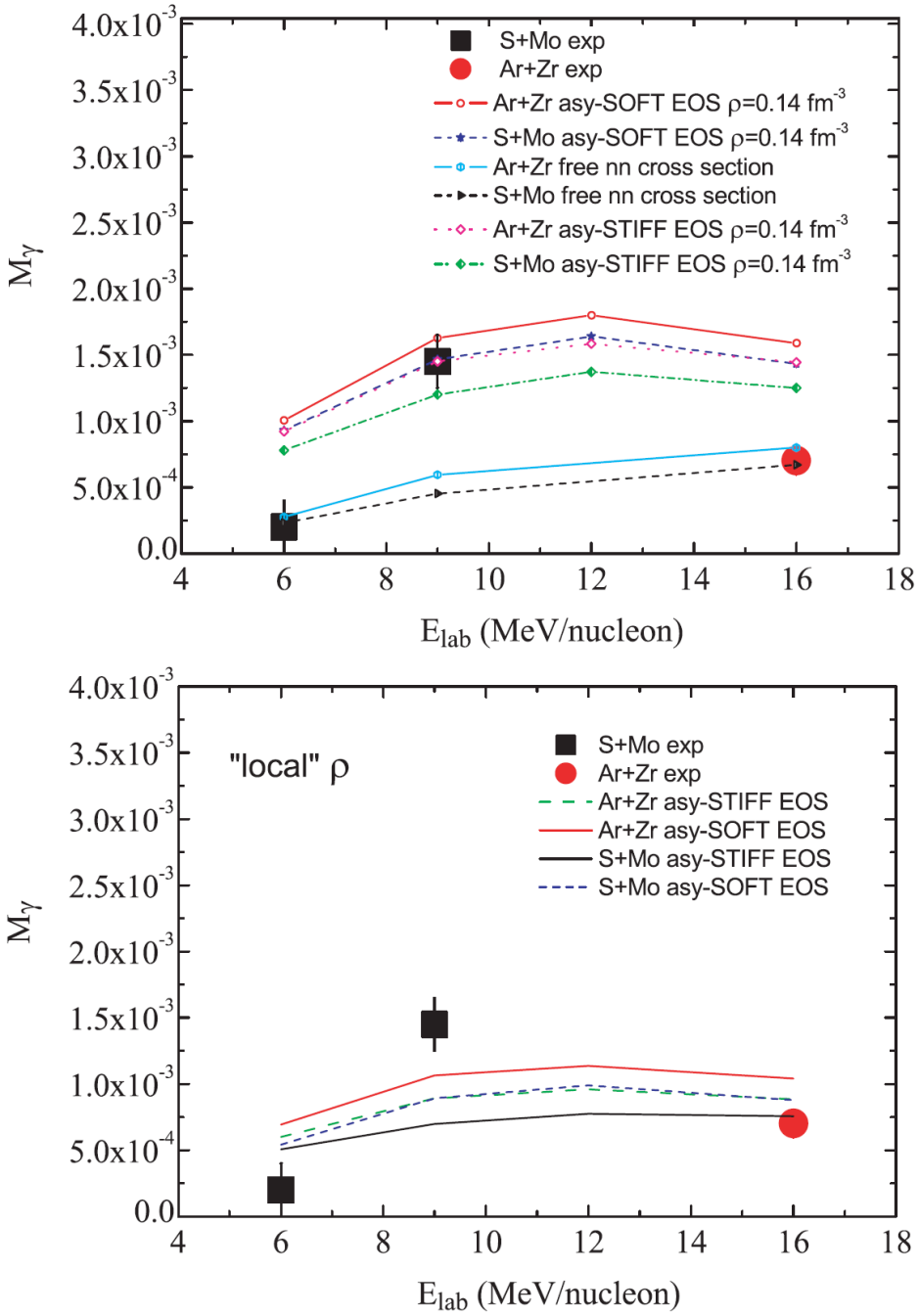

Fig.3. 4 (Color) (Up) Experimental multiplicity of the observed γ ray excess integrated over energy and over solid angle corrected by the experimental setup efficiency and theoretical calculations obtained for free *nn* cross sections (lower curves) and for ρ = 0.14 fm^{-3} and in-medium reduced *nn* cross sections (upper curves). (Down) Experimental multiplicity as in the left-hand side of the figure and theoretical calculations for a local density as described in the text and in-medium reduced *nn* cross sections.

From Fig.3.4 we also see effects due to the density dependence of the symmetry term of the used interaction in the region below saturation. Below ρ_0 the symmetry energy is larger for the Asysoft choice (see Fig.2.2), and in correspondence we have some larger yields for the extra dipole radiation. However, we notice that we are not able to draw a conclusion about the density dependence of the symmetry energy by using stable beams. The reason is that the experimental errors, together with the small difference in the dynamical dipole yield according to the different theoretical prescriptions, do not allow one to discriminate among them. Radioactive beams, like ^{132}Sn, are needed to maximize the difference of the dynamical dipole yield between the different prescriptions of the symmetry energy dependence on density, in order to allow an experimental discrimination.

The theoretical dynamical dipole centroid energies and widths were found to be $E_{dd,th}$~9MeV and $\Gamma_{dd,th}$~2MeV for all incident energies, thus in reasonable agreement with the corresponding experimental values writing in Tab. I.

The transport simulations allow also a consistent calculation of the radiation anisotropies, i.e. of the coupling between the rotation of the di-nuclear system and the γ emission [PIE09]. In this experiment the prompt dipole radiation has been investigated with a 4π gamma detector. The time scale of the radiative emission plays an essential role. Moreover, the comparison between the centre of mass angular distribution of the difference between the γ rays of the ^{36,40}Ar + ^{96,92}Zr reactions in the energy interval 9MeV<E_γ <21MeV and the theoretical angular distribution indicate that the largest contribution to the

prompt γ yield is given by the first collective oscillations in a time interval of 200 fm/*c*. A strong dipole-like photon angular distribution $M_\gamma(\vartheta_{\gamma,c.m.}) = M_0[1+a_2 P_2(\cos\vartheta_{\gamma,c.m.})]$, θ being the angle between the emitted photon and the beam axis, has been observed. It is anisotropic with a maximum around 90° and it is consistent with emission from a dipole oscillating along the beam axis. In fact in Fig.3.5 we have a photon angular distribution with the parameter a_2 =-1, $M_\gamma(\Theta_{\gamma,c.m.}) \sim \sin^2\Theta_{\gamma,c.m.}$

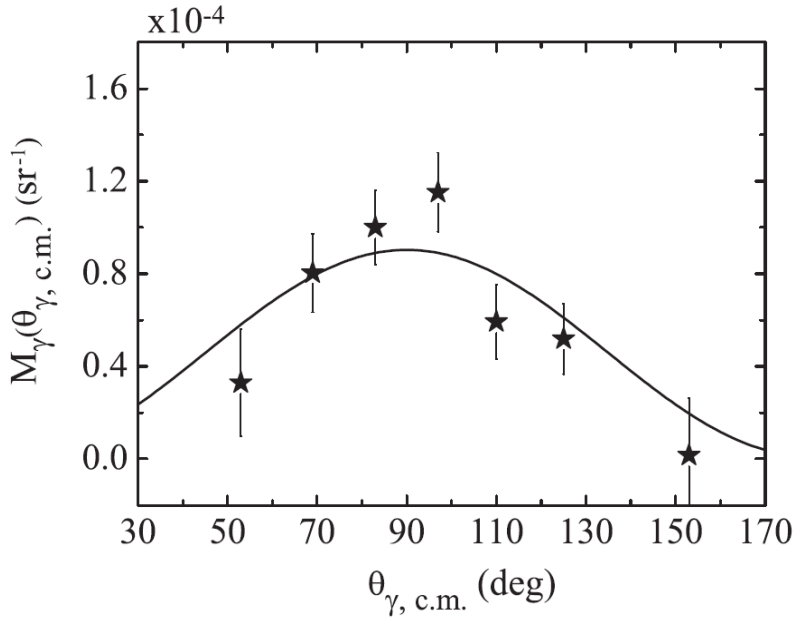

Fig.3. 5 Center-of mass angular distribution of the difference between the γ rays of the ^{36,40}Ar + ^{96,92}Zr reactions in the energy interval 9MeV<E_γ <21MeV corrected by the experimental setup efficiency.

The deviation from a pure dipole form could be interpreted as due to the rotation of the di-nucleus symmetry axis vs. the beam axis during the prompt dipole emission. So from accurate angular distribution measurements we can then expect to get a direct

information on the Dynamical Dipole Life Time. In this case the rotation of the symmetry axis is rather small, and this is in agreement with an almost pure dipole angular distribution with respect to the beam axis in near-central collisions.

However the symmetry energy could influence the damping mechanisms and consequently the di-nuclear rotation dynamics. In fact we can expect to see a sensitivity to the slope of the symmetry term below saturation in the presence of large rotation in events with high spin selection and with high dipole photons intensity.

3.4 Probing the symmetry energy with Exotic Proton-Rich Beams: the Prompt Dipole Radiation in Fusion Reactions with ^{34}Ar Beams

The use of unstable projectiles in fusion reactions would largely increase the effect, due to the possibility of larger entrance channel asymmetries. In particular the prompt of Dipole emission will be enhanced also with the use of exotic proton-rich projectiles [BAR09]. We have the chance to form the same compound nucleus with a more charge symmetric entrance channel and so the extra γ yield of the asymmetric case will be better revealed. All that allows to perform detailed studies on the behaviour of the symmetry term at low density.

In Fig.3.6 we report a comparison of the dipole mode in entrance channel for the p-rich ^{34}Ar(N/Z=0.89) beam vs. the more symmetric stable ^{36}Ar(N/Z=1) beam in fusion reactions with the same n-rich target, ^{96}Zr(N/Z=1.4). The bottom panels show the spiral correlation between Dipole moment in coordinate space D(t) and momentum dipole oscillation DK(t).

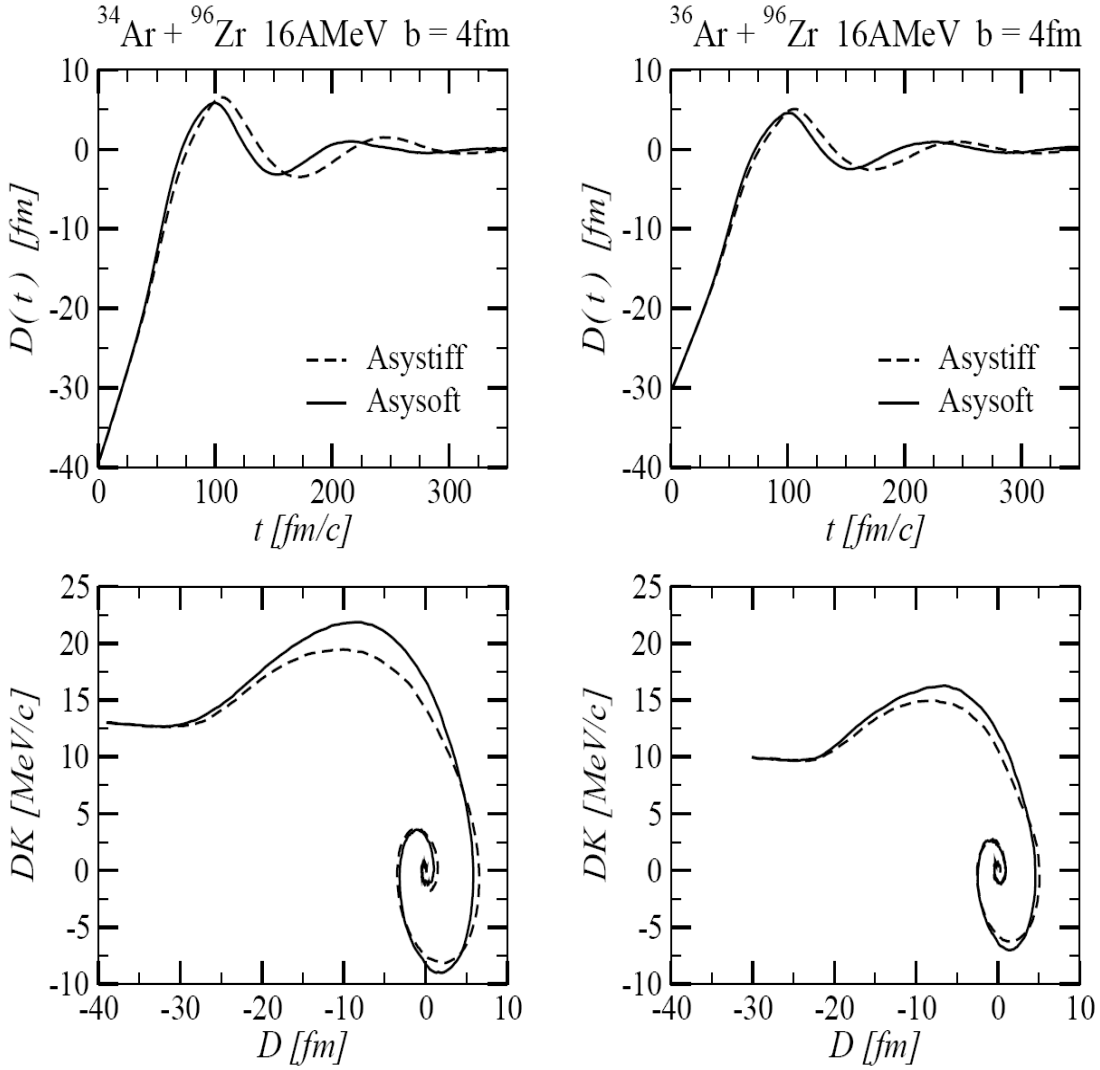

Fig.3. 6 Entrance channel Dipole Dynamics at 16AMeV, b = 4fm centrality. Left panels: Proton- rich unstable 34Ar beam. Right panels: Stable 36Ar beam. Top figures: Time evolution of dipole moment D(t) in real space. Bottom figures: Dipole phase-space correlation. Solid lines correspond to Asysoft EoS, the dashed to Asystiff EoS.

We see that in the p-rich beam case we get larger dipole oscillations because we have a larger spiral, more sensitive to the different choice of the isovector interaction.

In the top panels of Fig.3.7 we show a comparison of the fast nucleon emission rates. In the p-rich beam case we have less pre-equilibrium neutron emissions and this will enhance the prompt collective dipole mechanism for charge equilibration.

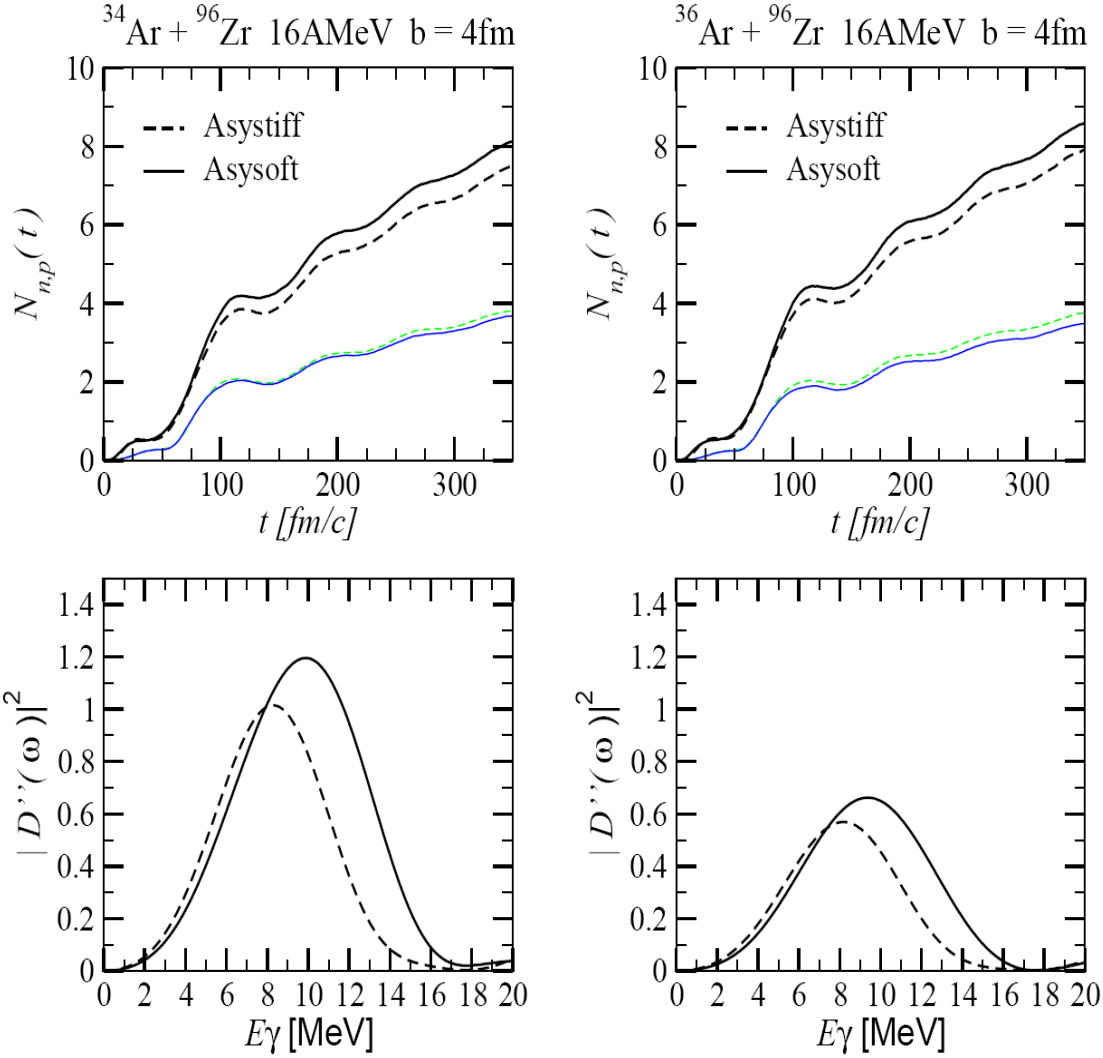

Fig.3. 7 Top panels: fast nucleon emission rates, upper lines for neutrons and lower lines for protons. Bottom panels: Strength distribution of the prompt dipole radiation. Solid lines correspond to Asysoft EoS, the dashed to Asystiff EoS.

In the bottom panels of Fig.3.7 we present the dynamical dipole γ emission strength for the same reactions. In p rich system, there is a slight decrease of evaporated neutrons which indicates the formation of a more stable compound system that damps the dipole more slowly.

We note stimulating expectations in the p-rich projectile case, in particular for the dipole radiation: larger yields and better sensitivity to the effective isovector forces. We see roughly a 70% increase of the yields and a more pronounced separation between the centroids varying the symmetry term. Moreover we remark that for the ^{34}Ar beam we can also choose the very charge symmetric ^{40}Ar+^{90}Zr as reference reaction in order to better reveal the entrance channel isospin effects.

At higher beam energies we expect a different charge equilibration dynamics, of exponential type like an over damped mode, very sensitive to the symmetry energy as well as to the interaction time and so to the total kinetic loss in the binary events.

3.5 The properties of the prompt dipole radiation in fusion reactions with ^{132}Sn exotic beams: the sensitivity to the density dependence of the symmetry energy below/around saturation.

In the following we shall study the features of the pre equilibrium dipole considering the reaction ^{132}Sn(N/Z=1.64) +^{58}Ni(N/Z=1.07) ("132" system) at 10MeV/A, as referred to the same reaction induced by a ^{124}Sn(N/Z=1.48) beam ("124" system) [BAR08]. We aspect a Monster Dynamical Dipole because we note that the initial dipole at touching configuration attains a value around 45fm for the exotic ^{132}Sn beam, to be compared to the smaller value 33fm for the stable "124" system, which can be considered as a reference partner in an experimental comparison.

In the numerical simulations a test particle approach with 200 Gaussian test particles per nucleon has been employed. In this way we get a good description of the phase space occupation, essential for the low energy reaction dynamics. In the collision integral in medium nucleon-nucleon cross sections are considered, where it is fixed for ρ=0.14fm^{-3} going to zero for nucleon-nucleon collisions below 50MeV of relative energy.

We perform calculations for three impact parameters: b= 0, 2, 4fm, to cover the region where fusion is mostly observed. In order to reduce the numerical noise we run twenty events for each set of macroscopic initial conditions and the displayed quantities are the averages over this ensemble.

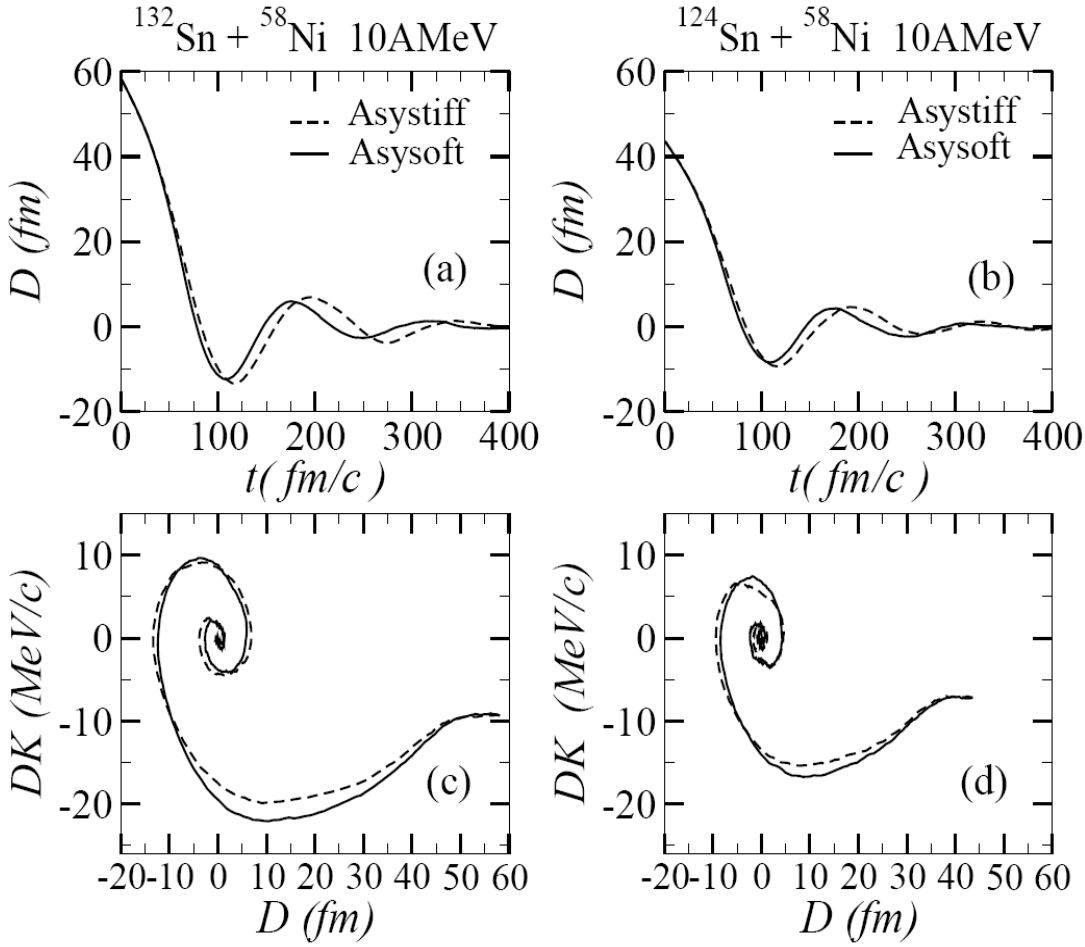

Fig.3. 8 Dipole Dynamics at 10AMeV, b = 4fm centrality. Exotic "132" system: (a) Time evolution of dipole moment D(t) in real space; (c) Dipole phase-space correlation. Panels (b) and (d): same as before for the stable "124" system. Solid lines correspond to Asysoft EoS, the dashed to Asystiff EoS.

In Fig.3.8 we report some global information concerning the dipole mode in entrance channel. The time evolution of the dipole moment D(t) for the "132" system at 4fm centrality is represented in Fig.3.8(a). At b = 0, 2 fm we observe very similar features for the spiral behaviour and for the power spectrum of the dipole acceleration as the ones shown in Fig.3.8 and in Fig.3.9 for b=4fm. We clearly notice the large amplitude of the first oscillation and the delayed dynamics for the Asystiff EOS related to the weaker isovector restoring force. We can also evaluate the quantity DK(t) the

canonically conjugate momentum of the X(t) coordinate. The phase space correlation (spiralling) between D(t) and DK(t) is reported in Fig.3.8(c). It nicely points out a collective behaviour which initiates very early, with a dipole moment close to the touching configuration value reported above. This can be explained by the fast formation of a well developed neck mean field which sustains the collective dipole oscillation in spite of the di-nuclear configuration with a central zone still at densities below the saturation value. The role of a large charge asymmetry between the two colliding nuclei can be seen from Fig.3.8(b,d) panels, where we show the analogous dipole phase space trajectories for the stable ^{124}Sn +^{58} Ni system at the same value of impact parameter and energy. A clear reduction of the collective behaviour is evidenced.

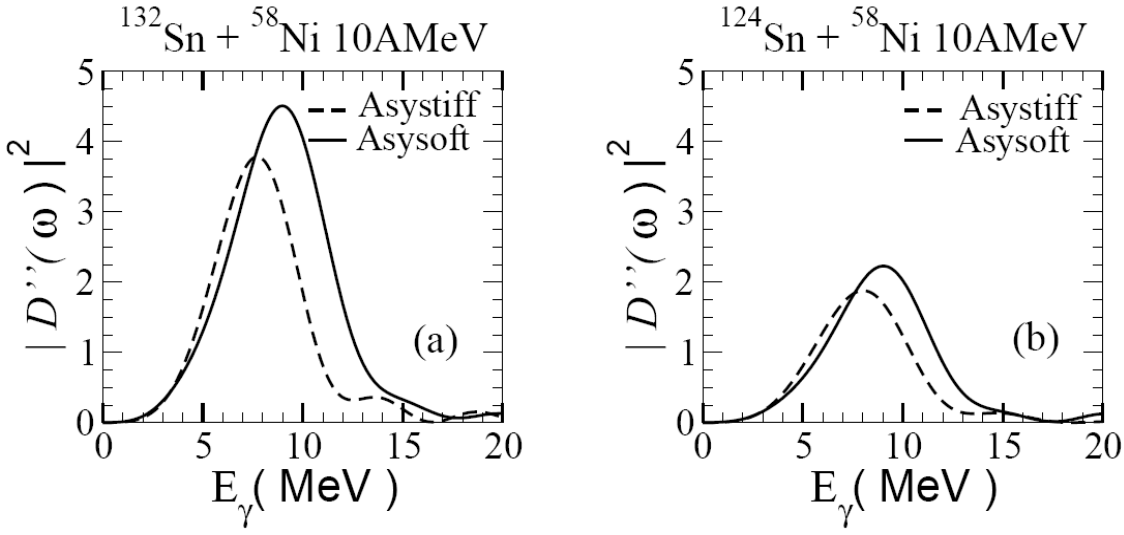

Fig.3. 9 (a) panel: Exotic "132" system. Power spectra of the dipole acceleration at b = 4fm (in c^2 units). (b) panel: Corresponding results for the stable "124" system. Solid lines correspond to Asysoft EoS, the dashed to Asystiff EoS.

In Fig.3.9(a) we report the power spectrum, $| D''(\omega) |^2$ in semi central "132" reactions, for the different Iso-EoS choices. The gamma multiplicity is simply related to it, see Equ.3.5. We clearly observe a lower value of the centroid, as well as a reduced total yield, in the Asystiff case, due to the weaker restoring force for the dynamical dipole in the dilute "neck" region, where the symmetry energy is smaller. Larger width of the "resonance" are obtained in the Asysoft case, due to the larger fast neutron evaporation (see Fig.3.10), that damps the collective oscillation.

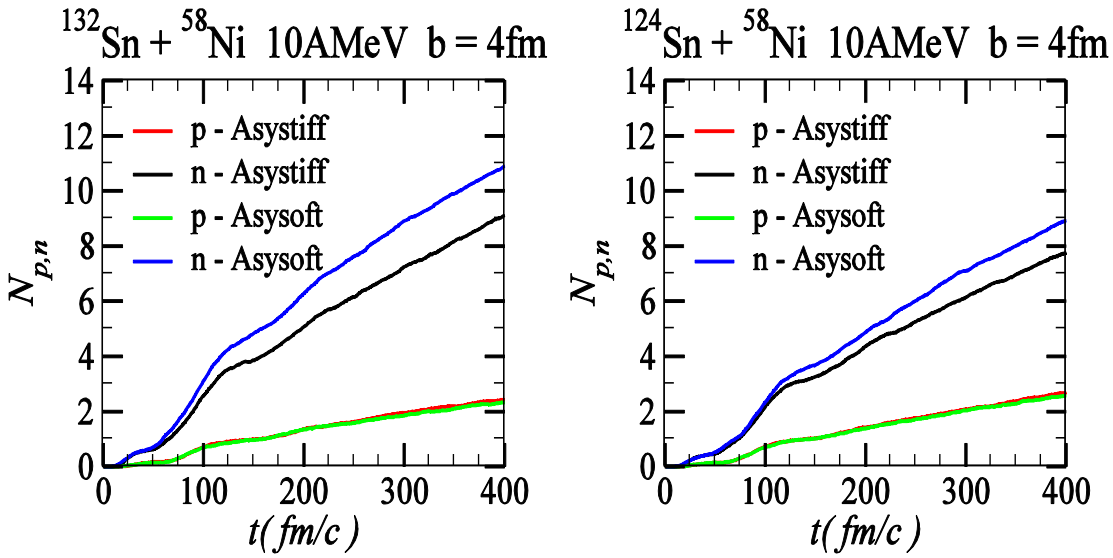

Fig.3. 10 Left curves: ^{132}Sn +^{58}Ni system (E = 10AMeV , b = 4fm). Right curves: same reactions but induced by ^{124}Sn: neutron (upper) and proton (lower) emissions.

The corresponding results for the stable "124" system are drawn in the Fig.3.9(b) panel. As expected from the larger initial charge asymmetry, the Prompt Dipole Emission is increased for the exotic n-rich beam.

From Equ.3.5 we can get the total, γ energy and impact parameter integrated, yield for the two systems and the two Iso-EoS. We find

3.0 10^{-3} for 124Sn and 5.7 10^{-3} for 132Sn in the Asysoft case and 2.5 10^{-3} for 124Sn and 4.4 10^{-3} for 132Sn in the Asystiff case. In conclusion we observe that: the yield is clearly sensitive to the Iso-Eos choice: a lower value is obtained in the Asystiff case.

3.6 The damped oscillator model.

A detailed analysis of the sensitivity of the results to the symmetry energy choice can be performed fitting the dipole oscillations by a simple damped oscillator model [BAR08]. From a mathematical point of view, considering only oscillations of small amplitude, i.e. attraction forces that obey the Hooke's law. The damping forces can generally be described by Stokes law. The one-dimensional equation of motion is:

$$\frac{d^2x}{dt^2}+\frac{1}{\tau}\frac{dx}{dt}+\omega_n^2 x=0$$

Equ.3. 6

where τ is the lifetime of the oscillator. The solution of the equation should reduce to the simple harmonic oscillator assuming that 1/τ=0 and that the velocity should decrease exponentially for the Stokes' law, we obtain the following expression:

$$x(t)=Ae^{-\frac{t}{2\tau}}sen(\omega_s t+\phi)$$

Equ.3. 7

where *A* is the amplitude of non damped oscillation, and where ω_s is the damped angular frequency related to that in the non-damping conditions: $\omega_s=\sqrt{\omega_n^2+1/4\mu^2}$.

Similarly, the behavior of the dipole moment in the pre equilibrium phase can be defined through the evolution of a oscillation as:

$$D(t)=D(t_0)e^{i(\omega_0+i/\tau)t}$$

Equ.3. 8

where $D(t_0)$ is the value at the onset of the collective dinuclear response, ω_0 the frequency, that depends on the symmetry energy choice, and τ the damping rate, related to two-body N-N collisions and neutron emission. The power spectrum of the dipole acceleration is given by

$$| D''(\omega) |^2 = \frac{(\omega_0^2 + 1/\tau^2)^2 D(t_0)^2}{(\omega - \omega_0)^2 + 1/\tau^2}$$

Equ.3. 9

which from Equ.3.5 leads to a total yield proportional to

$$\omega_0 \tau (\omega_0^2 + 1/\tau^2) D(t_0)^2 \simeq \omega_0^3 \tau D(t_0)^2$$

Equ.3. 10

since $\omega_0\tau > 1$. We clearly see the effect of the Iso-EoS on the total yield, through the quantity $\omega_0^3\tau$, that is slightly dependent on the system. Hence, from the above relation, the difference of the yields associated with two different systems, that is the quantity usually exploited in the experimental analysis [PIE05], depends on the Iso-EoS and the sensitivity is amplified when using exotic, more asymmetric beams, due to the factor $D(t_0)^2$, allowing for a clear experimental observation. It is worthwhile to mention that, according to our fit, we find that that the parameter $D(t_0)$ may be less than the touching point geometrical dipole amplitude D(t=0), equ.3.3, especially in the Asystiff case and for the exotic neutron-rich system. A delay in the onset of the collective response is expected and so a more reduced $D(t_0)$ with respect to the initial "geometrical" value.

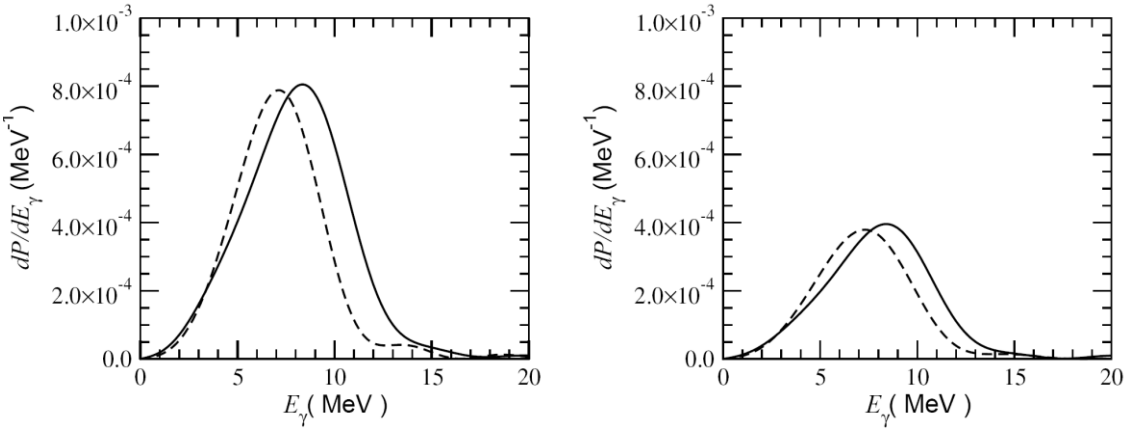

Fig.3. 11 Left Panels, Exotic "132" system: Gamma emission probability. Right Panels: Corresponding results for the stable "124" system. Solid lines correspond to Asysoft EoS, the dashed to Asystiff EoS.

In fact, we find that the ratio of the total, impact parameter integrated yields obtained with the two Iso-EoS (Asysoft relative to Asystiff) is larger in the ^{132}Sn case. We obtain 1.2 for the ^{124}Sn reaction and 1.3 in the ^{132}Sn case. This result points to other interesting Iso-EoS studies that can be performed from an accurate measurement of spectrum and yield of the prompt dipole radiation.

Since we could expect larger intensities we have also studied fusion reactions induced by the unstable ^{132}Te beams. We have compared the ^{132}Te(N/Z=1.54) +^{58}Ni system, D(t=0)=39fm, and the ^{132}Sn +^{58}Ni, D(t=0)=45fm, for central collisions at 5MeV/A, related to the case already studied in ^{132}Sn +^{58}Ni at 10MeV/A to prove the energy dependence and the charge asymmetry dependence on the dynamical dipole prompt. The calculation is done only with Asysoft EoS where we should have a larger contribution. We show the spirals and strength distribution vs. E_γ in Fig.3.12.

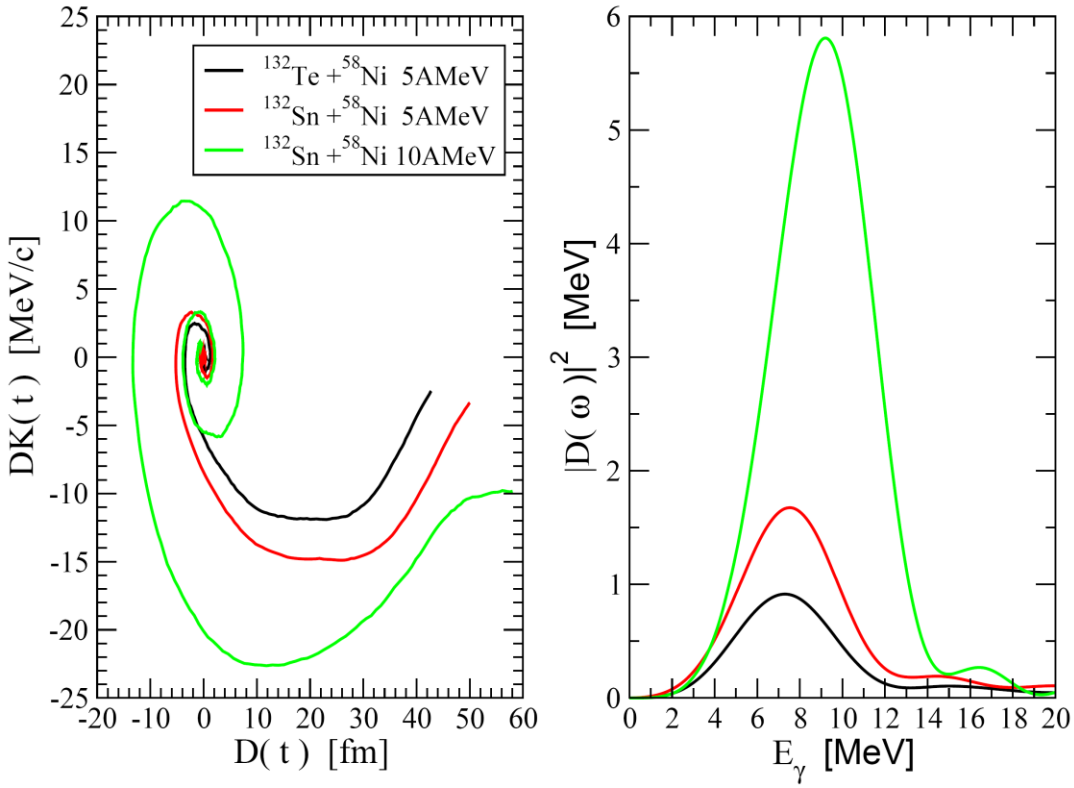

Fig.3. 12 Dipole phase-space correlation at b = 2fm centrality for exotic "132" system at incident energy of 10MeV/A (green line) and 5MeV/A (red line). The "132" system at 5MeV/A is compared to ^{132}Te + ^{58}Ni. Right Panel: Power spectra of the dipole acceleration. The calculation is done only with Asysoft EoS.

There is the effect due to the dipole mode but is generally small and even smaller in the case ^{132}Te. In fact a more reduced dynamics is observed in cases at 5MeV/A, especially for the ^{132}Te system due to its $D(t_0)^2$ (see Equ.3.10). This is mainly due to the delay between the start of the spiral behavior and the contact configuration time, it is caused by the formation of the di-nuclear mean field that also depends on the Iso-EoS. The fusion dynamics and the onset of the collective dipole oscillation are influenced by several isospin-dependent mechanisms, such as neutron evaporation and neutron diffusion to the neck region. In the early stage of the collision, when the overlap region becomes large enough to allow the migration of nucleons

between the colliding nuclei, the chaotic spread of nucleon tends to reduce the initial geometric dipole $D(t_0)$. This effect increases with decreasing the incident beam energy.

We also evaluated the photons yield: for the system ^{132}Te + ^{58}Ni we have 1.275 10^{-3} multiplicity and for ^{132}Sn +^{58}Ni we have 2.3 10^{-3}, while for the ^{132}Sn +^{58}Ni at 10MeV/A we come to 6.2 10^{-3}. It seems interesting that the yields ratio at 5MeV/A is about 1.80 while the ratio of $D(t=0)^2$ for each system would give 1.37. This seems to confirm that the two protons in excess of ^{132}Te (increased coulomb repulsion) significantly altered the fusion dynamics reducing the phase of collective oscillation.

Further comparisons were made with lighter SPES systems than the "132 system" in the output channel as ^{142}Cs(N/Z=1.58) + ^{40}Ca(N/Z=1) at E=10MeV/A and ^{90}Kr(N/Z=1.5) + ^{68}Zn(N/Z=1.27) at E=12MeV/A for fusion collisions. Each system has been reported with more stable systems as a possible term of experimental comparison test, respectively with ^{133}Cs(N/Z=1.42) + ^{48}Ca(N/Z=1.4) at E=10MeV/A and ^{70}Ge(N/Z=1.19) + ^{92}Mo(N/Z=1.19) at E=12MeV/A.

The systems that lead to the ^{182,181}Re in the output channel, since the calculated initial dipole moments strongly differ in the two cases (D(t=0)=36fm and 1.16fm, respectively), we expect a marked difference in the prompt collective resonance. One should verify the absence of the DDR in the ^{133}Cs + ^{48}Ca reaction and its hard presence in ^{142}Cs + ^{40}Ca. Instead in the system that leads to ^{158}Dy compound

nucleus there are also indications on some DDR dependence on the mass asymmetry between projectile and target.

In Fig.3.13 we present the time evolution of dipole moment in coordinate space evaluated for the ^{142}Cs + ^{40}Ca and ^{90}Kr + ^{68}Zn reactions at 2fm centrality, together with the simulations (red line in the figure) obtained with more symmetric systems.

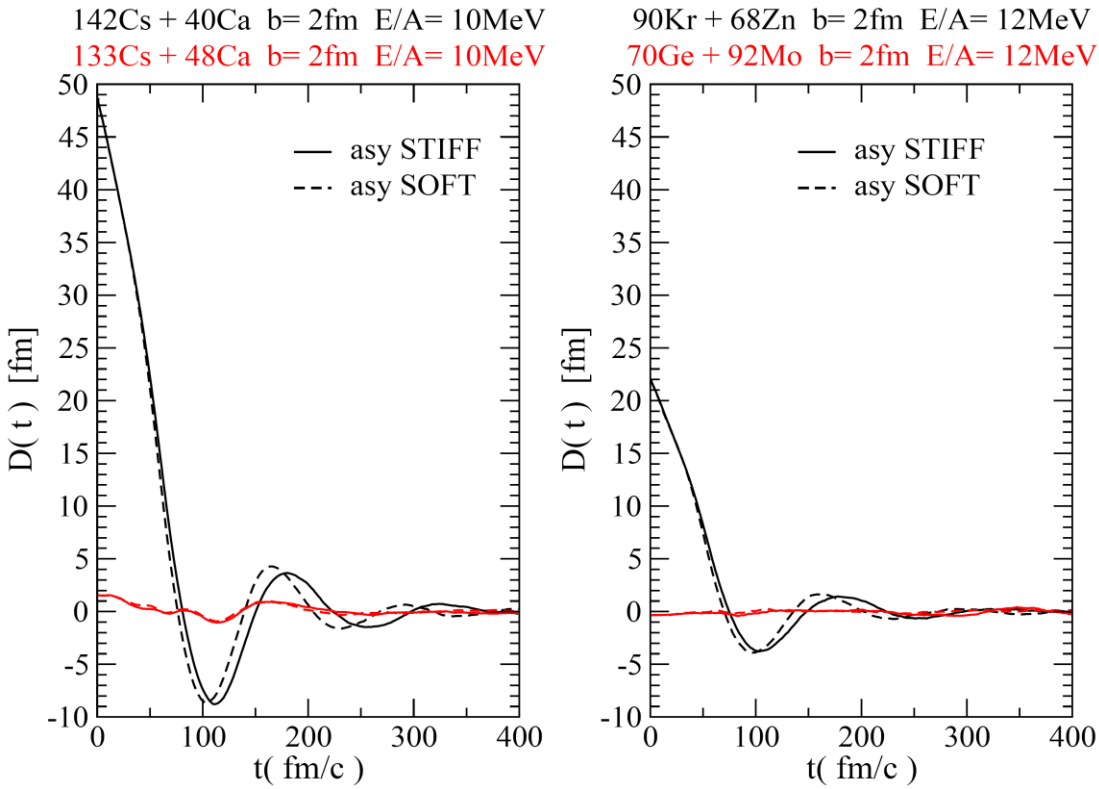

Fig.3. 13 Left Panels: Dipole Dynamics at 10MeV/A, b=2fm centrality, ^{142}Cs + ^{40}Ca (black line) and ^{133}Cs + ^{48}Ca (red line) system. Upper: Time evolution of dipole moment D(t) in real space; Lower: Dipole phase-space correlation. Right Panels: same as before for ^{90}Kr + ^{68}Zn (black line) and ^{70}Ge + ^{92}Mo (red line) system at 12MeV/A, b=2fm centrality. Solid lines correspond to Asysoft EoS, the dashed to Asystiff EoS.

Although the exchange of nucleons between the two colliding nuclei with different N/Z ratios in the di-nuclear phase tends to

diminish the ratio towards an equilibrium value of the compound nucleus. In this phase for the ^{133}Cs + ^{48}Ca and ^{70}Ge + ^{92}Mo system, the exchange of mass is dominated by a stochastic sequence of individual migrations of nucleons. As we can clearly see, in our simulations the dynamical dipole mode for the more charge symmetric reactions was found to be negligible. Therefore, the larger contribution refer to the dynamical dipole yield is related to the more charge asymmetric partners of each system.

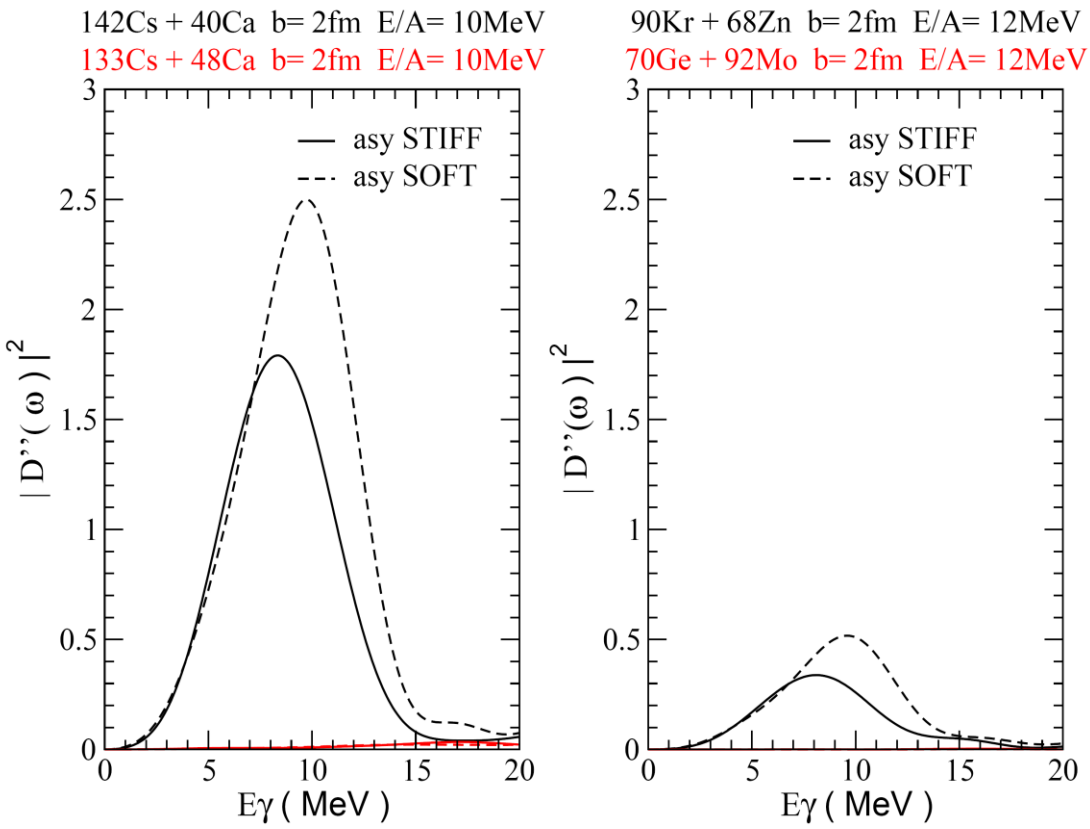

Fig.3. 14 Left Panels: Power spectra of the dipole acceleration at b = 2fm and 10MeV/A for ^{142}Cs + ^{40}Ca (black line) and ^{133}Cs + ^{48}Ca (red line) system. Right Panels: Corresponding results for the ^{90}Kr + ^{68}Zn (black line) and ^{70}Ge + ^{92}Mo (red line) system at 12MeV/A. Solid lines correspond to Asysoft EoS, the dashed to Asystiff EoS. The Iso-Eos effects and the yield on the more charge symmetric systems are negligible.

From Fig.3.14 we also see the typical effect observed above with the “132 system” due to the density dependence of the symmetry term in the region below saturation. These systems have very similar increase percentages compared to the previous case between Asysoft e Asystiff EoS.

However, we would not be able to draw a conclusion about the density dependence of the symmetry energy by using beams which correspond to little intensity of pre equilibrium photons. As said before the reason is that the experimental errors, together with the small difference in the dynamical dipole yield according to the different theoretical prescriptions, do not allow one to discriminate among them. Radioactive beams with a larger spectrum and yield of the prompt dipole radiation are needed to maximize the difference between the different prescriptions of the symmetry energy dependence on density and allow an experimental discrimination. For this reason we prefer the system with the ^{132}Sn beam because it show a increase factor of about 2 if compared to the larger yield in Fig.3.14. The difference between the yield associated with different systems clearly depends on the Iso-EoS and the sensitivity is amplified when using more asymmetric beams due to the factor $D(t_0)^2$ (see the equ.3.10).

3.7 Anisotropy of the angular distribution of the emitted pre equilibrium photon.

Aside the total gamma spectrum the corresponding angular distribution can be a sensitive probe to explore the properties of pre equilibrium dipole mode and the early stages of fusion dynamics [BAR08]. In fact a clear anisotropy vs. the beam axis has been observed in experimental data of the angular distribution of the difference between the γ rays of the ^{36,40}Ar + ^{96,92}Zr reactions [MAR08].

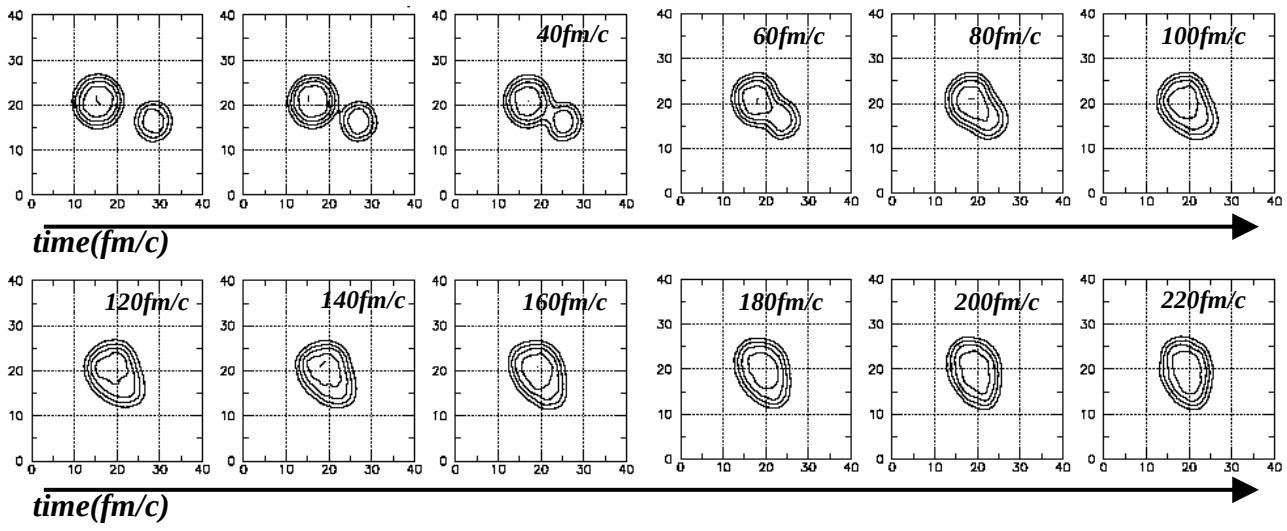

Fig.3. 15 Density plots at 4fm centrality of the neck dynamics for the ^{132}Sn +^{58}Ni system at incident energy of 10MeV/A .

For a dipole oscillation just along the beam axis we expect an angular distribution of the emitted photons like $W(\theta) \sim \sin^2\theta \sim 1+a_2P_2(\cos\theta)$ with $a_2=-1$, where θ is the polar angle between the photon direction and the beam axis. Such extreme anisotropy will be never observed since in the collision the prompt

dipole axis will rotate during the radiative emission. In fact the deviation from the $\sin^2\theta$ behaviour will give a measure of the time interval of the fast dipole emission. Just for comparison with statistical compound nucleus GDR radiation we remind that in the case of a prolate nucleus with a collective rotation, for the low energy component we can have an anisotropy parameter $a_2=-1/4$, averaging over all possible rotation angles and all possible orientations of the collective angular momentum (orthogonal to the beam axis), [HAR01]. Orientation fluctuations can even reduce such anisotropy, [ALH90]. These results cannot be translated directly to the case of the dynamical dipole. As we see from our calculations the pre equilibrium oscillations extend over the first 250−300fm/c. During this time interval, depending also on the centrality and energy, the deformed nucleus may not complete a full rotation on the reaction plane because the rugby ball form has a limited life before it becomes a CN spherical, so the symmetry axis can be detected only in a certain angle range.

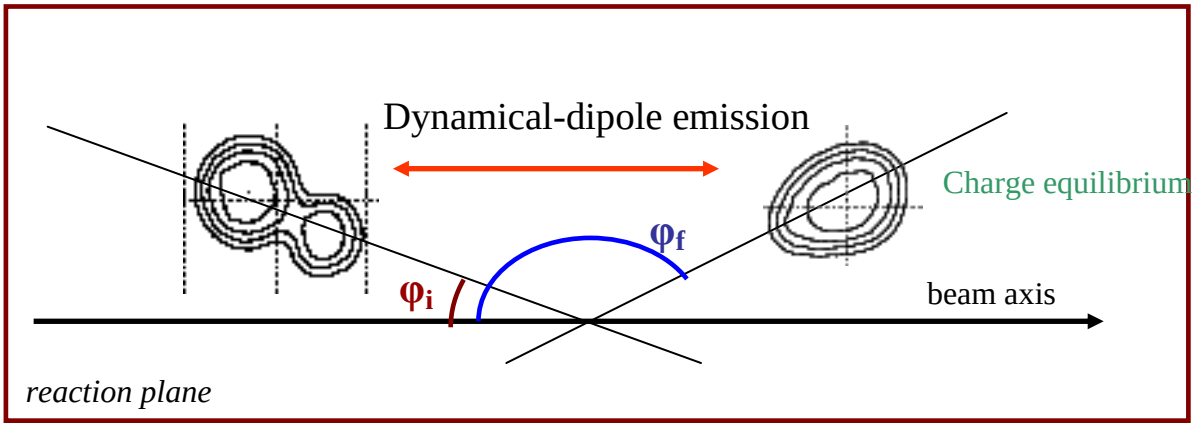

Fig.3. 16 Schematic time dependence of the rotation angle of the symmetry axis with respect to the beam axis. φ_i and φ_f the initial and final angles associat respectively to excitation and complete damping of the dynamical dipole emission.

From the experimental point of view it is convenient to have the angular distribution with respect to beam axis. Let us denote by φ_i and φ_f the initial and final angles of the symmetry axis (which is also oscillation axis) with respect to the beam axis, associated respectively to excitation and complete damping of the dipole mode. Then $\Delta\varphi=\varphi_f-\varphi_i$ is the rotation angle during the collective oscillations. We can get the angular distribution in this case by averaging only over the angle $\Delta\varphi$ obtaining

$$W(\theta) \sim 1 - (\frac{1}{4} + \frac{3}{4}x)P_2(cos\theta)$$

$$x = cos(\phi_f + \phi_i)\frac{sin(\phi_f - \phi_i)}{\phi_f - \phi_i}$$

Equ.3. 11

It is easy to see that for central collision when the di-nucleus deformation axis remains along the beam axis, $\Delta\varphi=0$, i.e. for $\varphi_f=\varphi_i=0$ we have x=1. This corresponds to the pure $\sin^2$, a2 =-1, angular distribution, (see in Fig.3.17, the dashed line). If $\Delta\varphi=2\pi$ then x = 0 and the angular distribution reduces to the statistical a2 =-1/4 expression mentioned above, (see also in Fig.3.17, the points line). Moreover if $\varphi_f = \varphi_i = \varphi_0$, i.e. the orientation is frozen at an angle φ_0 with respect to the beam axis, the Eq.(4) gives an $a_2=(-1+3/2\sin^2\varphi_0)$, with a change of sign for $\varphi_0 \geq 55^\circ$, i.e. a decrease of $W(\theta)$ around $\theta \approx \pi/2$. The point is that meanwhile the emission is damped.

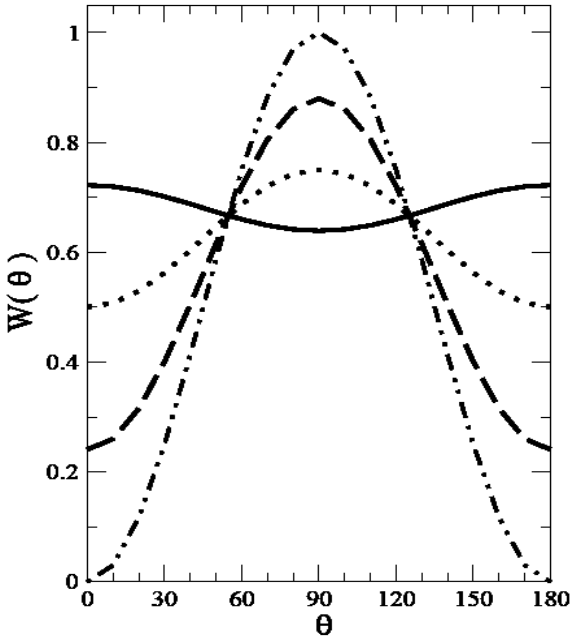

Fig.3. 17 The angular distributions for b = 2fm centrality considering a constant emission (dashed line) and b = 4fm (solid line). Dashed lines and two point for the a_2=-1 (beam axis) and point line for a_2=-1/4 (compound nucleus prolate).

In Fig.3.18(a) we plot the time evolution of the rotation angle, for the “132" system, extracted from dynamical simulations at b=2fm and b=4fm. The Iso-Eos effects on the rotation angle are negligible. By the simulations we can extract the values of the excitation and switching off angle of the dynamical dipole. The evolution of the symmetry axis angle show oscillations between 70 and 140fm/c which could be caused by isoscalar quadrupole and octupole surface modes in the entrance channel. A complete damping of the dipole oscillations is observed at about 300fm/c.

Assuming a constant radiation emission probability the corresponding angular distributions is calculated using as initial angle the contact configuration angle and as final angle that corresponding to 300fm/c for the two different impact parameters. The angular distribution shows in Fig.3.17 a remarkable sensitivity to the impact

parameter: we note that while at b = 2fm we still see a bump around $\pi/2$, in the more peripheral events we can have a minimum in the direction orthogonal to the beam axis just because now larger rotation angles are dominant.

However, the constant emission approximation is not valid because we have a photon emission that is concentrated largely in the first phase of the charge equilibration while a small portion is diluted over the time.

Within the bremsstrahlung approach we can perform an accurate evaluation of the prompt dipole angular distribution using a weighted form where the time variation of the radiation emission probability is accounted for

$$W(\theta) = \sum_{i=1}^{t_{max}} \beta_i W(\theta, \Phi_i)$$

Equ.3. 12

We divide the dipole emission time in Δt_i intervals with the corresponding ϕ_i mean rotation angles and the related radiation emission probabilities $\beta_i = P(t_i) - P(t_{i-1})$, where

$$P(t) = \int_{t_0}^{t} \mid D''(t) \mid^2 dt / P_{tot}$$

Equ.3. 13

with P_{tot} given by $P(t_{max})$, total emission probability at the final dynamical dipole damped time.

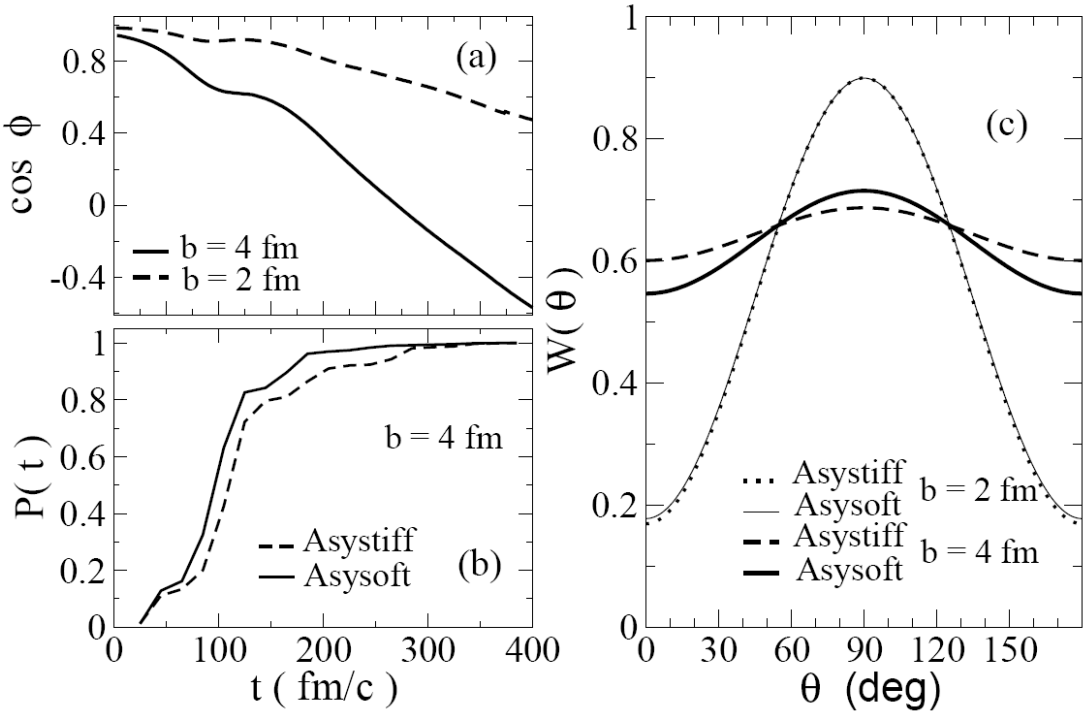

Fig.3. 18 "132" system. (a) panel: time dependence of the rotation angle at b=2fm (dashed line) and b=4fm (solid line). (b) panel: time evolution of the emission probability P(t), for b = 4fm impact parameter. (c) panel: weighted angular distributions for b = 2fm and b = 4fm centralities for different symmetry term choices. Dashed lines for the Asystiff choice, solid for Asysoft. The Iso-Eos effects on the rotation angle are negligible.

As mentioned above, we note in Fig.3.18(a) that essentially the same curves are obtained with the two Iso-EoS choices: the overall rotation is mostly ruled by the dominant isoscalar interactions. Instead symmetry energy effects will be induced by the different time evolution of emission probabilities. This is shown in Fig.3.18(b) for the "132" system at b = 4fm impact parameter. We clearly see that the dominant emission region is the initial one, between 50 and 150 fm/c, while the di-nuclear system rotates of about 20 degrees, roughly from 40◦ to 60◦. Another interesting point is the dependence on the symmetry energy. With a weaker symmetry term (Asystiff case) the P(t) is a little delayed and presents a smoother behaviour. As a

consequence we can expect possible symmetry energy effects even on the angular distributions.

This is shown in the (c) panel of Fig.3.18, where we have the weighted distributions, Equ.3.12, for b=2fm and b=4fm impact parameters, with the two choices of the symmetry energies below saturation. For more central collisions, due to the small rotation of the oscillation axis, the delay effect in the Asystiff case is not affecting the angular distribution. For more peripheral reactions we see a larger contribution at forward/backward angles, although the bump around $\pi/2$ is still present due to the decreasing emission probability at later times when the larger rotations contribute. Altogether we get wider "dipole" angular distributions with respect to the beam axis, in agreement with the first available data on the angular distribution of the difference between the γ rays of the ^{36,40}Ar + ^{96,92}Zr reactions. Moreover, as evidenced by the results at b = 4fm, we expect to see a sensitivity to the slope of the symmetry term below saturation in presence of larger rotation velocities, i.e. in fusion events with high spin selection, in fact the sensitivity to Iso-EoS is clearly seen only for not too central impact parameters, where the elongated system may get to larger rotation during the prompt dipole lifetime. From the experimental point of view, this signal can be sought by selecting fusion events with high spin.

As a consequence we would expect to see more evident anisotropy effects of the DDR radiation in fusion-fission events. This effect should be clearly observed even in deep-inelastic binary cases where we still expect the presence of a DDR emission, see the Chapter 4, as in fact in ref. [PIE03]

Summarizing we have shown that in fusion with exotic nuclei an enhanced pre equilibrium dipole emission can be observed with a peculiar angular distribution related to its early emission. The features of this collective mode are sensitive to the density dependence of symmetry energy below saturation. For the system ^{132}Sn +^{58}Ni at 10MeV/A, the γ multiplicity appears about 25% greater for the Asysoft choice of the symmetry term comparing to the Asystiff case. The angular distributions are sensitive to the fusion dynamics and dipole excitation mechanism and lifetime.

In conclusion the dynamical dipole mode can constitute a suitable probe to test the symmetry energy term in the nuclear EoS as well as to scrutinize the early entrance channel dynamics in dissipative reactions with radioactive beams.

Chapter 4: SYMMETRY ENERGY EFFECTS ON FUSION CROSS SECTIONS.

Dissipative mid-peripheral collisions, including binary and three-body breakings, offer a unique opportunity to study phenomena occurring in nuclear matter under extreme conditions with respect to shape, intrinsic excitation energy, spin, isospin, etc., together with the possibility to control these conditions by choosing appropriate entrance and exit channels. Thus, it is possible to probe the mechanisms of nuclear excitation, how intrinsic degrees of freedom are converted into collective modes, how these modes decay and how relaxation processes occur within a small quantal system that is initially far from equilibrium. The velocity and the angular distribution of the reaction products furnish natural clocks from which it is possible to determine the equilibration times of the various degrees of freedom, (e.g. N/Z ratio, mass, excitation energy).

We focus our investigation on the interplay fusion vs. break-up (fast-fission, deep-inelastic) for Heavy Ion Collisions, HIC, with exotic nuclear beams at low energies. For such systems the competition between reaction mechanisms can be used to study

properties of the symmetry energy term at densities below and around the normal value. In particular since for dissipative collisions at low energy the interaction times are quite long we can have a large coupling among various mean field modes that may eventually lead to a two-body break-up of the system. The Coulomb and angular momentum (deformation) effects can also lead to three-body breakings, where a light cluster is emitted from the neck region [COL95]. In this reaction mechanism, the development of surface (neck-like) instabilities, that would help ternary breaking, is also sensitive to the structure of the symmetry term.

The idea in this work is to probe how the symmetry energy will influence such couplings in neutron-rich systems with direct consequence on the fusion probability.

The method that we have adopted, based on the event by event evolution of quadrupole collective modes, in coordinate and momentum space, will nicely allow to extract the fusion probability at relatively early times, of the order of 200-300 fm/c, when the transport results are reliable.

We can see measurable symmetry energy effects for intermediate impact parameters, where the competition fusion-break-up is more important. Same differences are observed with respect to the predictions of macroscopic models, such as PACE4 [GAV79, TAR03]. Finally the collective charge equilibration mechanism (the Dynamical Dipole already discussed in Chapter 3) is revealed in both fusion and break-up events, also depending on the stiffness of the symmetry term below saturation.

4.1 Competition of reaction mechanisms.

Isospin is expected to govern the competition between fusion and deep inelastic reactions in semi-central collisions, at energies around and slightly below the Fermi energy [BAR05]. In FigS.4.1 and 4.2 we show plots, for two choices of the symmetry term, of the time evolution of the density projection on the reaction plane in semicentral collisions, at b=4 fm, of neutron rich ions ^{46}Ar$(N/Z$=1.56$)$ + ^{64}Ni$(N/Z$=1.29$)$ and neutron poor ions, $N = Z$, ^{46}V + ^{64}Ge at 30MeV/A.

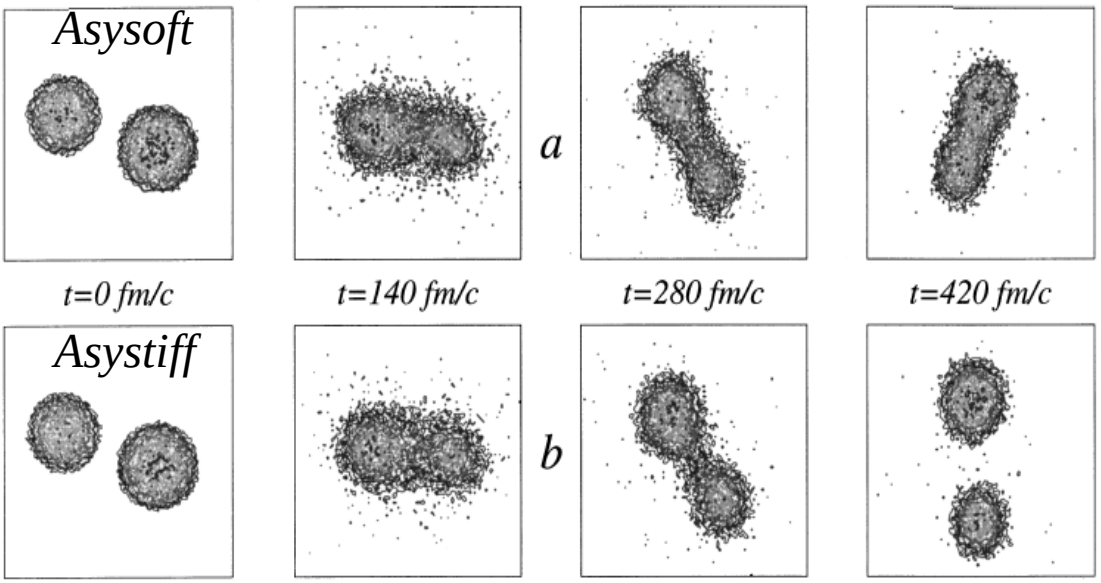

Fig.4. 1 Density plots at different times in a reaction between neutron-rich ions ^{46}Ar+ ^{64}Ni at Elab = 30 MeV/A, b = 4 fm. Asy-soft EoS more dissipative.

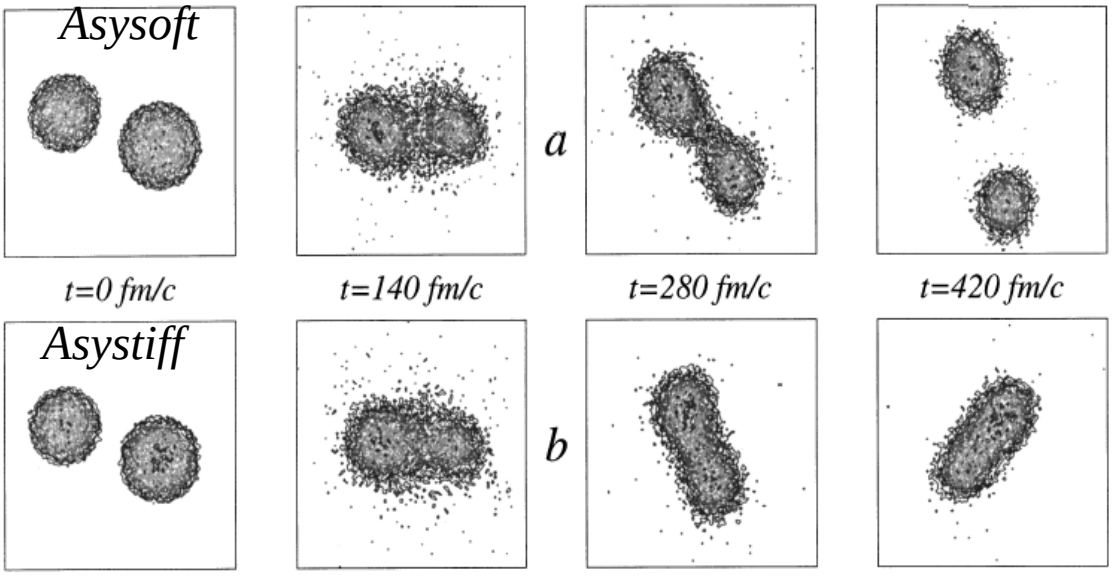

Fig.4. 2 Density plots in a reaction between neutron-poor ions ^{46}V + ^{64}Ge at Elab = 30 MeV/A, b = 4 fm. Asy-stiff EoS more dissipative.

The effect on the reaction mechanism of the different density dependences of the symmetry term is quite evident in Fig.4.1. The effect of isospin can be understood in terms of the amount of

attraction or repulsion existing during the approaching phase of the two nuclei. During this phase, for a density slightly above saturation density, the symmetry energy is larger in the Asy-stiff case. So for neutron-rich systems, the fusion is favoured with an Asy-soft EoS: neutrons are dominant, and their effect is less repulsive in this case. In fact we see in Fig.4.1(a) a stronger interaction between the two partners, leading to a larger dissipation of the relative energy, and thus the system will more likely enter a fusion path. Experimentally this means a larger (incomplete) fusion cross section at medium energies. In reaction between neutron-poor ions $^{46}V + {}^{64}Ge$, we would expect more repulsion since we have larger Coulomb and direct $n-p$ collision contributions. In fact, for neutron-poor systems in the Asy-soft case, we have a dominant binary deep-inelastic mechanism (Fig.4.2a). However, in the Asy-stiff choice (Fig.4.2b) we get a clear fusion dominance. This result is amazing for two reasons: the dynamics of a symmetric $N = Z$ system appears to be isospin-dependent and the stiffer symmetry term leads to a larger attractive potential. This observation could be related to the appearance in the symmetric system, of a "proton skin", which is overlapping in the interaction zone. The fusion is easier for an Asy-stiff EOS, because initially the dominant protons have a larger attractive symmetry potential for a density slightly above saturation density in the overlap region.

Afterwards, when the density goes below normal density in the interaction zone, the protons in the Asy-stiff case are less attracted and are more easily promptly emitted. As a consequence, the two partners feel a smaller Coulomb repulsion and more likely fusion can

be reached. Consistently, a larger yield of fast proton emission is predicted with the Asy-stiff parameterization [COL98+].

These results suggest that in low-energy dissipative collisions an observable sensitive to the stiffness of the symmetry term can be just the relative yield of incomplete fusion vs. deep-inelastic events.

The dependence of the interaction time on the stiffness of the symmetry term will also influence the competition between binary and *neck-fragmentation* events [COL95, BER84], where intermediate mass fragments (IMF, in the range $3<Z<10$) are formed in the overlapping region, roughly at mid-rapidity in semicentral reactions .

The isospin effects on the reaction dynamics were experimentally studied at Fermi energies [AMO09]: targets of ^{40}Ca, ^{46}Ti, and ^{48}Ca were bombarded by a ^{40}Ca beam accelerated at 25MeV/A. Charged reaction products were detected with the CHIMERA 4π array. The competition between fusion and deep inelastic reactions in central collisions was explored through the study of the variable $\Delta M_{nor}=(M_1-M_2)/M_{tot}$, M_1, M_2 being the masses of the largest and second largest detected fragment and $M_{tot}=M_1+M_2$ the total mass of the incident system. A fusion reaction, ending with a heavy residue and evaporated light charged particles will be associated with large values of ΔM_{nor}. Conversely deep inelastic reactions, for these almost symmetric systems, should have ΔM_{nor} values closer to zero. ΔM_{nor} minimizes the effects due to the mass differences between the targets and enhances those coming from their isotopic content.

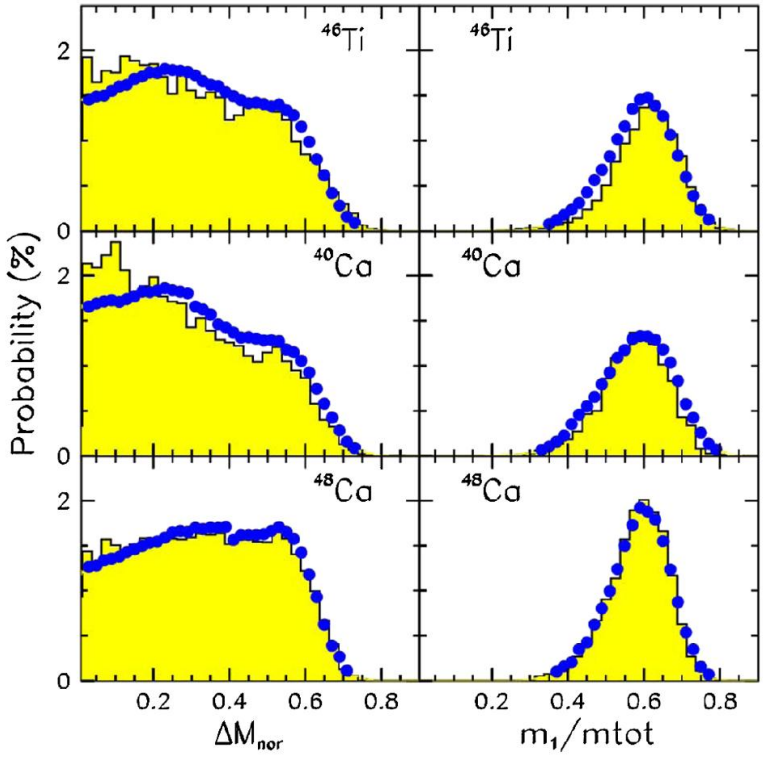

Fig.4. 3 Probabilities of _Mnor (left) and of the normalized mass of the largest fragment (right) for the 3 studied systems. Blue dots represent experimental data whereas the shaded histograms show the results of a CoMD+GEMINI calculation, [AMO09].

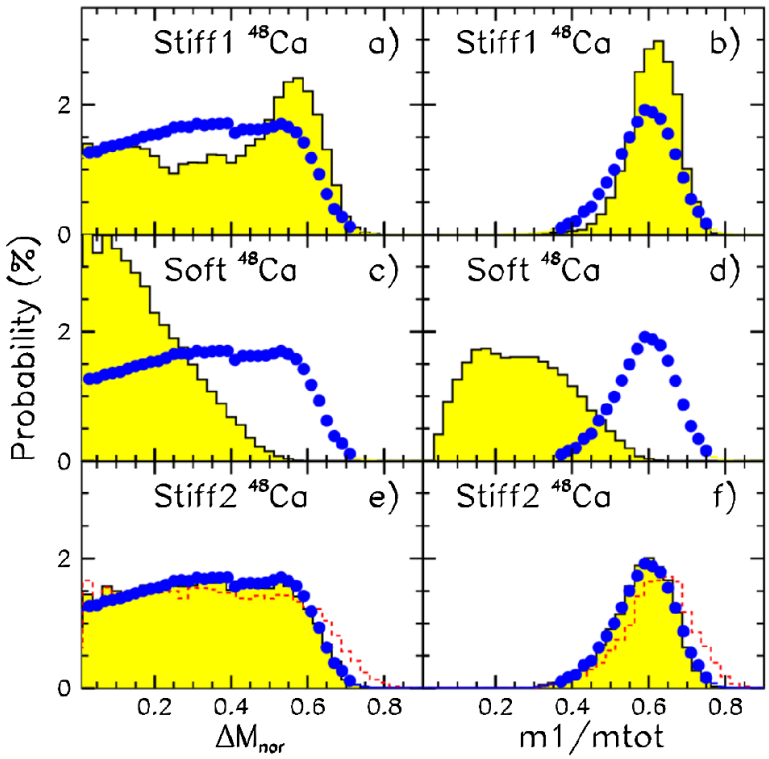

Fig.4. 4 Same as Fig.4.3 for the ^{40}Ca + ^{48}Ca CoMD + GEMINI calculations with different parametrizations are shown. The dashed lines correspond to CoMD without the GEMINI.

The distributions of ΔM_{nor} clearly show that there are more fusion events (characterized by ΔM_{nor} larger than 0.4) for the heavy ^{48}Ca target than for the two others. Indeed, due to the neutron richness of ^{48}Ca the corresponding compound nucleus is close to the valley of stability while the other ones lie near the proton-drip line. Information on symmetry energy was extracted by comparing experimental findings to the results of constrained molecular dynamics (CoMD) simulations [PAP01].

4.2 Fusion dynamics for ^{132}Sn induced reaction: Average dynamics of shape observables.

The purpose of this work is to understand what happens at lower energies in the framework of the Stochastic Mean-Field (SMF) approach, extension of the microscopic Boltzmann-Nordheim-Vlasov transport equation, see equ.1.29.

We focus the attention on the interplay of fusion vs. deep-inelastic mechanisms for dissipative HIC with unstable ion beams at low energies [RIZ10]. These collisions are characterized by interaction times that are quite long and by a large coupling among various mean field modes that may eventually lead to the break-up of the system. Hence the idea is to probe how the slope of the symmetry term around the saturation density will influence such couplings in neutron-rich exotic systems with direct consequences on the fusion probability.

Similarly to the simulations conducted so far, the fluctuating term $\delta I[f]$ is implemented by stochastic spatial density fluctuations, and to map the particle occupation at each time step, Gaussian phase space wave packets (test particles) are considered. Stochasticity is essential to get distributions, as well as to allow the growth of dynamical instabilities. In these simulations 100 test particles per nucleon have been employed for an accurate description of the mean field dynamics. In the collision integral, I_{coll}, an in-medium depending nucleon-nucleon cross section, via the local density, is employed, and it is set equal to zero for nucleon-nucleon collisions below 50MeV of relative energy. In this way we avoid spurious effects, that may dominate in this energy range when the calculation time becomes too large.

In spite of that, we are not able to draw a conclusion about the final outcome of the reaction because the simulations cannot be trusted on the time scale of a compound nucleus formation, mainly for the increasing numerical noise. As it will be explained, we will seek a new procedure to evaluate the fusion probability: on the basis of a shape analysis in phase space, we can separate fusion and break-up trajectories at rather early times, of the order of 200-300 fm/c, when the calculation can still be fully reliable.

To study isospin and symmetry energy effects on the competition between fusion and break-up we consider the reactions $^{132}Sn + ^{64,58}Ni$ at 10 MeV/A, and we have performed collision simulations for semi-peripheral impact parameters (from b =4.5 fm to b = 8.0 fm, with Δb= 0.5 fm), to explore the region of the transition from fusion to break-up dominance. The transport equations clearly give fusion events at central impact parameters and break-up events for peripheral collisions, but there are some problems when we consider semi-peripheral impact parameters at such low energies, since the time scales for break-up are not compatible with the transport treatment, as already noted. Then based on a phase space analysis of Quadrupole collective modes, the information on the final reaction path is deduced investigating the fluctuations of the system at early times (200-300 fm/c), when the formation of composite elongated configurations is observed and phenomena associated with surface meta stability and/or instability may take place.

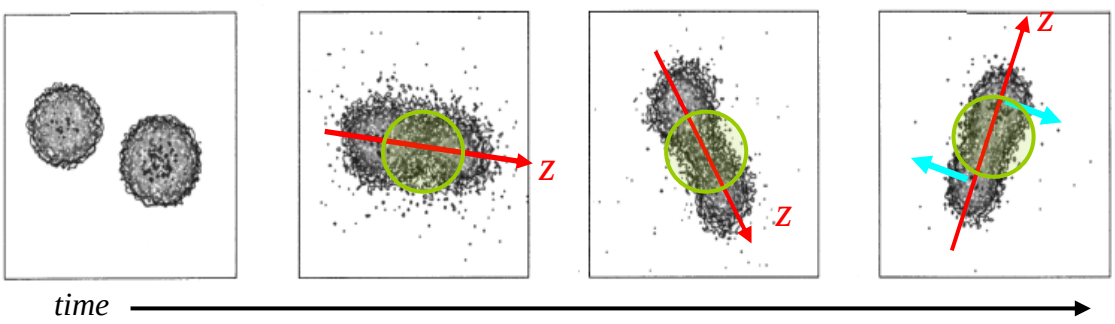

Fig.4. 5 Schematic description of the z-axis along the rotating projectile-like/target-like direction and spatial region around the center of mass where we have calculated the Quadrupole moment in momentum space.

We start considering the time evolution, in each event, of the Quadrupole moment in coordinate space which is given by:

$$Q(t) = < 2z^2(t) - x^2(t) - y^2(t) >,$$

Equ.4 1

averaged over the space distribution in the composite system. At the same time-steps we construct also the Quadrupole moment in momentum space:

$$QK(t) = < 2p_z^2(t) - p_x^2(t) - p_y^2(t) >,$$

Equ.4 2

in a spatial region around the center of mass. The z-axis is along the rotating projectile-like/target-like direction, the x-axis is on the reaction plane. We run 200 events for each set of macroscopic initial conditions and we first consider the average over this ensemble.

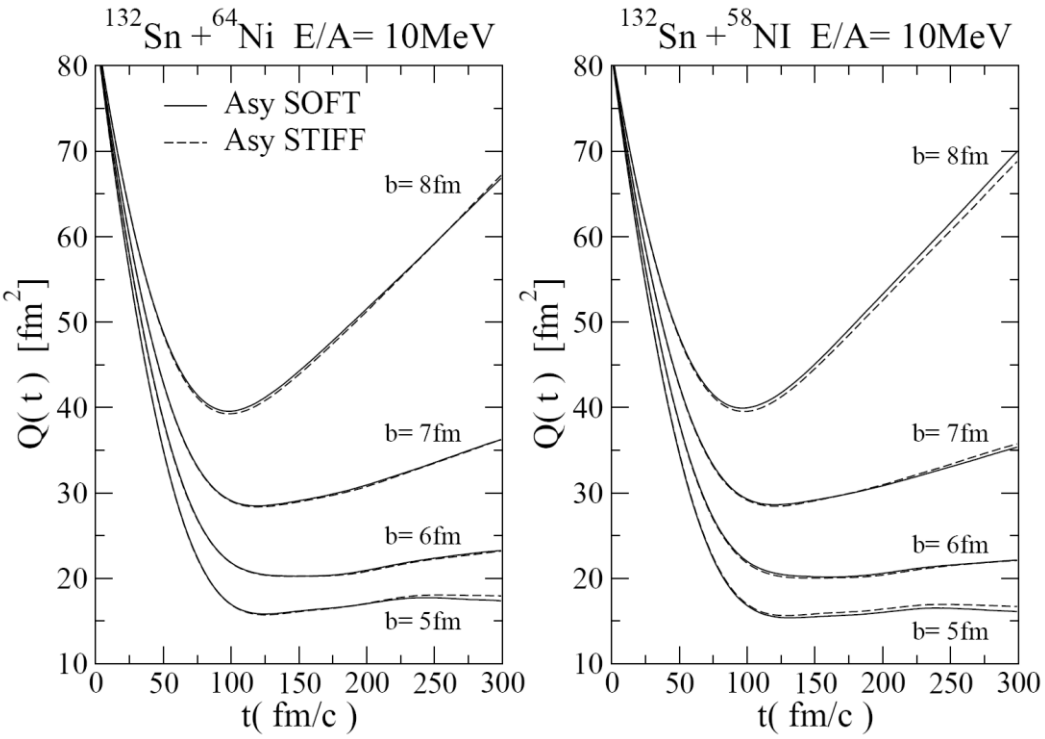

Fig.4. 6 Time evolution of the space Quadrupole moments for different centralities and for the two systems. Solid line: Asysoft. Dashed line: Asystiff.

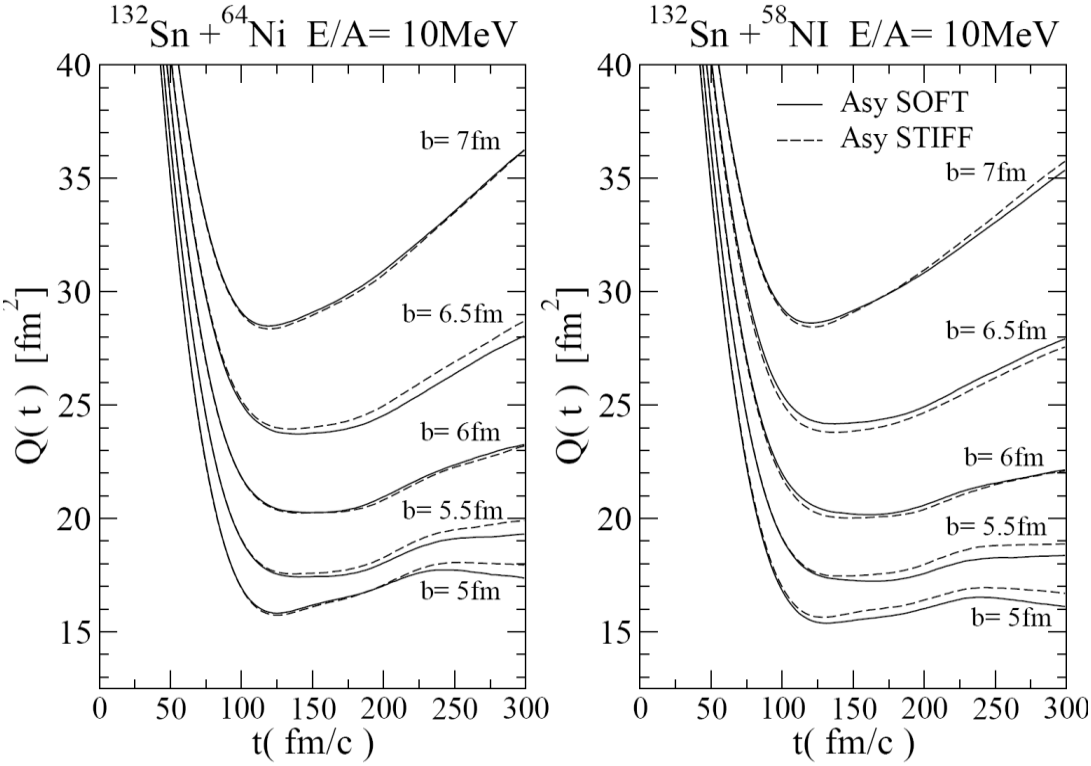

Fig.4. 7 Like Fig.4.6 but more detailed in the angular momentum transition region, between b=5 and 7 fm. Solid line: Asysoft. Dashed line: Asystiff.

In Fig.4.6 and in Fig.4.7 we present the time evolution of the mean space Quadrupole moment at various centralities for the two reactions and for the two choices of the symmetry term. We notice the difference in Q(t) between the behaviour corresponding to more peripheral impact parameters and that obtained for b=5-6 fm, where we have still a little oscillation in the time interval between 100 and 300 fm/c, good indication of a fusion contribution. We can interpret these observations assuming that starting from about b = 5 fm, we have a transition from fusion to a break-up mechanism, like deep-inelastic. Positive values of the Q(t)-slope should be associated with a Quadrupole deformation velocity of the dinuclear system that is going to a break-up exit channel. We notice a slight systematic difference, especially in the most neutron-rich system, with a larger deformation velocity in the Asystiff case, see the more detailed picture of Fig.4.7. Hence, just from this simple analysis of the average space Quadrupole "trajectories" we can already appreciate that the Asysoft choice seems to lead to larger fusion cross sections, at least for less peripheral impact parameters, between b=5fm and b=6,5fm. The latter point can also be qualitatively seen from the time evolution of the space density distributions projected on the reaction plane, as shown in Fig.4.8.

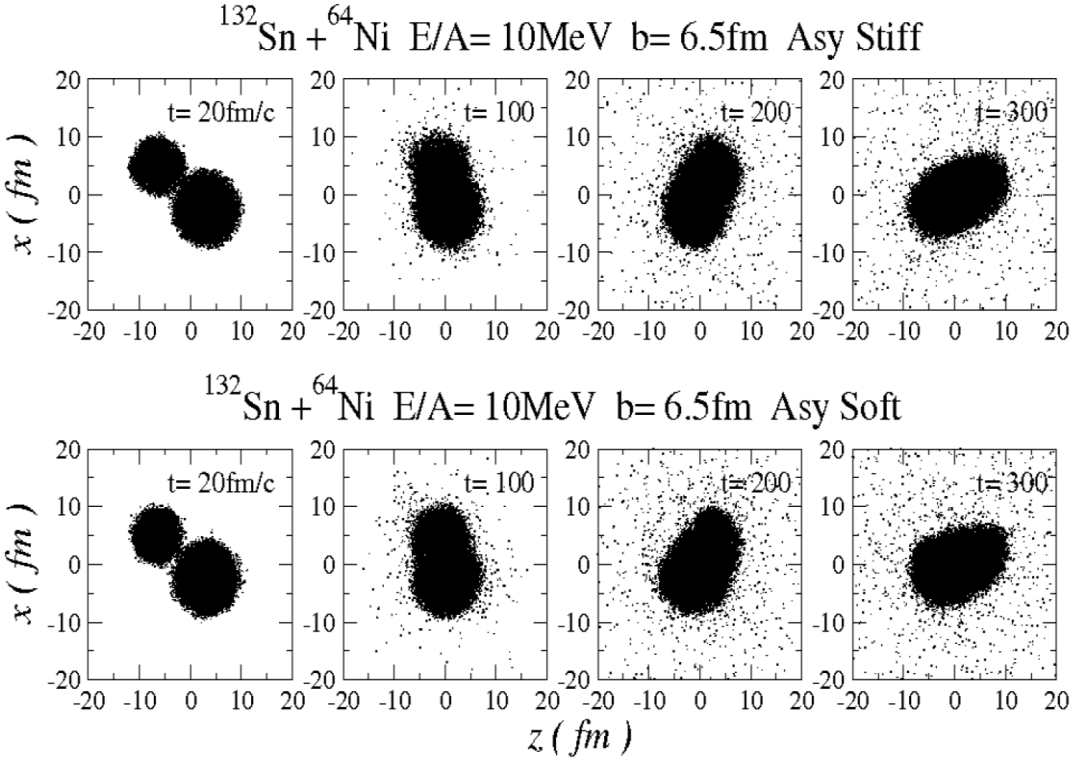

Fig.4. 8 Time evolution of the space density distributions for the reaction ^{132}Sn + ^{64}Ni (n-rich systems), 10 MeV/A beam energy, for semicentral collisions, b=6.5 fm impact parameter. Upper Panel: Asystiff. Lower Panel: Asysoft.

The formation of a more compact configuration in the Asysoft case can be related to a larger fusion probability. It is very instructive to look also at the time evolution of the Quadrupole deformations in momentum space. For each event we perform the calculation in a spherical cell of radius 3 fm around the system center of mass.

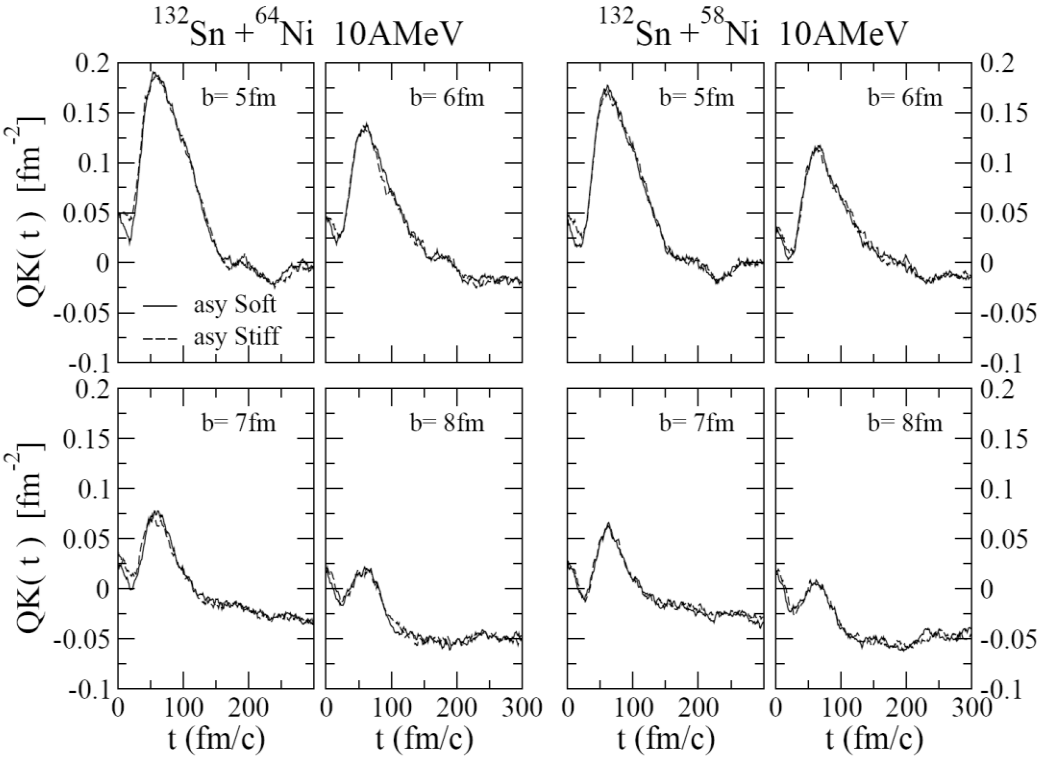

Fig.4. 9 Time evolution of the momentum quadrupole moments, in a sphere of radius 3fm around the center of mass, for different centralities and for the two systems. Solid line: Asysoft. Dashed line: Asystiff.

In Fig.4.9 we present the time evolution of the average p-Quadrupole moments at various centralities for the two systems and the two choices of the symmetry term. We notice a difference between the plots corresponding to peripheral or central collisions. With increasing impact parameter the Quadrupole QK(t) becomes more negative in the time interval between 100 and 300 fm/c: the components perpendicular to the symmetry axis, that is rotating in reaction plane, are clearly increasing. We can interpret this effect as due to the presence, in the considered region, of Coriolis forces that are enhanced when the angular momentum is larger. These forces help to break the deformed dinuclear system. Then the break-up probability will be larger if the Quadrupole moment in p-space is more negative. From Fig.4.6 and Fig.4.9 one can see that there is a

region of impact parameter (b = 5 – 6,5fm) where the derivative of the Quadupole moment in coordinate space, Q′, and the Quadrupole moment in momentum space, QK, are both rather close to zero. This is the region where we expect that fluctuations of these quantities should play an important role in determining the fate of the reaction and event-by-event analysis is essential to estimate fusion vs. break-up probabilities.

4.3 Analysis of fluctuations and fusion probabilities for ^{132}Sn induced reactions.

To define a quantitative procedure to fix the event by event fusion vs. break-up probabilities, we undertake an analysis of the correlation between the two Quadrupole moments introduced in the previous Section, in the time interval defined before (100-300 fm/c). Another important suggestion to look at correlations comes from the very weak presence of isospin as well as symmetry energy effects in the separate time evolution of the two Quadrupole moments, as we can see from Figs.2,3 and Fig.5. Negative QK values denote the presence of velocity components orthogonal to the symmetry axis, due to angular momentum effects, that help the system to separate in two pieces. At the same time, the observation of a velocity component along the symmetry axis indicates that the Coulomb repulsion is dominating over surface effects (that would try to recompact the

system), also pushing the system in the direction of the break-up. Hence, in order to get the fusion probability from the early evolution of the system we assume positive Q' and negative QK for break-up events. In other words, we suppose that, in the impact parameter range where the average value of the two quantities is close to zero, the system evolution is decided just by the amplitude of shape fluctuations, taken at the moment when the formation of a deformed composite system is observed along the SMF dynamics (t=200-300 fm/c, see the contour plots of Fig.4). Within our prescription, the fusion probability is automatically equal to one for central impact parameters, where the system goes back to the spherical shape and Q' is negative, while it is zero for peripheral reactions, where Q' is always positive and QK always negative.

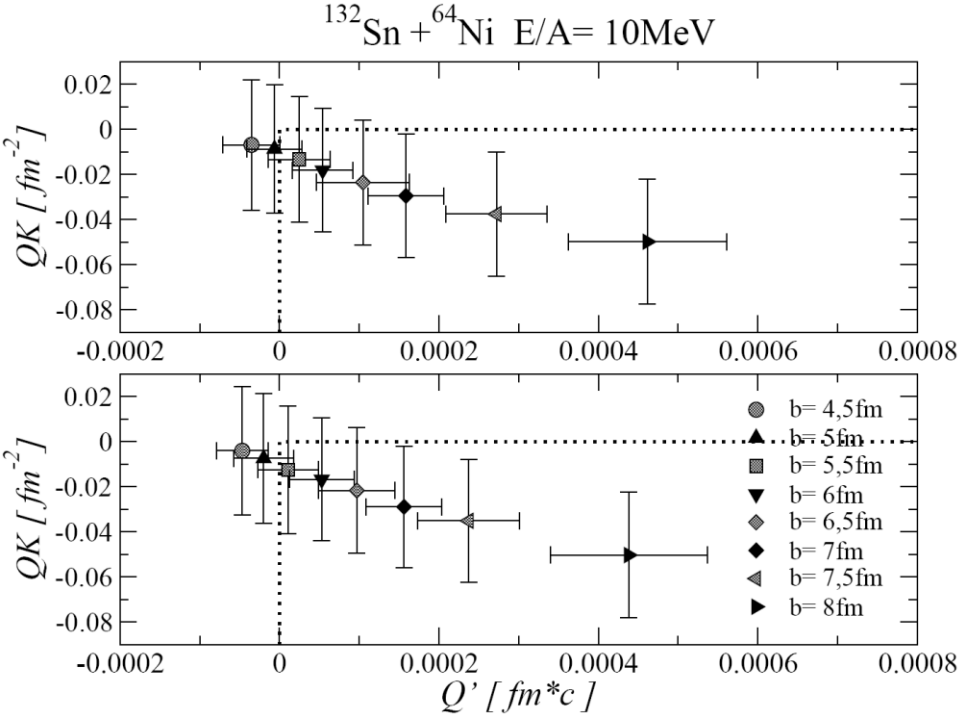

Fig.4. 10 ^{132}Sn + ^{64}Ni system. Mean value and variance of QK vs. Q', averaged over the 100-300 fm/c time interval, at various centralities in the transition region. The box limited by dotted lines represents the break-up region. Upper panel: Asystiff. Bottom Panel: Asysoft.

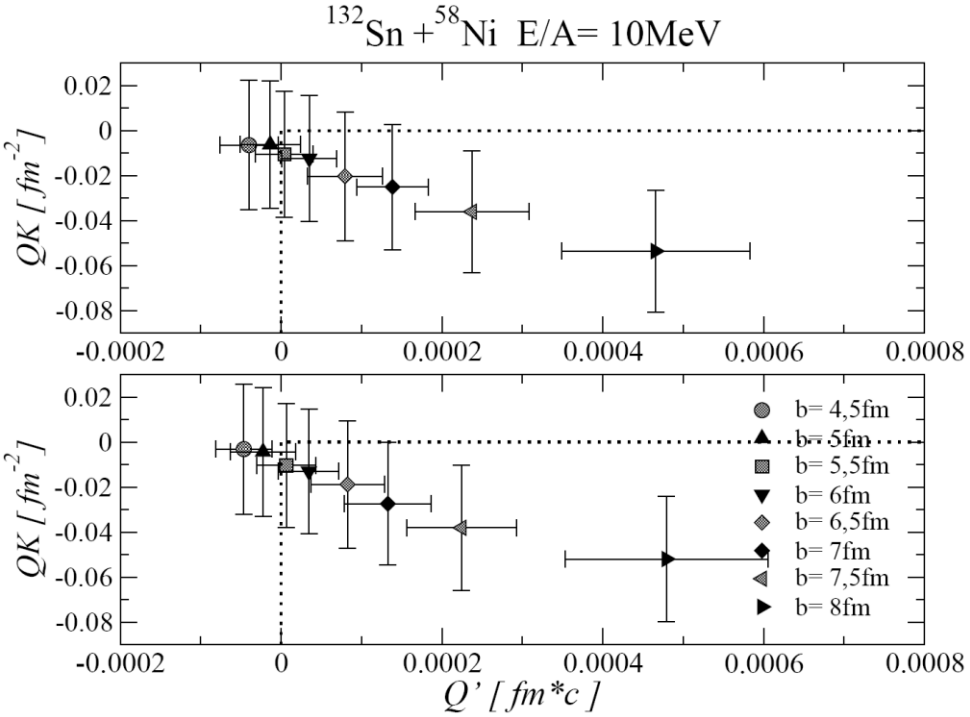

Fig.4. 11 Like in Fig.4.10 but for the ^{132}Sn + ^{58}Ni system.

The correlation plots for the two systems studied and the two Asy-EOS are represented in Fig.4.10 and Fig.4.11, respectively.

Through the quantities displayed in the figures, mean value and variance of the two extracted properties of the phase space moment evolution, we can evaluate the normal curves and the relative areas for each impact parameter in order to select the events: break-up events will be located in the regions with both positive slope of Q(t) and negative QK. In this way, for each impact parameter we can evaluate the fusion events by the difference between the total number of events and the number of break-up events. Finally the fusion cross section is obtained (in absolute value) by

$$\frac{d\sigma}{dl} = \frac{2\pi}{k^2} l \frac{N_f}{N_{tot}}$$

Equ.4 3

where l is the angular momentum calculated in the semi classical approximation, k is the relative momentum of the collision, N_f the number of fusion events and N_{tot} the total events in the angular momentum bin. In Fig.4.12 we present the fusion spin distribution plots.

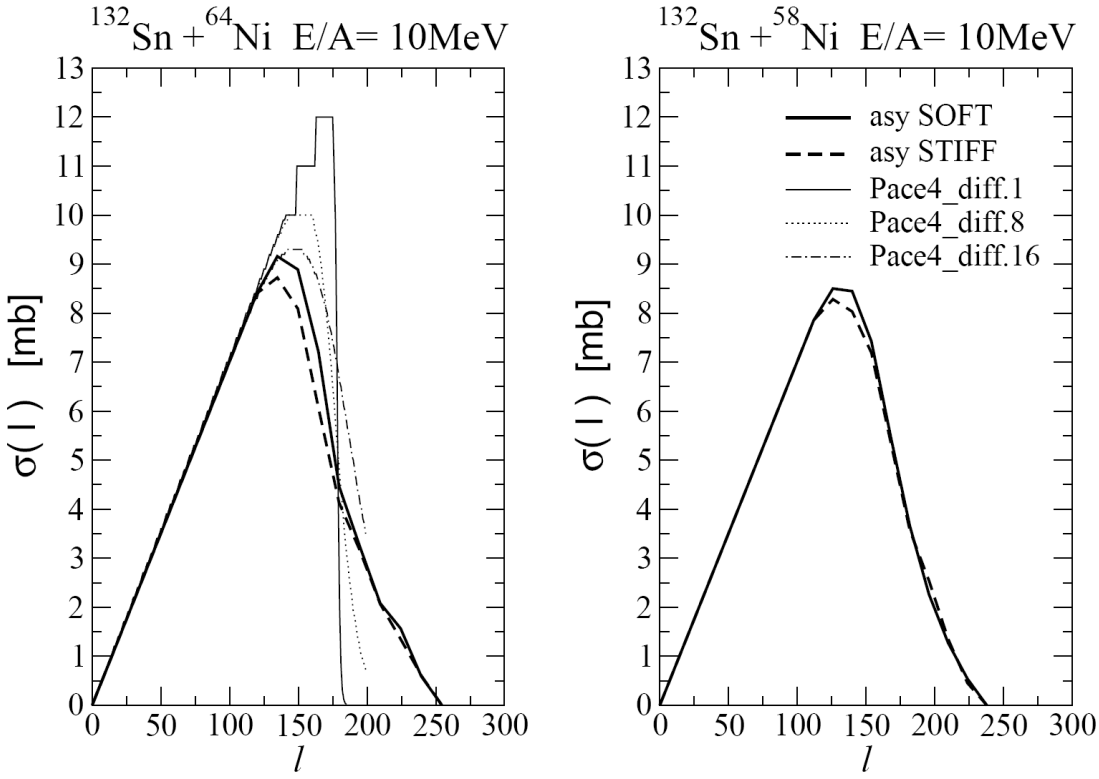

Fig.4. 12 Angular momentum distributions of the fusion cross sections (mb) for the two reactions and the two choices of the symmetry term. For the 132Sn + 64Ni system (left panel), the results of PACE4 calculations are also reported, for different l-diffuseness.

We note that just in the centrality transition region there is a difference between the fusion cross section corresponding to the two different Iso-EOS, with larger values for Asysoft. In fact, the total cross sections are very similar: the difference in the area is about 4-5 % in the neutron rich system, 1128 mb (Asysoft) vs. 1078 mb

(Asystiff), and even smaller, 1020 mb vs. 1009 mb, for the ^{58}Ni target. However, through a selection in angular momentum, $130 \leq l \leq 180\ (\hbar)$, we find that the Asysoft curve is significantly above the Asystiff one, and so in this centrality bin the fusion cross section difference can reach a 10% in the case of the more neutron-rich system. Then it can be compared to experimental data as an evidence of sensitivity to the density dependence of the symmetry energy.

From the comparison of the total areas for the two systems we can also estimate isospin effects on the total fusion cross section, with a larger value in the more neutron-rich case, as also recently observed in fusion reactions with Ar + Ni [MAR10] and Ca + Ca isotopes [AMO09]. We note that this effect is also, slightly, dependent on the symmetry term: The total fusion cross section for the more neutron rich system is 10% larger in the Asysoft calculation and about 7% in the Asystiff case. Finally we like to note that for the neutron-rich case, ^{132}Sn+^{64}Ni, our absolute value of the total fusion cross section presents a good agreement with recent data, at lower energy (around 5 MeV/A), taken at the ORNL [LIA07].

In Fig.4.12 for the same system (left panel) we show also the results obtained with the macroscopic fusion probability evaluation code PACE4, obtained with different *l*-diffuseness parameters, fixing, as input parameters, our total fusion cross section and maximum angular momentum. We see that in order to have a shape more similar to our $\sigma(l)$ distribution we have to choose rather large diffuseness values, while the suggested standard choice for stable systems is around Δl=4. This seems to be a nice evidence of the neutron skin effect.

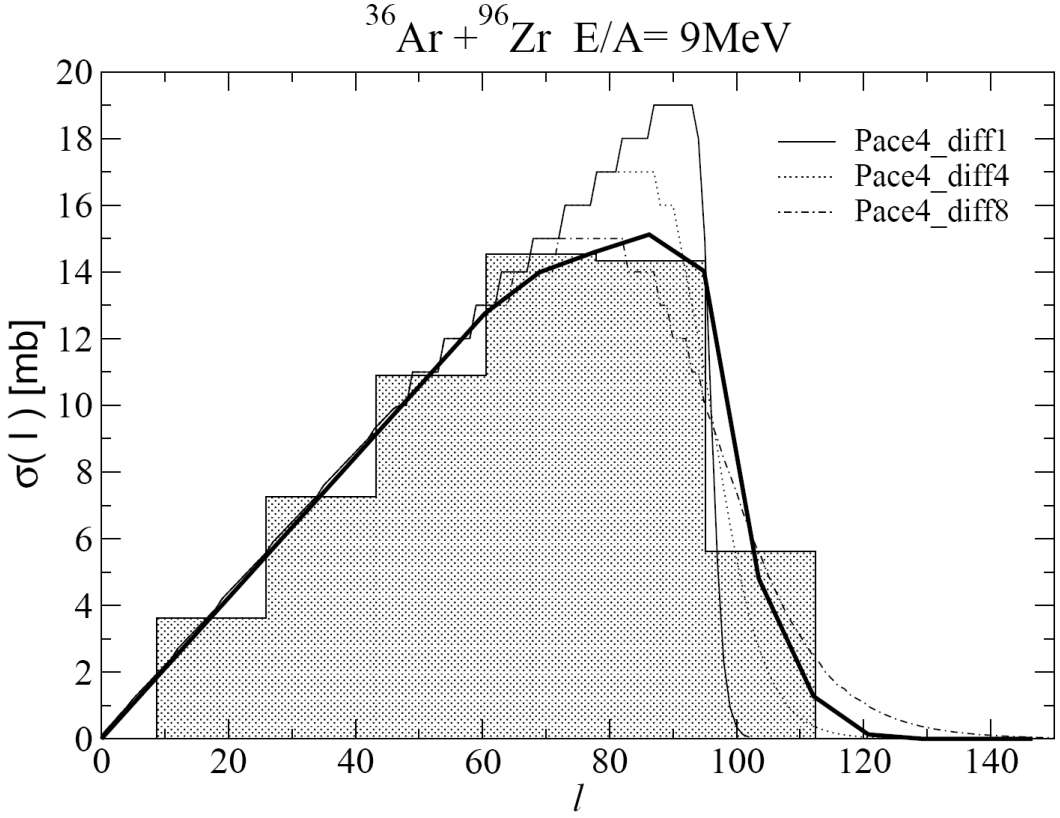

Fig.4. 13 Angular momentum distributions of the fusion cross sections (mb) for the reaction ^{36}Ar + ^{96}Zr at 9 MeV/A (solid line). The dashed histogram corresponds to the results of ref.[21]. The PACE4 evaluations are also reported, for different l-diffuseness.

In order to have a further cross-check of our procedure to evaluate fusion probabilities we compare in Fig.4.13 our fusion spin distributions with the ones derived from a Langevin treatment of fluctuations in a dynamical evolution of the system shape observables [SHV10]. The reaction is ^{36}Ar + ^{96}Zr at 9 MeV/A ; the solid line shows our "early time" estimation (Asysoft choice) while the dashed histogram corresponds to the result of ref.[SHV10]. The good agreement is interesting since the thermal fluctuations used in this reference to fix the stochastic force are consistently giving the same fusion probabilities in our transport approach based on the study of shape fluctuations at early times ($t \approx 200 - 300$ fm/c).

In the same figure we also show the PACE4 results, again fixing as input parameters our total fusion cross section (990mb) and maximum angular momentum (*120ħ*). We nicely see that in order to have an agreement with our microscopic estimation we need now a diffuseness $\Delta l \approx 6$, much smaller than in the ^{132}Sn + ^{64}Ni case where, probably due to larger neutron skin effects, we find $\Delta l \approx 16$.

Our main conclusion is that we can extract significant signals on the event by event reaction mechanism by the fluctuations of the Quadrupole moments in phase space evaluated in a time region well compatible with the interval where the transport results are reliable.

4.4 Analysis of Symmetry energy effects.

The larger fusion probability obtained with the Asysoft choice, especially in the more n-rich system, seems to indicate that the reaction mechanism is regulated by the symmetry term at suprasaturation density, where the Asysoft choice is less repulsive for the neutrons, see Fig.2.2 and Fig.2.3.

In order to check this point we have performed a detailed study of the density evolution in the region of overlap of the two nuclei, named neck in the following. We present results obtained for the system ^{132}Sn + ^{64}Ni at impact parameter b = 6,5fm. To account for the system mass asymmetry, this "neck" region is identified by a sphere of radius 3fm centered on the symmetry axis, at a distance from the projectile center of mass equal to $d(t) \approx D(t)R_2/(R_1 + R_2)$, where R_1 and R_2 are the radii of projectile and target, and D(t) is the distance between the centers of mass of the two colliding nuclei. In fact, in the time interval of interest for the fusion/break-up dynamics it will almost coincide with the system center of mass, see also the contour plots of Fig.4.8.

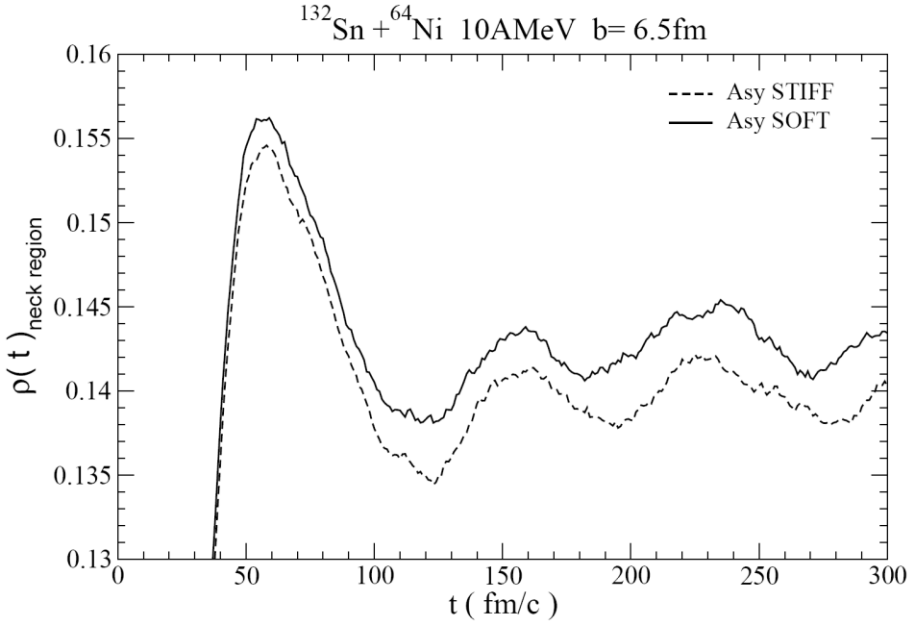

Fig.4. 14 Reaction ^{132}Sn+ ^{64}Ni semi peripheral. Time evolution of the total density in the "neck" region.

The time evolution of the total density in this "neck" region is reported in Fig.4.14 for the two choices of the symmetry energy . We note that in the time interval of interest we have densities above or around the normal density and so a less repulsive symmetry term within the Asysoft choice, corresponding to larger fusion probabilities.

This also explains why larger fusion cross sections are seen for the neutron rich system, mainly in the Asysoft case. In fact, the neutron excess pushes the formed hot compound nucleus closer to the stability valley, especially when the symmetry energy is smaller.

Other nice features are: i) the density values found in the Asysoft case are always above the Asystiff ones, to confirm the expectation of a smaller equilibrium density for a stiffer symmetry term [BAR05];

ii) collective monopole oscillations are present after 100 fm/c, showing that also at these low energies we can have some compression energy.

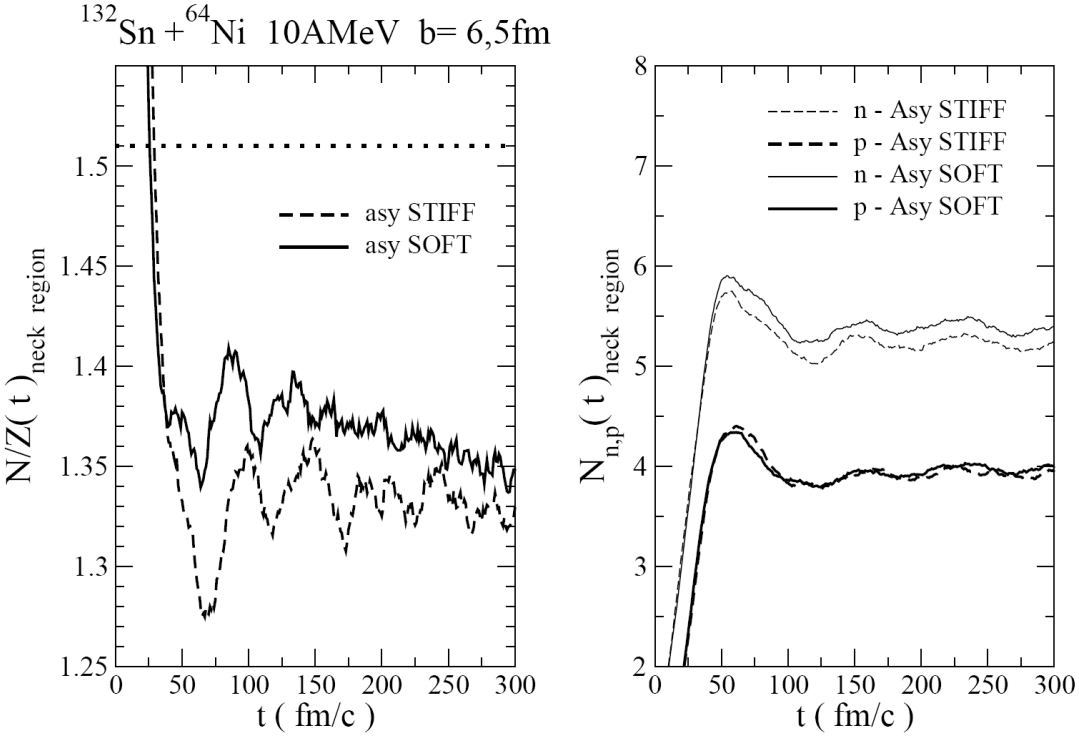

Fig.4. 15 Reaction 132Sn +64 Ni semi peripheral. Left panel: time evolution of the neutron/proton ratio in the "neck" region. The dotted line corresponds to the initial isospin asymmetry of the composite system. Right panel: time evolution of the neutron and proton densities.

It is also instructive to look at the evolution of the isospin content, the N/Z ratio, in this "neck" region, plotted in Fig.4.15. As reference we show with a dotted line the initial average isospin asymmetry. We see that in the Asysoft choice a systematic larger isospin content is appearing (Left Panel). This is consistent with the presence of a less repulsive neutron potential at densities just above saturation probed in the first 100fm/c, when the fast nucleon emission takes place (Fig.4.14 and Fig.4.15, Left Panel). All that is confirmed by the

separate behaviour of the neutron and proton densities shown in the Right Panel of Fig.4.15.

It is finally very interesting the appearance of N/Z oscillations after 100 fm/c. This can be related to the excitation of isovector density modes in the composite system during the path to fusion or break-up. Since initially a charge asymmetry is present in the system (N/Z=1.64 for ^{132}Sn and 1.28 for ^{64}Ni) we expect the presence of collective isovector oscillations during the charge equilibration dynamics for all dissipative collisions, regardless of the final exit channel. The features of this isovector mode, the Dynamical Dipole already observed in fusion reactions with stable beams [BAR08] in chapter 3.

4.5 Ternary breaking.

Within the same transport approach, a first analysis of symmetry energy effects on break-up events in semiperipheral collisions of $^{132}Sn+^{64}Ni$ at 10 MeV/A has been reported in ref.[DIT07]. Consistently with the more accurate study presented here, smaller break-up probabilities have been seen in the Asysoft choice. Moreover the neck dynamics on the way to separation is found also influenced by the symmetry energy below saturation.

Semi-peripheral reactions, corresponding to impact parameters b=6, 7, 8 fm have been considered, for which one observes mostly binary exit channels. It appears that the neck dynamics is rather different when one considers the Asysoft or the Asystiff parameterization. This can be qualitatively seen on Fig.4.16 and Fig.4.17, where density contour plots of events obtained with the two iso-EOS at 7fm centrality are represented.

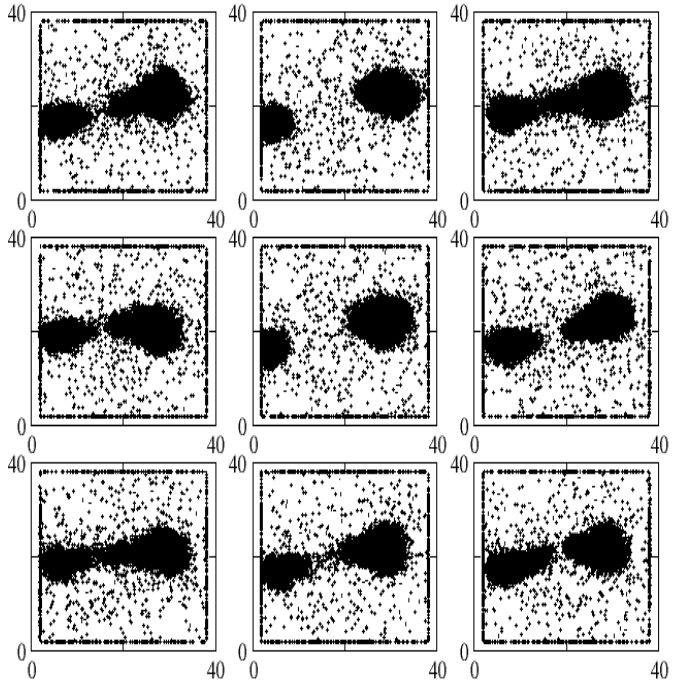

Fig.4. 16 Density contour plots on the reaction plane of the reaction $^{132}Sn+^{64}Ni$ at 10 MeV/A, b = 7fm, at t = 500 fm/c. Asystiff interaction [DIT07]

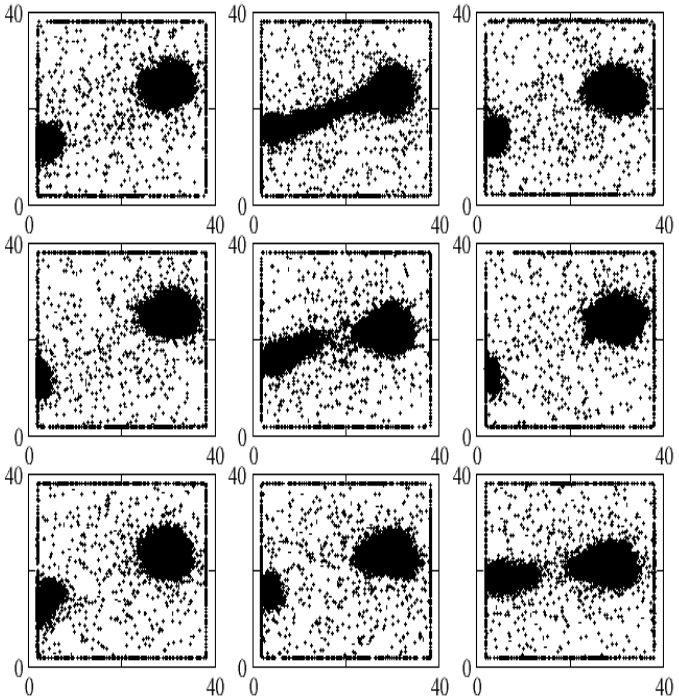

Fig.4. 17 Density contour plots on the reaction plane of the reaction $^{132}Sn+^{64}Ni$ at 10 MeV/A, b = 7fm, at t = 500 fm/c. Asysoft interaction.

Larger deformations, strongly suggesting a final three-body outcome, are seen in the majority of the events in the Asystiff case corresponding to a smaller symmetry repulsion at the low densities probed in the separation region. The neutron-rich neck connecting the two partners can then survive a longer time producing very deformed primary PLF/TLF. Even small clusters can be eventually dynamically emitted leading to ternary/quaternary fragmentation events [SKW08, WIL10].

This can be observed in the different deformation pattern of the Projectile-Like and Target-Like Fragments (PLF/TLF), as shown in Fig.4.18 :

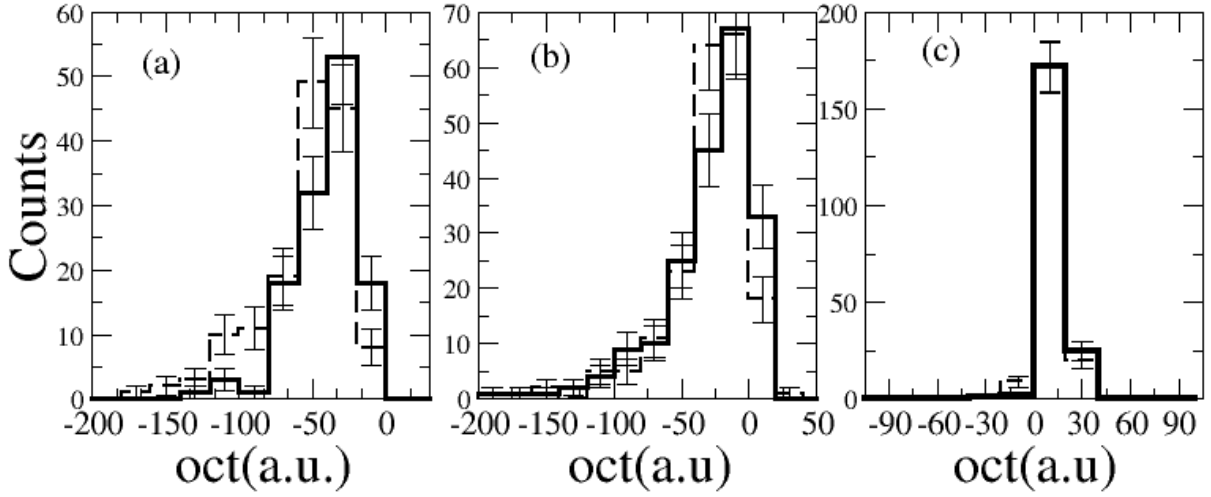

Fig.4. 18 Distribution of the octupole moment of primary fragments obtained in the reaction $^{132}Sn + ^{64}Ni$ at 10 MeV/A at b = 6 fm (left), 7 fm (middle), 8 fm (right). Full line: asysoft; dashed line: asystiff [DIT07]

To perform a quantitative analysis, we can evaluate the Quadrupole or Octupole moment of PLF and/or TLF, that are related to the degree of deformation of these objects and, hence, to the probability to get a ternary break-up. The distribution of the Octupole moment over an ensemble of events is shown in Fig.4.18 for the two

Asy-EoS (the dashed histogram corresponds to Asystiff and the full histogram to Asysoft) and three impact parameters. The Asystiff symmetry term leads to more dissipative events, due to lower value of the symmetry energy, [DIT07].

In conclusion not only the break-up probability but also a detailed study of fragment deformations in deep inelastic (and fast-fission) processes, as well as of the yield of 3-4 body events, can give independent information on the symmetry term around saturation.

4.6 The prompt dipole mode in fusion and break-up events.

From the time evolution of the nucleon phase space occupation it is possible to extract at each time step the isovector dipole moment of the composite system. In our study we have focused the attention on the system with larger initial charge asymmetry, the ^{132}Sn on ^{58}Ni case, already studied in the Chapter 3. Here we focus on results obtained in a different, more peripheral, impact parameter window.

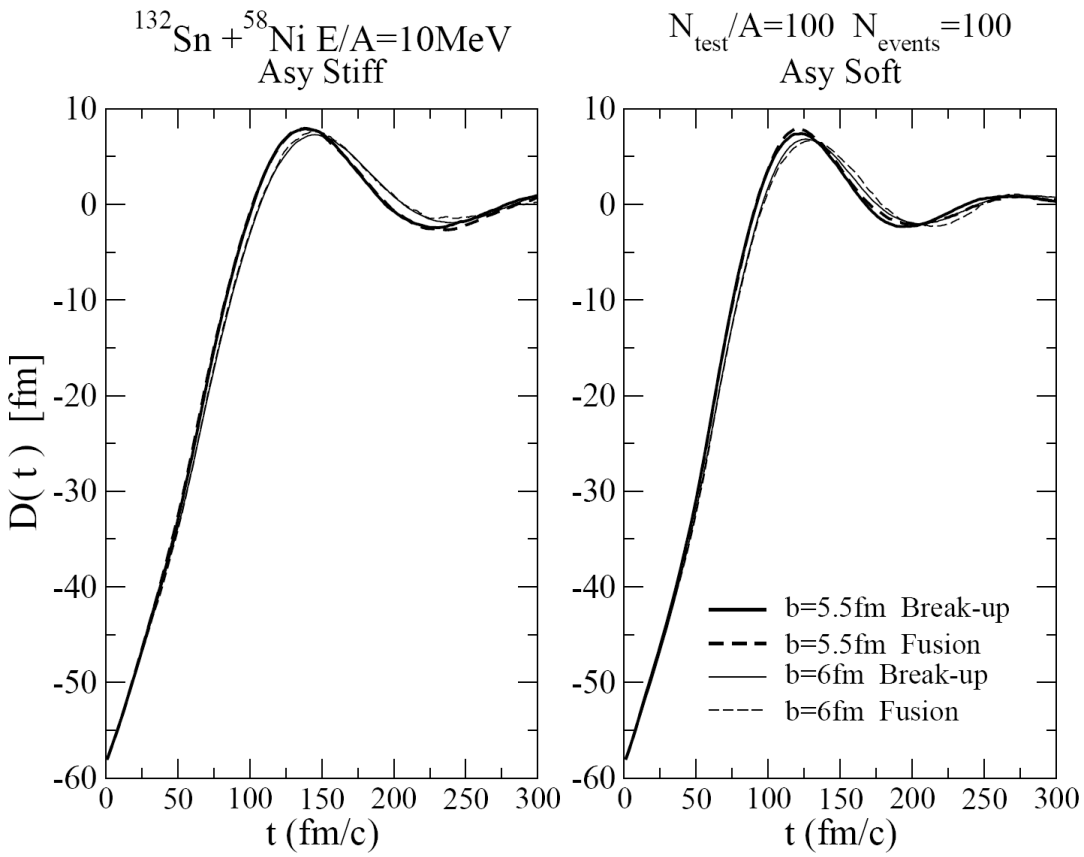

Fig.4. 19 Reaction ^{132}Sn + ^{58}Ni semi-peripheral. Prompt Dipole oscillations in the composite system for break-up (solid lines) and fusion (dashed lines) events. Left Panel: Asystiff. Right Panel: Asysoft.

In Fig.4.19 we present the prompt dipole oscillations obtained for semicentral impact parameters, in the fusion/break-up transition zone. We nicely see that in both classes of events, ending in fusion or deep-inelastic channels, the dipole mode is present almost with the same strength. We note that such fast dipole radiation was actually observed even in the most dissipative deep-inelastic events in stable ion collisions [PIE02, PIE05, AMO04].

The corresponding emission rates can be evaluated, through the ”bremsstrahlung” mechanism (see chapter 3), in fusion or deep-

inelastic processes [BAR01]. In fact from Equ.3.5 we can directly evaluate, in absolute values, the corresponding pre-equilibrium photon emission yields, integrated over the dynamical dipole region.

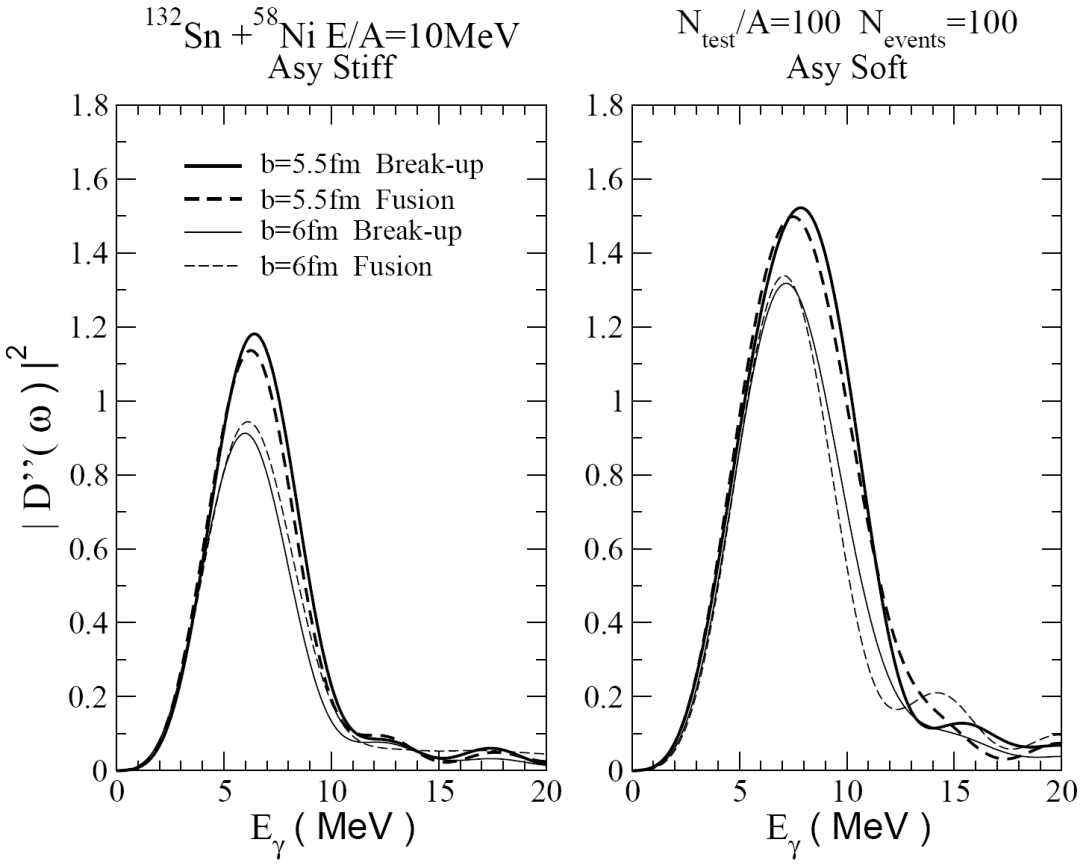

Fig.4. 20 Reaction ^{132}Sn + ^{58}Ni semi-peripheral. Prompt Dipole strengths (in c^2 units), see text, for break-up (solid lines) and fusion (dashed lines) events. Left Panel: Asystiff. Right Panel: Asysoft.

In Fig.4.20 we report the prompt dipole strengths |D″(ω)|2 for the same event selections of Fig.4.19.

The dipole strength distributions are very similar in the fusion and break-up selections in this centrality region where we have a strong competition between the two mechanisms. In any case there is a smaller strength in the less central collisions (b=6.0fm), with a

centroid slightly shifted to lower values, corresponding to more deformed shapes of the dinuclear composite system.

In the Asysoft choice we have a systematic increase of the yields, roughly given by the area of the strength distribution, of about 40% more than in the Asystiff case, for both centralities and selections. For centrality b=5.5fm we get 2.3 10−3 (1.6 10−3) in the Asysoft (Asystiff) choice, and for b=6.0fm respectively 1.9 10−3 (1.3 10−3), with almost no difference between fusion and break-up events.

We know that Asysoft corresponds to a larger symmetry energy below saturation. Since the symmetry term gives the restoring force of the dipole mode, our result is a good indication that the prompt dipole oscillation is taking place in a deformed dinuclear composite system, where low density surface contributions are important, as already observed in ref.[BAR08].

In the previous Sections we have shown that the Asysoft choice leads to a large fusion probability since it gives a smaller repulsion at the supra-saturation densities of the first stage of the reaction. Here we see that for the dipole oscillation it gives a larger restoring force corresponding to mean densities below saturation. This apparent contradictory conclusion can be easily understood comparing Fig.4.14 and Fig.4.19. We note that the onset of the collective dipole mode is delayed with respect to the first high density stage of the neck region since the composite system needs some time to develop a collective response of the di-nuclear mean field.

In this way fusion and dynamical dipole data can be directly used to probe the isovector part of the in medium effective interaction below and above saturation density.

Another interesting information is derived from Fig.4.21 where we show the prompt dipole oscillations only for break-up events at centralities covering the range from semicentral to peripheral.

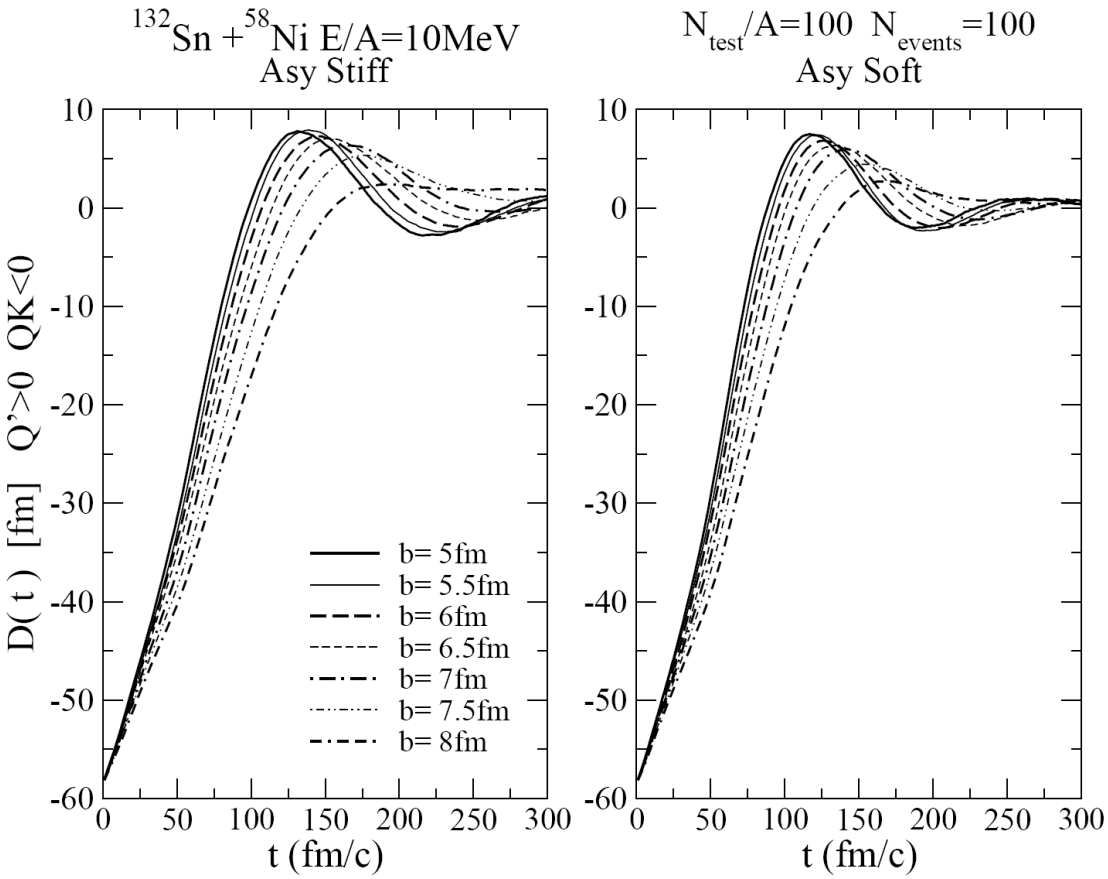

Fig.4. 21 Reaction ^{132}Sn + ^{58}Ni semiperipheral to peripheral.Prompt Dipole oscillations in the composite system for break-up event selections at each impact parameter. Left Panel: Asystiff. Right Panel: Asysoft.

We nicely see that the collective mode for charge equilibration, due to the action of the mean field of the dinuclear system, is disappearing for the faster, less dissipative break-up collisions.

4.7 Anisotropy emission in semi-peripheral reactions.

Aside the total gamma spectrum the corresponding angular distribution can be a sensitive probe to explore the properties of pre-equilibrium dipole mode and the early stages of reaction dynamics (see section 3.7).

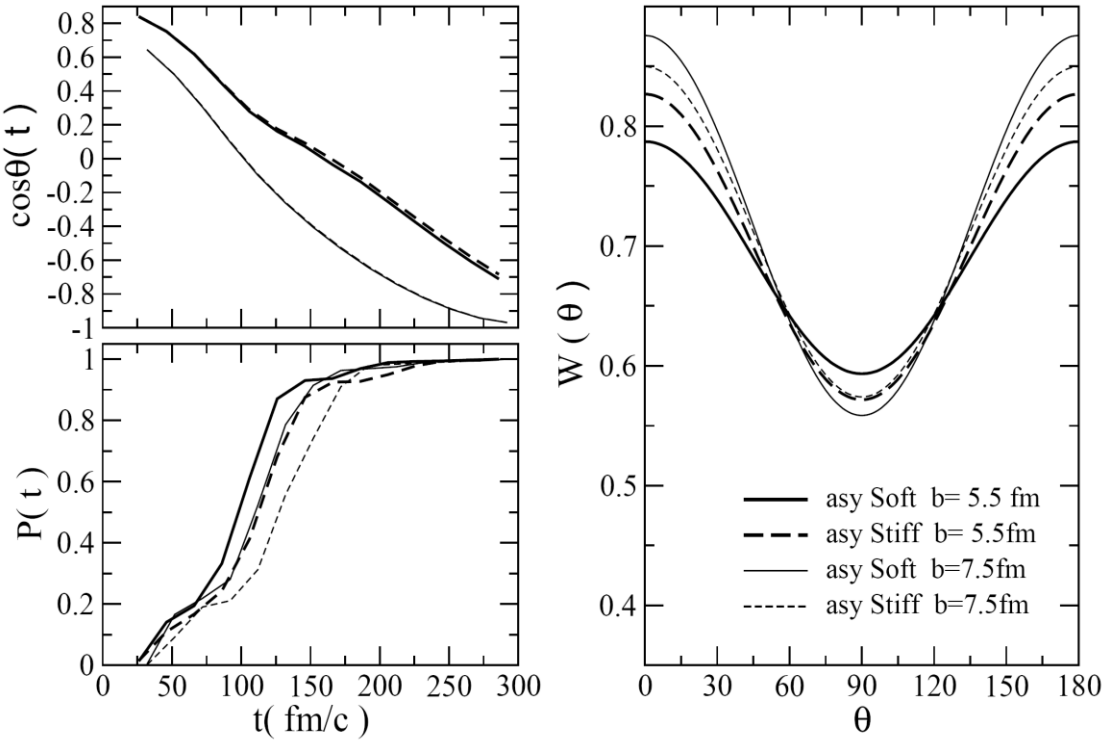

Fig.4. 22 Reaction ^{132}Sn + ^{58}Ni semi-peripheral. Upper Left panel: Rotation angle. Bottom Left Panel: emission probabilities. Right panel: Weighted angular distribution.

In Fig.4.22, upper left panel, we plot the time dependence of the rotation angle, for the ^{132}Sn + ^{58}Ni system, extracted from all the events, fusion and break-up, at two semi-peripheral impact parameters, for the two symmetry terms. As already shown in Chapter 3, we note that essentially the same curves are obtained with the two Iso-EoS choices (the overall rotation is mostly ruled by the dominant

isoscalar interaction), and the symmetry energy effects are induced by the different time evolution of the emission probabilities, as shown in the bottom left panel.

We clearly see that the dominant emission region is the initial one, just after the onset of the collective mode between 80 and 150 fm/c, while the emitting dinuclear system has a large rotation. Another interesting point is the dependence on the symmetry energy. With a weaker symmetry term at low densities (Asystiff case), the P(t) is a little delayed and presents a smoother behaviour. As a consequence, according to equ.3.12, we can expect possible symmetry energy effects even on the angular distributions.

This is shown in the right panel of Fig.4.22, where we have the weighted distributions, for the two impact parameters and the two choices of the symmetry energies. We see some sensitivity to the stiffness of the symmetry term. Hence, from accurate measurements of the angular distribution of the emitted γ's, in the range of impact parameters where the system rotation is significant, one may extract independent information on the density behaviour of the symmetry energy.

4.8 Mass symmetry effects on the fusion cross section.

It is well known that the mass symmetry of the colliding partners is also affecting the fusion probability. Mass symmetric cases are expected to lead to a reduced fusion events for the combined effect of larger Coulomb barrier and smaller dissipation (in a macroscopic "window" model). Since the Dynamical Dipole mode is also related to the fusion dynamics we have analysed both the fusion-break-up competition and the DDR emission for n-rich systems selecting entrance channels with roughly the same charge asymmetry but with rather different mass asymmetry [RIZ11].

We report here some preliminary results for the reactions ^{124}Sn(N/Z = 1.48)+ ^{56}Fe(N/Z = 1.15) vs. ^{90}Kr(N/Z = 1.5) + ^{90}Zr(N/Z = 1.25) at 10 MeV/A , i.e. with same average < N/Z >= 1.37, close charge asymmetry and rather different mass symmetry in the entrance channel. In Fig.4.23 we show the time evolution of the mean space Quadrupole moments for the two reactions and the two choices of the symmetry term.

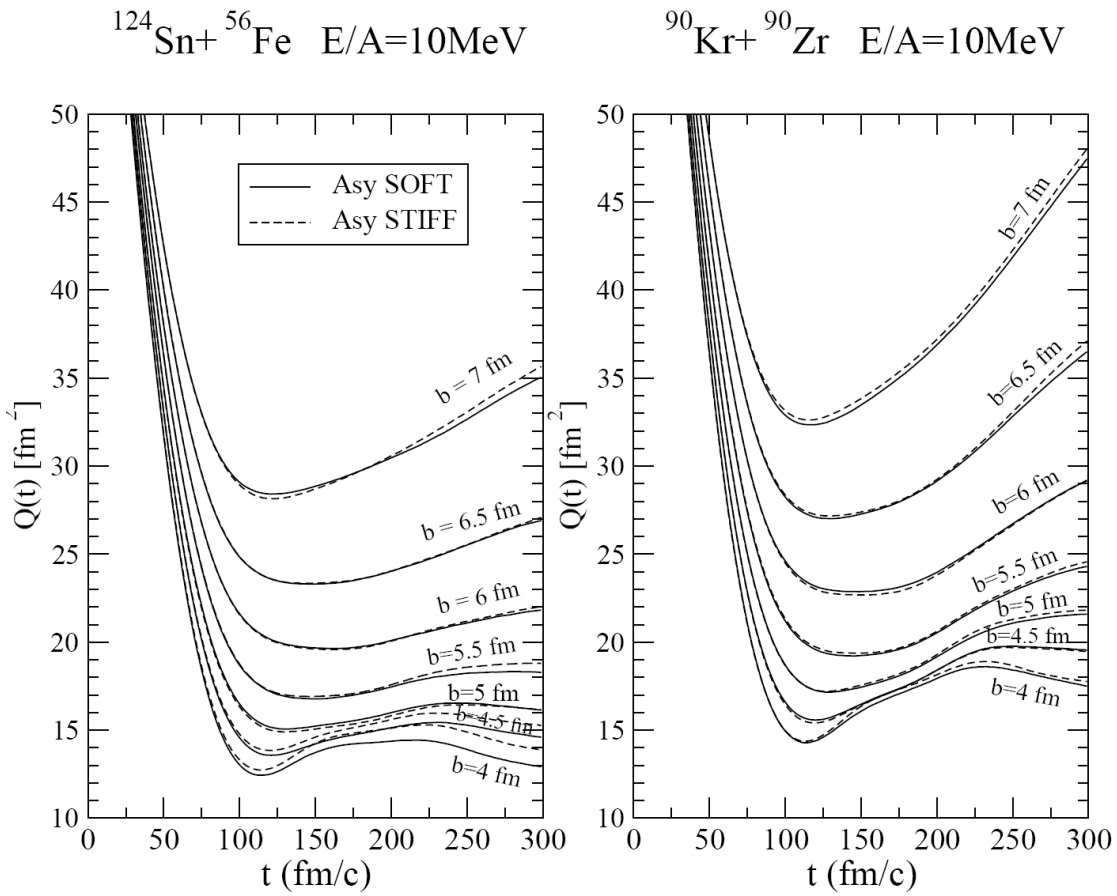

Fig.4. 23 Reactions ^{124}Sn+ ^{56}Fe vs. ^{90}Kr+ ^{90}Zr at 10 MeV/A . Time evolution of the space quadrupole moments in the angular momentum transition region, between b=4 and 7fm. Solid line: Asysoft. Dashed line: Asystiff.

We see that for the mass asymmetric case (Sn/Fe) we have more definite oscillations in the centrality transition region, clear indication of a larger fusion probability. We note also that in mass symmetric Kr/Zr case the fusion process is slower and at the same t=300 fm/c we do not see yet clear asymptotic trends for the space Quadrupoles in the transition region (and the same is observed for the momentum Quadrupoles, QK). It is then difficult to distinguish symmetry energy effects but we can clearly evaluate the impact of mass symmetry on the fusion cross sections. This is shown in Fig.4.24.

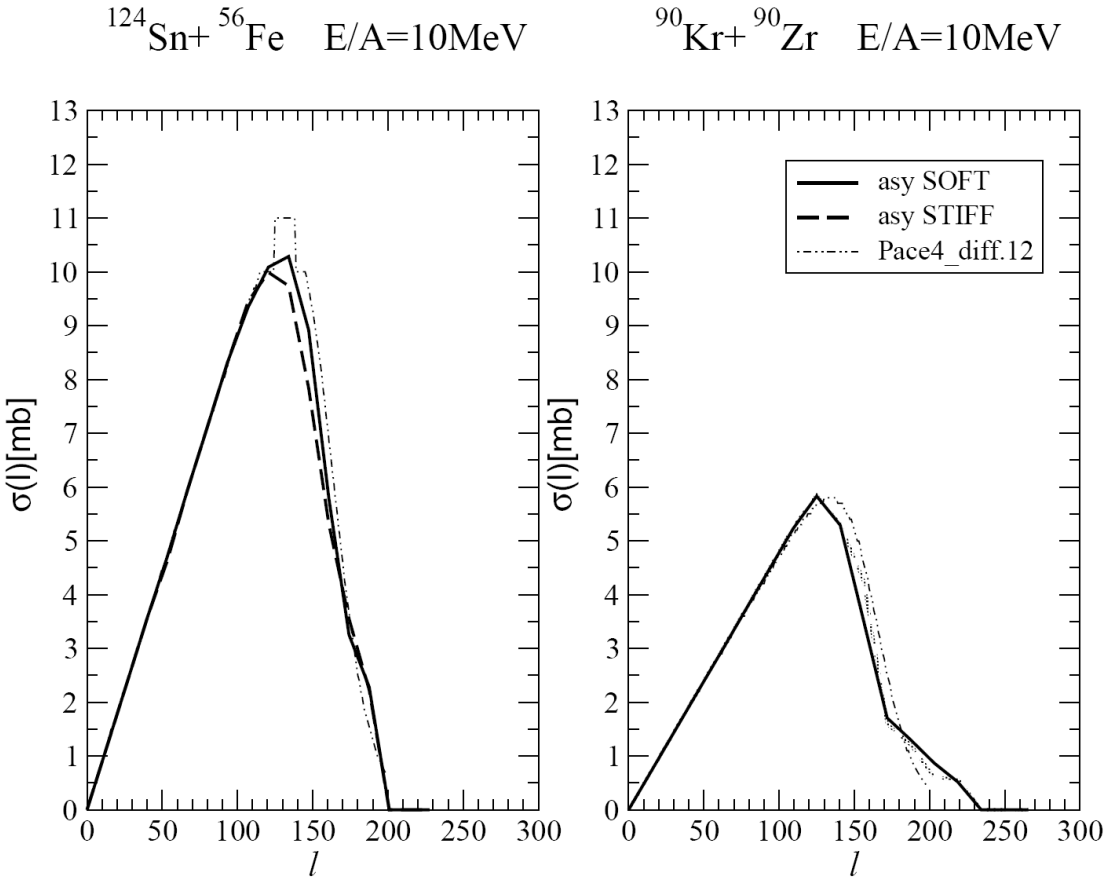

Fig.4. 24 Reactions ^{124}Sn + ^{56}Fe vs. ^{90}Kr + ^{90}Zr at 10 MeV/A . Angular momentum distributions of the fusion cross sections (mb) for the two choices of the symmetry term. The results of PACE4 calculations are also reported, l-diffuseness 12ħ.

The total cross sections are 1115 mb and 630 mb respectively for the mass asymmetric and symmetric cases (Asysoft choice). Extensions of the calculation to later times would probably allow to evaluate the dependence on the stiffness of the symmetry terms. Also for this n-rich systems we find that, in order to have similar *σ(l)* distributions from the PACE4 simulations, we have to use a rather large l-diffuseness value.

These systems are also interesting to investigate the DDR excitation. In Fig.4.25 we report the dipole strength distribution $|D''(\omega)|^2$ for the fusion/break-up event selection in the impact parameter transition region.

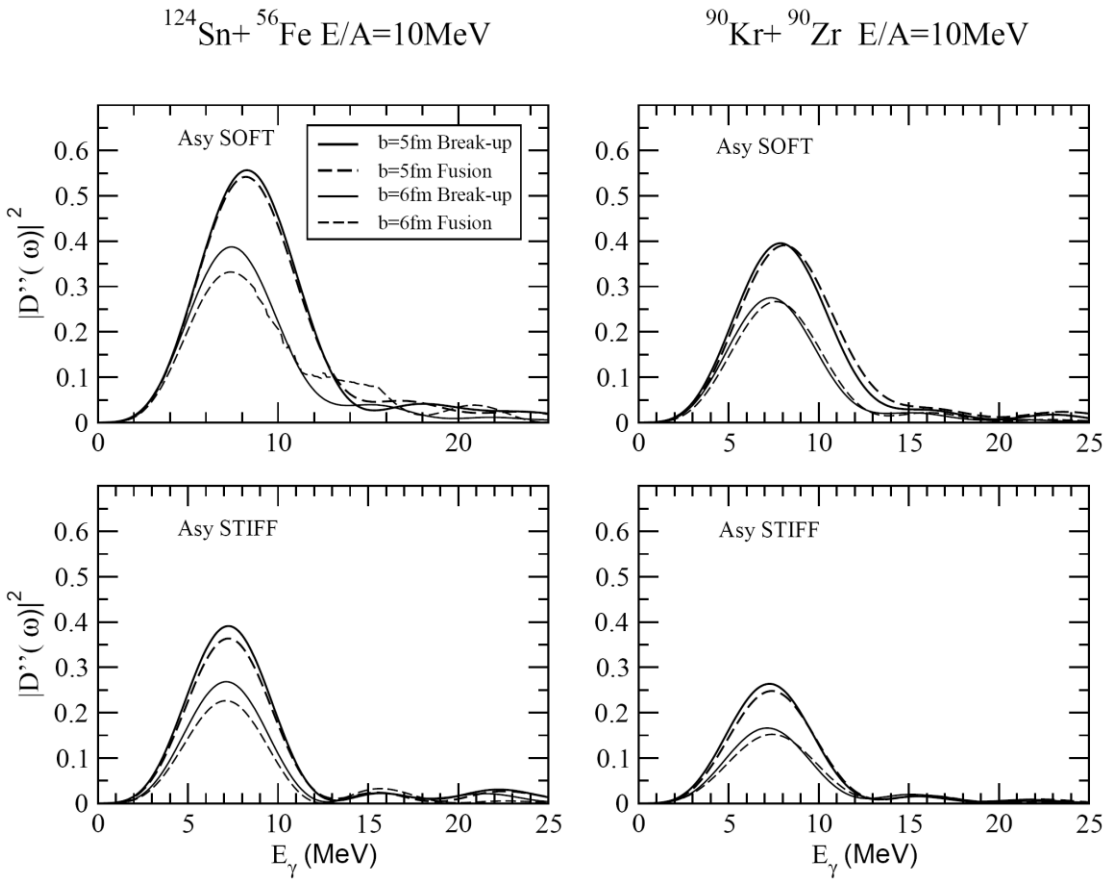

Fig.4. 25 Reactions ^{124}Sn + ^{56}Fe vs. ^{90}Kr +^{90}Zr at 10 MeV/A . Prompt Dipole strengths (in c^2 units) for break-up (solid lines) and fusion (dashed lines) events for impact parameters in the transition region. Left Panel: Asystiff. Right Panel: Asysoft.

As in the previous ^{132}Sn+^{58}Ni system, the DDR emission is larger in the Asysoft choice and not much different for the two reaction mechanism selections. An important point to remark is the larger emission probability for the mass-asymmetric Sn/Fe case. However this effects is almost exactly scaling with the square of the initial Dipole moment D(t = 0), 26.3 fm for Sn/Fe vs. 22.4 fm for Kr/Fe. This indicates that only the initial charge asymmetry really matters for the prompt dipole emission, which then is not much affected by the different fusion dynamics. All that is fully consistent with the very fast nature of the Dynamical Dipole mode.

4.9 Conclusions.

We have undertaken an analysis of the reaction path followed in collisions involving exotic systems at beam energies around 10 MeV/A. In this energy regime, the main reaction mechanisms range from fusion to dissipative binary processes, together with the excitation of collective modes of the nuclear shape. In reactions with exotic systems, these mechanisms are expected to be sensitive to the isovector part of the nuclear interaction, yielding information on the density dependence of the symmetry energy. Moreover, in charge asymmetric systems, isovector dipole oscillations can be excited at the early dynamical stage, also sensitive to the behaviour of the symmetry energy. We have shown that, in neutron-rich systems, fusion vs. break-up probabilities are influenced by the neutron repulsion during the approaching phase, where densities just above the normal value are observed. Hence larger fusion cross sections are obtained in the Asysoft case, associated with a smaller value of the symmetry energy at supra-saturation densities. On the other hand, the isovector collective response, that takes place in the deformed dinuclear configuration with large surface contributions, is sensitive to the symmetry energy below saturation.

The relevant point of our analysis is that it is based on the study of the fluctuations that develop during the early dynamics, when the transport calculations are reliable. Fluctuations of the Quadrupole moments, in phase space, essentially determine the final reaction path.

Conclusions and perspectives.

In this thesis we have studied the reaction path followed by HIC with exotic nuclear beams at low energy. We have focused on dissipative collisions to study the symmetry term of the EoS at densities below and around the saturation density.

The purpose of this investigation has been to analyze in detail the reaction mechanisms occurring in collisions involving exotic systems and to indentify observables which are sensitive to the still controversial Iso-EoS. We have employed two typically different Iso-EoS (Asysoft and Asystiff), for which one expects to see characteristic signatures, associated with the value and the derivative of the symmetry energy.

In particular, we have discussed the excitation of collective modes in dissipative reactions of charge asymmetric systems : isovector dipole oscillations can be excited at the early stage of a nuclear reaction in systems with different N/Z ratio. Our results are a good indication that the prompt dipole oscillation, due to the neutron/ proton oscillation along a definite symmetry axis, takes place in a deformed di-nuclear composite system , where low density surface contributions are dominant.

The corresponding emission rate, with a peculiar angular distribution has been evaluated, through a “bremsstrahlung” mechanism, within a consistent transport approach to the reaction

dynamics, which account for the whole contribution along the dissipative non equilibrium path, in fusion or deep-inelastic processes.

We have discussed different input channels, changing the beam energy and considering the use of exotic beams. We find a rise and fall of the photon emission multiplicity when increasing the beam energy: the peak of the excitation curve is located around 10MeV/A.

Furthermore, employing radioactive beams, new possibilities for the investigation of the symmetry energy at sub-saturation density are foreseen: we have shown that the Asysoft choice leads to a larger dipole emission since it gives a larger restoring force corresponding to mean densities below saturation. The high beam intensity and the use of exotic systems with a larger initial geometrical dipole moment, as in the $^{132}Sn+^{58}Ni$ reaction, trigger higher amplitude isovector oscillations, increasing the chance of a clear experimental observation and allowing to discriminate the DDR dependence on the symmetry term. Moreover a clear anisotropy in the angular distribution of the γ-emission, vs. the beam axis, is observed in the simulations, also sensitive to the density dependence of the symmetry energy.

We have investigated also the effect of the mass asymmetry in the entrance channel, for systems with the same overall isospin content and similar initial charge asymmetry. We observe that the DDR strength is not much affected. In fact, our results show that only the initial charge asymmetry is important for the prompt dipole emission, which then is not much affected by the different fusion dynamics. All that is fully consistent with the very fast nature of the Dynamical

Dipole mode with respect to the time evolution of the reaction mechanism.

Finally, we would like to stress that the dynamical dipole mode could represent a new cooling mechanism of the composite system, becoming thus of interest for the synthesis of super heavy elements. In fact, we know that the composite system survival probability against fission and the shell structure stabilization effects increases by decreasing the composite system excitation energy. The emission of pre-equilibrium dipole photons in charge asymmetric “hot” fusion reactions would produce a lowering of the compound nucleus excitation energy by about 10–15 MeV that could result in an increase of its survival probability against fission.

Around 10MeV/A of beam energy, the main reaction mechanisms range from fusion to dissipative binary processes. In reactions with exotic systems, the competition between these mechanisms is sensitive to the isovector part of the nuclear interaction.

Indeed we have shown, by performing a shape analysis, that, in neutron-rich systems, fusion vs. break-up probabilities are influenced by the neutron repulsion during the approaching phase, where densities just above the normal value are observed. Hence larger fusion cross sections are obtained in the Asysoft case, associated with a smaller value of the symmetry energy at supra-saturation densities.

Our analysis is based on the study of the fluctuations of quadrupole moments in phase space, that are developed during the early dynamics, but determine the final reaction path.

We stress that the collective charge equilibration mechanism, i.e. the DDR discussed above, is revealed in both fusion and break-up events at semi-peripheral impact parameters. Also in these cases we find a systematic increase of the DDR yields in the Asysoft choice.

Hence we have shown that the Asysoft choice leads to a large fusion probability since it gives a smaller repulsion at the supra-saturation densities of the first stage of the reaction, but at the same time gives a larger restoring force for the dipole oscillation, corresponding to mean densities below saturation. This apparent contradictory conclusion can be easily understood: we note that the onset of the collective dipole mode is delayed with respect to the first high density stage of the overlap region between colliding nuclei since the composite system needs some time to develop a collective response of the di-nuclear mean field.

As far as the transport approach employed here and possible improvements are concerned, we would like to note that the fluctuations discussed here are essentially of thermal nature. It would be interesting to include also the contribution of quantal (zero-point) fluctuations of surface modes and angular momentum. Indeed the frequencies of the associated collective motions are comparable to the temperature ($T \approx 4MeV$) reached in our reactions [LAN80]. This would increase the overall amplitude of surface oscillations, inducing larger fluctuations in the system configuration and a larger break-up probability. Such quantum effect has been recently shown to be rather important for fusion probabilities at near and sub-barrier energies [AYI10]. The qualitative agreement of our semi-classical procedure

with present data above the barrier could be an indication of a dominance of thermal fluctuations at higher excitation energy.

In conclusion, we have shown that considerable isospin effects, concerning reaction mechanisms and dynamical dipole radiation, are revealed especially in the impact parameter window corresponding to semi-peripheral reactions. Interesting perspectives are opening for new experiments on low energy collisions with exotic beams focused to the study of the symmetry term below and above saturation density. We like to conclude by listing again the observables that, according to our investigations, appear very promising:

i) Larger fusion probabilities for more neutron-rich systems with a clear enhancement in the Asysoft choice in the semi-central transition region;

ii) Larger fragment deformations in break-up processes in the Asystiff choice, with related larger probabilities for ternary/quaternary events;

iii) Evidence of the Dynamical Dipole Radiation in both fusion and dissipative break-up events for charge asymmetric entrance channels.

iv) Sensitivity of the DDR γ-yields and anisotropies to the stiffness of the symmetry term around saturation;

v) The entrance channel mass-asymmetry is influencing the fusion probabilities but not the Prompt Dipole emission, nice confirmation of the fast nature of this isovector oscillation.

Bibliography

[ALH90] Y. Alhassid, B. Bush, Phys. Rev. Lett. 65, 2527 (1990)

[AMO04] F. Amorini et al., Phys. Rev. C69, 014608 (2004)

[AMO09] F. Amorini, G. Cardella et al., Phys. Rev. Lett. 102, 112701 (2009)

[AYI88] S. Ayik, C. Gregoire, Phys. Lett. B212, 269 (1988); Nucl. Phys. A513, 187 (1990)

[AYI10] S. Ayik, B. Yilmaz, D. Lecroix, Phys. Rev. C81, 034605 (2010)

[BAR96] V.Baran, M. Colonna, M. Di Toro, A. Guarnera, A. Smerzi, Nucl. Phys. A600, 111 (1996)

[BAR00] V.Baran, M. Cabibbo, M. Colonna, M. Di Toro, N. Tsoneva, Nucl. Phys. A679, 373 (2001)

[BAR01] V.Baran, D.M. Brink, M. Colonna, M. Di Toro, Phys. Rev. Lett. 87, 18, 182501 (2001)

[BAR02] V. Baran et al. Nucl. Phys. A703, 603 (2002)

[BAR05] V.Baran, M. Colonna, V. Greco, M. Di Toro, Phys. Rep. 410, 335 (2005)

[BAR08] V. Baran, C. Rizzo, M. Colonna, M. Di Toro, and D. Pierroutsakou, Phys. Rev. C **79**, 021603(R) (2009)

[BAR09] V. Baran, M. Colonna, M. Di Toro, C. Rizzo "Probing the symmetry energy with exotic proton rich beams" Proposal for the upgrading of the FRIBS beam production line (2009)

[BER84] G.F. Bertsch, Phys. Lett. B 141, 9 (1984)

[BER88] G. F. Bertsch, S. Das Gupta, Phys. Rep. 160 N° 4 , 189 (1988)

[BOM91] I. Bombaci, U. Lombardo, Phys. Rev. C 44, 1892 (1991)

[BON89] A. Bonasera et al., Phys. Lett. B221, 233 (1989)

[BON94] A. Bonasera et al., Phys. Rep. 243 N° 1-2 (1994)

[BON04] L. Bonanno, Effetti di radiazione diretta dipolare sulla sintesi degli elementi superpesanti, Master Thesis, Catania Univ. (2004)

[CAB98] M. Cabibbo, V.Baran, M. Colonna, M. Di Toro, Nucl. Phys. A637, 374 (1998)

[CHA97] E. Chabanat, P. Bonche, P. Haensel, J. Meyer, R. Schaeffer, Nucl. Phys.A627, 710 (1997); Nucl. Phys. A635, 231 (1998); Nucl. Phys. A643, 441 (1998)

[CHO93] P. Chomaz, M. Di Toro, A. Smerzi, Nucl. Phys. A563, 509 (1993)

[COL95] M.Colonna, M.Di Toro, A.Guarnera, Nucl .Phys. **A589,** 160 (1995)

[COL98] M. Colonna, M. Di Toro, A. Guarnera, S. Maccarone, M. Zielinska-Pfabè, H.H. Wolter, Nucl. Phys. A642, 449-460 (1998)

[COL98+] M. Colonna et al. Phys. Rev. C57, 1410 (1998)

[DIT84] M. Di Toro, Nuclear Dinamics in Phase Space; Proceeding of the Winter College on Fundamental Nuclear Physics, World Scientifics(1984)

[DIT07] M. Di Toro et al, Nucl. Phys. A787, 585c (2007)

[GAA92] J. J. GaardhΦje, Ann. Rev. Nucl. Part. Sci.42, 483 (1992)

[GAV79] A. Gavron, Phys. Rev. 21, 230 (1979)

[HAR01] M.N. Harakeh, A. van der Woude, *Giant Resonances*, Oxford Univ.Press (2001)

[HUA63] K. Huang, Statistical Mechanics , Wiley & Sons (1963)

[LAN80] L. D. Landau, E. M. Lifsits, 'Statistical Physics', Part.1, Vol.5 (3rd ed.), Butterworth-Heinemann, (1980)

[LEF76] M. Lefort, Rep. Prog. Phys. 39, 129 (1976)

[LIA07] J.F. Liang et al., Phys. Rev. C75, 054607 (2007)

[LI94] G. Q. Li e R. Machleidt, Phys. Rev. C49, 566 (1994)

[LI04] B. A. Li, C. B. Das et al., Phys. Rev. C 69, 011603 (2004)

[MAR08] B. Martin, D. Pierroutsakou et al., Phys. Lett. B664, 47 (2008)

[MAR10] P. Marini, B. Borderie, A. Chbihi, N. Le Neindre, M.-F. Rivet, J.P. Wieleczko, M. Zoric et al. (Indra-Vamos Collab.), IWM2009 Int.Workshop, Eds.J.D.Frankland et al., SIF Conf.Proceedings Vol.101, pp.189-196, Bologna (2010)

[MYE77] D. W. Meyers et al., Phys. Rev. C15, 6, 2032 (1977)

[PAP01] M. Papa, T. Maruyama and A. Bonasera, Phys. Rev. C64, 024612 (2001)

[PIE02] D. Pierroutsakou et al., Nucl. Phys. A687, 245C (2003)

[PIE03] D. Pierroutsakou et al., Eur. Phys. J. A16, 423 (2003)

[PIE05] D. Pierroutsakou et al., Phys. Rev. C71,054605 (2005)

[PIE09] D. Pierroutsakou et al., Phys. Rev. C**80**, 024612 (2009)

[RAN90] J. Randrup, B. Remaud, Nucl. Phys. A514, 339-366 (1990)

[RIN80] P. Ring, P. Schuck, The Nuclear Many-Body Problem, Springer-Verlag (1980)

[RIZ08] J. Rizzo, P. Chomaz, M. Colonna, Nucl. Phys. A806, 40 (2008)

[RIZ10] C. Rizzo, V. Baran, M. Colonna, A. Corsi, M. Di Toro, Symmetry Energy Effects on Fusion Cross Sections, Phys. Rev. C in press. (2010)

[RIZ11] C. Rizzo, V. Baran, M. Colonna, M. Di Toro, M. Odsuren, Symmetry Energy Effects on Low Energy Dissipative Heavy Ion Collisions, Proceeding International Symposium: Quasifission Process in Heavy Ion Reactions, Messina, Journal of Physics: Conference Series (IOP) in press (2010)

[SIM07] C. Simenel et al., Phys. Rev. Lett. 86, 2971(2001); Phys.Rev. C76, 024609 (2007)

[SNO86] K. A. Snover, Ann. Rev. .Nucl. Part. Sci.36, 545 (1986)

[SHV10] L. Shvedov, M. Colonna, M. Di Toro, Physi. Rev. C81, 054605 (2010)

[SKW08] I. Skwira-Chalot et al. (Chimera Collab.), Phys. Rev. Lett. 101, 262701 (2008)

[TAR03] O.B. Tarasov, D. Bazin, Nucl. Inst. Methods, B204, 174 (2003)

[TSA89] M. B. Tsang, J. F. Bertsch, W. G. Lynch, M. Tohyama, Phys. Rev. C40, 1685 (1989)

[VLA45] V. Vlasov, J. Phys. 9 (Acad. Of Sci.), 25 (1945)

[WIG32] E. Wigner, Phys. Rev. C38, 2967 (1988)

[WIL10] J. Wilczynski et al. (Chimera Collab.), Phys. Rev. C81, 024605 (2010)

[WON82] Cheuk-Yin Wong, Phys. Rev. C25, 1460 (1982)